DISSERTATION

CATALYTIC STRATEGIES FOR ENHANCING ELECTROCHEMICAL OXIDATION OF 1,4-DIOXANE: TiO_2 DARK ACTIVATION AND MICROBIAL STIMULATION

Submitted by

Jeramy R. Jasmann

Department of Chemistry

In partial fulfillment of the requirements

For the Degree of Doctor of Philosophy

Colorado State University

Fort Collins, Colorado

Summer 2016

Doctoral Committee:

Advisor: Thomas Borch
Co-Advisor: Jens Blotevogel

Delphine Farmer
William Sanford
James Neilson
Michael Elliot

ABSTRACT

CATALYTIC STRATEGIES FOR ENHANCING ELECTROCHEMICAL OXIDATION OF 1,4-DIOXANE: TiO_2 DARK ACTIVATION AND MICROBIAL STIMULATION

1,4-dioxane, a probable human carcinogen, is an emerging contaminant currently being reviewed by the U.S. Environmental Protection Agency for possible health-based maximum contaminant level regulations. As both stabilizer in commonly used chlorinated solvents and as a widely used solvent in the production of many pharmaceuticals, personal care products (PPCPs), 1,4-dioxane has been detected in surface water, groundwater and wastewater around the U.S. It is resistant to many of the traditional water treatment technologies such as sorption to activated carbon, air stripping, filtering and anaerobic biodegradation making 1,4-dioxane removal difficult and/or expensive. State-of-the art technologies for the removal of 1,4-dioxane usually apply advanced oxidation processes (AOPs) using strong oxidants in combination with UV-light and sometimes titanium dioxide (TiO_2) catalyzed photolysis. These approaches require the use of expensive chemical reagents and are limited to *ex situ* (i.e. pump and treat) applications.

Here, at Colorado State University's Center for Contaminant Hydrology, innovative flow-through electrolytic reactors have been developed for treating groundwater contaminated with organic pollutants. The research presented in this dissertation has investigated catalytic strategies for enhancing electrochemical oxidation of 1,4-dioxane in flow-through reactors. Two types (abiotic and biotic) of catalysis were also explored: (1) dark, electrolytic activation of insulated, inter-electrode TiO_2 pellets to catalyze the degradation of organic pollutants in the

bulk solution by reactive oxygen species (ROS), and (2) adding permeable electrodes upstream of dioxane-degrading microbes, *Pseudonocardia dioxanivorans* CB1190, to pre-treat mixed contaminant water and provide O_2 stimulation to these aerobic bacteria.

For the abiotic form of catalysis, we characterized the properties of novel TiO_2 inter-electrode material, and elucidated the properties most important to its catalytic activity, using 1,4-dioxane as the model contaminant. The TiO_2 was novel in its use as an "inter-electrode" catalyst (not coated on the electrode and not used as a TiO_2 slurry) and in the mechanism of its catalytic activation occurring in dark (not photocatalysis) and insulated (not typical electrocatalysis) conditions. Further studies were performed using electrochemical batch reactors and probe molecules in order to gain mechanistic insights into dark catalysis provided by detached TiO_2 pellets in an electrochemical system. The results of our investigations show that electrolytic treatment, when used in combination with this catalytically active inter-electrode material, can successfully and efficiently degrade 1,4-dioxane. Benefits of catalyzed electrolysis as a green remediation technology are that (1) it does not require addition of chemicals during treatment, (2) it has low energy requirements that can be met through the use of solar photovoltaic modules, and (3) it is very versatile in that it could be applied *in situ* for contaminated groundwater sites or installed in-line on above-ground reactors to remediate contaminated groundwater.

Although, 1,4-dioxane appears to be resistant to natural attenuation via anaerobic biodegradation, some aerobic bacteria have been shown to metabolize and co-metabolize 1,4-dioxane. For example, growth-supporting aerobic metabolism/degradation of 1,4-dioxane by *Pseudonocardia dioxanivorans* CB1190, has been demonstrated in laboratory studies. However, previous studies showed that this biodegradation process is inhibited by the presence of

chlorinated solvents such as 1,1,1-trichlorethane (1,1,1-TCA) and trichloroethene (TCE). This could dramatically impact the success for *in situ* 1,4-dioxane biodegradation with *P. dioxanivorans* since chlorinated solvents are common co-contaminants of 1,4-dioxane. Our previous investigations into electrolytic treatment of organic pollutants both *ex* and *in situ* showed that effective degradation of chlorinated solvents like TCE was achievable. In addition, the electrolysis of water generates molecular O_2 required by the CB1190 bacteria as well. This led us to hypothesize that the generation of O_2 could enhance aerobic biodegradation processes, and the concurrent degradation of co-solvents could reduce their inhibitory impact on 1,4-dioxane biodegradation. In flow-through sand column studies presented here, we investigate the electrolytic stimulation of *Pseudonocardia dioxanivorans* CB1190, with the expectation that anodic O_2 generation would enhance aerobic biodegradation processes, and concurrent degradation of TCE would reduce the expected inhibitory impact on 1,4-dioxane biodegradation. Results show that when both electrolytic and biotic processes are combined, oxidation rates of 1,4-dioxane substantially increased suggesting that aerobic biodegradation processes had been successfully stimulated. In summary, the results of this dissertation provide evidence of (1) efficient removal of recalcitrant 1,4-dioxane, especially with the addition of inter-electrode TiO_2 catalysts, (2) elucidate possible mechanistic pathways for electro-activated dark TiO_2 catalysis, and (3) provide evidence for successful synergistic performance for electro-bioremediation treatment during simulated mixed, contaminant plume conditions.

ACKNOWLEDGEMENTS

Thank you God for this amazing opportunity and for bringing so many special people into my life during this time. Thank you God for listening to my prayers, providing me with blessing when I needed them most [Matthew 6:25-34], and helping my family to make it through this challenging financial season as an intact, active, healthy and truly joyous family of five: "The Jasmann Five" (only we don't sing…well). By diving deeper into science, I continue to be impressed by your creation and the natural laws you have put into motion [Romans 1:19-20]. These laws of chemistry, thermodynamics, electromagnetism and others, are what provide endless discoveries for us to make as scientist.

I would like to thank my advisors Dr. Thomas Borch and Dr. Jens Blotevogel who have provided invaluable guidance and helped me to establish a remarkable foundation in hypothesis-driven research. Without their advice, support, and friendship, my journey to this publication would not have been possible. I would like to thank Dr. Borch for his enthusiasm for science and for working with me to find an interdisciplinary research problem with applicable outcomes relevant to the protection of human health and the environment; it was exactly what I had hoped for. I would like to thank Dr. Blotevogel for his desire to research practical remediation solutions for recalcitrant environmental contaminants (a tough and uncertain field at times), and his outstanding intellectual contributions when discussing difficult scientific problems, especially when providing critical revisions and structure to my writing near the end of my time here.

I would like to thank Dr. Tom Sale of the Center for Contaminant Hydrology (CCH) who has been a close collaborator throughout my doctoral work and who made it possible for my entire Ph.D. program to be funded by industry-university collaborations he has formed over the years.

Dr. Sale has an uncanny ability to distill industry problems down to their most important needs in order to target the problem and investigate solutions most efficiently. I would also like to thank Gary Dick, our laboratory manager in the CCH, who was instrumental in the experimental design phase when building my flow-through electrochemical reactors. His retirement midway through my program left a gaping hole, losing his unmatched mechanical expertise and losing the continuous stream of oddly funny jokes and quips he seemed to always have at the ready. I would like to recognize the financial assistance that made this work possible. I thank Dr. Masayuki Shimizu for conducting the synchrotron radiation-based XRD with me at the Stanford Synchrotron Radiation Lightsource, SLAC National Accelerator Laboratory, supported by the U.S. Department of Energy, Office of Science, Office of Basic Energy Sciences under Contract No. DE-AC02-76SF00515. Thank you to Dr. Yury Desyaterik, Ali Boris and Robert Young for their patient guidance in the use of LC/ESI-TOF-MS, and LC/UV, respectively.

My work was primarily supported by E. I. du Pont de Nemours and Company (DuPont) and The Chemours Company, along with complementary support from General Electric, three outstanding companies who recognize the environmental concern posed by 1,4-dioxane, and were committed to fully funding my research to discover novel, effective, and economical remediation options.

I met many fellow researchers and students throughout this processes that I consider both friends and colleagues. Many members of the Borch group and CCH laboratory group have made lasting impressions on me for their valuable input and for being great co-workers: Ellen Daugherty, Kevin McKoy, Helen Dungan, Ali Hawkins-Haron, Kevin Saller, Missy Tracy, Calista Campbell, Wess Tuli, Dr. Rong (Rhoya) Wei, Dr. Masayuki Shimizu, Dr. Saeed Kiaalohosseini, Dr. J.J. Stone, and Dr. Lyndsay Troyer. Thank you to the undergraduate

laboratory technicians who helped out so much with some of my later experiments: Nolan Platt and Alexa Kinsinger. Thanks for putting up with the old guy in the group; never thought that would be me. Thank you to my environmental analytical chemistry "crew" Raymond Detweiler, Penny Osborne, and Dr. Pat Brophy for all the good times and making it fun to be back in school again.

A special acknowledgement to my Bri'ish mate Dr. Gina McKee who eats peas by lining them up on the backside of a fork (really), but also is so kind, intelligent and organized and helped to keep the laboratory group cohesive. To the soon-to-be Dr. Genevieve Kahrilas, thanks for keeping it real, and being a friend to me. It was great having you as my writing buddy near the end; your revisions and witty comments were fun to read, and I'll never forget about Oxford commas again! I would especially like to thank Maria Irianni-Renno, Dr. Mitch Olson, and Dr. Robert Young for their friendship, their advice, and in having disgruntled conversations about the failures and trouble-shooting requirements of modern analytical instruments. I knew Maria was always up for lunch at The Mayor's if I needed to talk, especially when Horse & Dragon's Sad Panda was on tap. Maria's assistance in preparing sterile biological nutrient media, training me on the ATP analysis, and modeling best practices when working with microbes were essential for me to obtain credible and reproducible data in my electro-bioremediation experiments. Mitch's help in general maintenance and troubleshooting the gas chromatography-mass spectrometer was "instrumental" (*pun intended*) to the development of my technical skills that have already paid dividends with me beginning my new career as a research scientist. And Robert, an aged man like myself and research scientist being his second career like myself, was a great companion I could count on for beers and cheers, and a colleague I could rely on for

valuable input on chemical analysis and life. I look forward to continuing these friendships both professionally and personally.

Dr. Delphine Farmer, Dr. James Neilson, and Dr. William Sanford: thank you to for agreeing to serve on my committee. You are all great academic examples and people of excellence whom I have the utmost respect for. A special thank you is in order for Dr. Michael Elliot, the electrochemistry expert on my team, who unfortunately died suddenly of a heart attack in 2014. I really could have used his electrochemical input and sharp wit as I was struggling to finalize my dissertation. I would also like to acknowledge other members of my CSU graduate school support team: Dr. Melissa Reynolds and Dr. Chuck Henry for being true professionals and authentic individuals that I could count on when I needed advice; and Dr. Brian Bledsoe for being openly passionate about your teaching and for your engaging conversations ranging from environmental health to life decisions.

In addition, I would like to say thank you to organizations that recognized my scientific contributions. It was nice to be recognized for all the hard work that goes into novel research, and the added benefit of financial rewards were always helpful when living on graduate student pay. Thank you to the Sustainable Remediation Forum (SURF) for the Outstanding Performance Award in 2013, to the American Chemical Society for the Outstanding Environmental Chemistry Graduate Student Award in 2015, to the Rocky Mountain Society of Environmental Toxicology and Chemistry (RMSETAC) for the Best Student Platform Award in 2015, and to sponsors of the Emerging Contaminants Summit for second place in the Student Presentation Competition in 2016.

Thank you to all of my friends outside of my working environment whom I had a blast with camping, biking, skiing, BBQ'ing or doing all those things I used to do much more

regularly before the time-sucking whirlpool that is graduate school became my life. You know who you are; I look forward to seeing you all a lot more soon!

To my family in California: especially my parents and brother, Roland Jasmann, Betty Jasmann and Ben Jasmann, it was ALWAYS so nice to get to see you when you flew out, or when you'd pay to fly us out to Cali to see you. I am so appreciative that I have a caring brother like you Ben. And Mom and Dad, thank you for your truly unconditional love and encouragement regardless of the personal and professional goals and career paths I choose to follow. Thank you for instilling in me integrity and worthwhile values that guide my decisions today. Your high moral character and unsurpassed work ethic are legacy qualities that I continually strive to maintain, and hope to pass them along to my children as well.
Your upbringing, along with the close family I had growing up and still have today, have allowed me to achieve what I have today. Thank you Grandma and Grandpa Jasmann (Gertrude and Alex) and thank you Grandma and Pop Sullivan (Jimmie and Dale); I could not have asked for more loving and perfect grandparents. And thank you Grandpa Cale, who passed away when I was far too young but still occupies many, many fond memories of camping, fishing, walking alongside the railroad tracks together and passing along catchy euphemisms which I still use today, like "spider bark" and "buck snort". I know you would be proud of me today, just as you were when cheering me on along the sidelines at my soccer games when I was in grammar school. Thank you to my in-laws Pam Wee and Greg Bridwell for being supportive of my PhD aspiration, and contributing in a gigantic way by taking care of Addison two days a week. She loves being there with the two of you.

Most importantly, I COULD NOT have done this PhD program without the unequivocal love and support of my wife AND children. Sometimes I wonder how we did it. Thank you

Carson (8 years old), Bryce (6), and Addie (2) for continually bringing joy into my life! It was a blessing to be with you every morning and walk you to school each day. Riding bikes with you, camping, and snow skiing on the weekends protected my sanity throughout this program, and reminded me of what is truly important in this life, FAMILY. Thank you for making me feel special by running up to hug me and so enthusiastically tell me about your days, especially when I had to work many long nights in the laboratory. I am already so proud of you all for your kind hearts, joyful and adventurous spirits, and your passion for outdoor activities and protecting the environment, or "Mother Earth" as you call it. I also am proud to hear when any of you tell others you want to grow up to be a scientist like me, even if this is not what you truly end up becoming. If I were brilliant enough as a scientist, I would try to slow down how quickly you are growing up so that I could have just that much more time with you living in the house and sharing life with you.

Last, but not least, I wholeheartedly and enthusiastically thank my beautiful wife Christine Jasmann. You are the glue who kept our family functioning, when I did not have the time to be there. Thank you for making me laugh always, and making me feel successful as a husband and father when research disappointments were bringing me down. Thank you for healthy dinners, and for binge-watching Netflix shows with me late into the night because I just needed to clear my head. Thank you for supporting me to be the best person I can be, encouraging me to get the exercise and activities that I need, listening to me when I needed to vent about failures of analytical instruments (even when these venting sessions are far too detailed and lengthy to be of interest to you), and thanks for being willing and able to be the financial bread-winner for our family during this season of our lives. Most of all, I appreciate

your unconditional love for me and the kids, and the consistency of your spiritual strength and positive attitude through this all. I LOVE YOU.

DEDICATION

To my energetic, intelligent and compassionate children,

Carson, Bryce and Addison

This research, and all of my future work, is motivated by my desire to be a faithful steward of this earth, and to make the world a better place for my children, and my children's children.

We do not inherit the earth from our ancestors;

we borrow it from our children.

Amish Saying? Native American Proverb?

Ralph Waldo Emerson? Wendell Barry?

TABLE OF CONTENTS

LIST OF FIGURES

CHAPTER 1

INTRODUCTION

RESEARCH OBJECTIVES

Our overarching goal is to develop an above-ground electrochemical reactor or *in situ* electrolytic permeable reactive barrier that is an effective, economical, and environmentally responsible treatment for recalcitrant pollutants, such as 1,4-dioxane (our model contaminant). 1,4-dioxane has demonstrated high recalcitrance to biodegradation in anoxic groundwater environments and conventional groundwater treatments, such as filtration, sorption to activated carbon, and air stripping, are extremely inefficient for 1,4-dioxane removal.[1]

Currently UV-light based advanced oxidation processes (AOPs) like UV/H_2O_2 are able to effectively treat 1,4-dioxane through the production of hydroxyl radicals, which are powerful non-selective oxidants. However, these UV-based processes are expensive and limited to *ex situ* (i.e. pump and treat) systems. An efficient and practical technology, like advanced chemical oxidation (AEO) is needed as an alternative to UV/AOPs. The first main objective was to investigate the treatment efficacy of 1,4-dioxane in flow-through electrochemical reactors (FTERs), both with and without the addition of inter-electrode TiO_2 catalysts. To create conditions more representative of contaminated groundwater environments, we built laboratory-scale, flow-through electrochemical reactors, and used groundwater-relevant flow velocities and electrical conductivities. Previous electrolytic studies pertaining to 1,4-dioxane using simple electrochemical batch reactors showed successful degradation was possible with boron-doped diamond (BDD) anodes, however this material is not available in the mesh format and is

considered to be prohibitively expensive for field-scale applications at this time.[2] Experiments were designed to derive optimal conditions and potential challenges applying to flow-through remediation technologies in the field. In addition, this study is the first to test the selective electrochemical activity toward 1,4-dioxane of Ti/IrO_2-Ta_2O_5, a different electrode material, and to include inter-electrode TiO_2 pellets as a heterogeneous catalyst that is electrically insulated and blocked from exposure to any light .This work is described in Chapter 2.

Principal hypotheses related to TiO_2-catalyzed permeable electrolytic barriers:

- Flow-through electrochemical reactors with permeable, mesh Ti/IrO_2-Ta_2O_5 electrodes can provide effective degradation of 1,4-dioxane under simulated groundwater conditions.
- Relative 1,4-dioxane degradation efficiencies will be higher under certain water quality and flow characteristics, such as having lower 1,4-dioxane concentrations, higher ionic strength, and slower seepage velocities.
- Certain operational parameters, such as voltage, current density, and the number of polarized electrodes in use, can be controlled to achieve targeted 1,4-dioxane removal outcomes, providing the opportunity for utilizing the least amount of energy and materials resources whenever possible.
- Inter-electrode TiO_2 pellets will catalyze the electrochemical degradation kinetics of 1,4-dioxane in the absence of light and while electrically insulated from the anode.

The second main objective was to gain mechanistic insights into the dark catalytic activity of TiO_2 in electrochemical systems. In these studies, we explored which catalyst properties were most relevant to the electrochemical activity of different compositions of TiO_2 pellets with regards to 1,4-dioxane degradation efficiencies in FTERs and electrolytic batch

reactors. In addition, numerous probe molecules (e.g. 1,4-benzoquinone, *tert*-butyl alcohol, carbon tetrachloride) were used in electrolytic batch reactors to gain insight into what mechanisms were governing the catalytic activity of TiO_2 in the dark electrochemical reactors. Again, previous studies have examined TiO_2 as a photocatalyst or as a non-active electrode coating material for electrocatalysis. However, previous studies have not examined TiO_2 as a separated and insulated inter-electrode catalyst in dark (non-photocatalytic) conditions. This work is described in Chapter 3.

Principal hypotheses related to the mechanisms responsible for the improved contaminant degradation kinetics observed in the presence of electrically insulated TiO_2:

- TiO_2 pellets will have higher catalytic activity with greater specific surface area, smaller crystallite size, and high percentage of TiO_2 in the anatase phase. Since, this is not a photocatalytic process, it is unclear whether the band gap energy will affect activity.
- Electrode-generated $^{\bullet}OH$ radicals will "drift" downstream (downgradient in an aquifer) and adsorb onto TiO_2 surfaces, forming "surface-active complexes" capable of oxidizing co-adsorbed pollutants (i.e. 1,4-dioxane and its transformation products).
- The electric field will induce charge migration/separation within the electrically insulated TiO_2 pellets creating localized partial negative (e^- majority) and partial positive (hole or h^+ majority) regions, which then are able to perform chemical reactions with molecules adsorbed to the surface (i.e. 1,4-dioxane, its intermediates, and H_2O).

The third main objective was to examine possible synergistic effects of the electrolytic degradation of 1,4-dioxane and a common co-solvent, TCE, while also stimulating aerobic bacteria capable of biodegrading 1,4-dioxane. Previous work has demonstrated the microaerophilic bacteria *Pseudonocardia dioxanivorans* CB1190 is capable of metabolizing 1,4-

dioxane as its sole energy and carbon source.[3-5] However, further studies revealed a possible limitation for *in situ* field applications in which groundwater is anoxic and/or contains chlorinated co-contaminants like TCE which can greatly inhibit the microbial degradation of 1,4-dioxane.[6] This work is described in Chapter 4.

Principal hypotheses related to the synergistic effects observed when combining electrochemical and microbial degradation of 1,4-dioxane:

- Electrolysis of water will generate O_2 at the upstream anode of flow-through reactors, providing a necessary e^- acceptor for aerobic 1,4-dioxane biodegradation by *P. dioxanivorans* CB1190, leading to improved degradation kinetics when compared to control experiments of microbes without the addition of electrolysis.
- Direct anodic oxidation of 1,4-dioxane will synergistically contribute to the overall removal of 1,4-dioxane, resulting in mineralization to CO_2, or transformation to more easily biodegradable products.
- The highest abundance of CB1190 bacteria will primarily occur downstream of the charged electrodes due to optimal microbial conditions, rather than between the charged electrodes where harsh redox and pH conditions are expected to exist.
- Electrolytic degradation of chlorinated co-contaminants (i.e. TCE) will reduce or remove the microbial inhibition associated with the biotoxicity impacts of chlorinated solvents.

RESEARCH RATIONALE

Contaminants of emerging concern. The intensification of industrial activities and development of synthetic chemicals since the latter half of the 19th century has inevitably caused environmental pollution with dramatic consequences for atmosphere, soils, and waters. Because of known or potential risks to human and environmental health, these environmental pollution

problems need to be effectively managed, both with strong regulatory enforcement as well as adaptation to environmentally benign industrial practices on the front end and comprehensive remediation strategies on the back end. Despite noble legislative attempts at environmental protection in the 1970s such the Clean Water Act, Safe Drinking Water Act, and Toxic Substances Control Act (TSCA), our efforts at environmental remediation have fallen tragically short.

Unfortunately, scientific literature and recent environmental problems in the news clearly indicate our surface and groundwater environments continue to become polluted, so much so that even providing safe drinking water for our homes can be at risk. In 2014, after cost-cutting measures that switched the source of municipal water for Flint, Michigan, many of the 99,000 residents were exposed to high levels of lead and disinfection byproducts (trihalomethanes) in their drinking water for 18 months.[7] In Ann Arbor, Michigan, accidental releases of 1,4-dioxane used to produce medical filters created a large 1,4-dioxane plume (levels > 1000 µg/L) under residential neighborhoods (first discovered in 1984) that continues to contaminate groundwater used for municipal drinking water, and persists towards the Huron River, another municipal source of water. No treatment has worked well enough to stops its progression, and just this year new reports of 1,4-dioxane vapor intrusion into Ann Arbor homes has exceeded safe limits.[8] And in another case in North Carolina, multiple wastewater treatment effluents are thought to be the culprit of 1,4-dioxane hot spots of up to 1000 µg/L in the Cape Fear River Basin. Other examples of decades-long environmental challenges include river sediment and aquifer exposure to the insulation chemicals PCBs (polychlorinated biphenyls) used in electrical transformers and the ubiquitous industrial use of vapor-degreasing, chlorinated solvents like TCE (trichloroethylene).[9]

Although many of our industrial processes and pollutant management systems have improved over the last 40 years, the majority of Superfund sites have yet to be comprehensive remediated, accidental releases still happen, and new chemicals with new environmental problems present themselves each year. The TSCA inventory contains about 85,000 contaminants registered for commercial use and the Chemical Abstracts Service (CAS) of the American Chemical Society (ACS) registers approximately 15,000 new chemicals and biological sequences each day.[10] This is a daunting number of synthesized chemicals which, while they surely supply societal benefits, will inevitably produce unknown or unintended negative consequences when released into the environment. And while other chemicals may not be new, new information concerning high risk factors has recently emerged, as is the case for perfluorochemical compounds (PFCs) and 1,4-dioxane. These contaminants of concern (whether legacy or emerging) create a great need for scientific research into effective remediation strategies to preserve the environment and protect human health. My research motivation is to contribute scientifically to finding practical & effective remediation processes particularly for recalcitrant pollutants in groundwater. Therefore, the overarching goal of my research is to investigate the best operational parameters for advanced electrochemical oxidation to provide an alternative treatment option for recalcitrant contaminants that persist in groundwater, with 1,4-dioxane being the primary model contaminant of my investigations.

LITERATURE REVIEW

1,4-Dioxane in the environment and its remediation challenges. 1,4-dioxane ($C_4H_8O_2$) is a contaminant of emerging concern according to the U.S. EPA. 1,4-dioxane has been detected in surface water and groundwater all across the U.S., including many federal superfund

facilities.[11-13] This chemical can have chronic toxic effects to liver and kidney,[14, 15] and is designated as a probable human carcinogen, partially based upon reported cancers in liver, nasal, and mammary glands in animal research models exposed to high levels of 1,4-dioxane in drinking water.[15, 16]

1,4-Dioxane a cyclical ether and an aprotic solvent that is miscible in water, making it a desirable organic solvent for certain industrial processes. It is especially desirable when reactions are carried out at higher temperatures, because it has a relatively high boiling point of 101°C. Its two oxygens are Lewis bases and therefore the molecule can serve as a chelating diether ligand. The Lewis base properties of 1,4-dioxane are what allow for it to form ligand adducts to "poison" the unwanted catalytic $AlCl_3$ and prevent degradation of chlorinated solvents stored in aluminum barrels. Historically, this stabilizer function of 1,4-dioxane was widely used to preserve chlorinated solvents in vapor-degreasing applications, and due to improper disposal and accidental spills is the most common environmental exposure route.[12, 14]

Environmental exposure can come from many other sources as well due to 1,4-dioxane's continued use in industry. It is still used as a wetting agent in paint strippers, textiles, and paper processing.[17, 18] 1,4-Dioxane is also generated as a by-product or impurity during the synthesis of many important products such as polyethylene terephthalate (PET), polyoxyethylene nonionic surfactants, and cosmetics.[12, 14] Additionally, residues of 1,4-dioxane may be present on certain food packaging materials and on food crops treated with pesticides containing 1,4-dioxane (such as vine ripened tomatoes).[14]

In comparison to many other organic solvents, 1,4-dioxane has very low octanol-water and organic carbon partition coefficients ($\log K_{ow}$= -0.27 and $\log K_{oc}$= 1.23) allowing accidental releases to rapidly leach into groundwater, forming large and dilute plumes, often in combination

with other industrial solvents. U.S. state regulations for potable water and groundwater currently mandate maximum contaminant levels (MCLs) very near to the current EPA guideline for 1,4-dioxane in potable water of 0.3 µg/L. 1,4-dioxane is not only persistent, but once released into groundwater it is also difficult to treat due to its miscibility with water, low sorption affinity, and low volatility. Current conventional water treatment practices such as sorption to activated carbon, air stripping, filtration, and anaerobic biodegradation have proven to be relatively ineffective at removing 1,4-dioxane from water. Therefore, more aggressive technologies are needed for remediation of groundwater contaminated with 1,4-dioxane.

Currently applied technologies that effectively degraded 1,4-dioxane are UV/AOPs that generate ·OH radicals by the application of high energy UV light to chemical reagents such as ozone (O_3) or hydrogen peroxide (H_2O_2) and are sometimes enhanced by aqueous slurries of TiO_2 to catalyze production of ·OH from the surrounding water. [19] [18, 20, 21] The need for UV light and input of additional chemical reagents (H_2O_2, O_3, Fe^{+2}) has been a critical limitation in full scale treatment technologies due to high operation and maintenance costs of powering racks of UV lamps and continually supplying strong chemical reagents. Other obstacles preventing widespread use of UV-based AOPs include the low quantum efficiency of incident photon to electron transfer oxidation reactions due to fast electron/hole recombination reactions, difficulty in post-treatment recovery of TiO_2 catalyst often used as a slurry, and unwanted quenching of reactive oxygen species by non-target organic molecules in the environmental matrix.[22, 23] Furthermore, UV-based AOPs are limited to more costly *ex situ* applications such as "pump and treat" where groundwater is pumped from underground to be chemically treated in above-ground reactors before the treated water is then reinjected into the aquifer. Due to these limitations, there is high interest in alternative 1,4-dioxane removal technologies that are more cost-effective and able to treat

groundwater via *in situ* applications. Based upon other UV-based AOPs in the literature which were effective at degrading 1,4-dioxane and previous successes our laboratory group had with electrochemical degradation of other organic contaminants, we hypothesized that electrolytic oxidation of 1,4-dioxane may be a feasible alternative treatment, even in a flow-through application.

Advanced electrochemical oxidation. Many studies of water treatment spanning the last two decades have established the efficacy of electrochemical degradation for aqueous organic contaminants, including the removal of textile dyes, pesticides, chlorinated solvents, and highly persistent perfluorinated compounds[24-29]. Previous research has also demonstrated the advantages of electrochemical degradation, including the tunability and versatility of oxidation and reduction potentials, the ability to achieve high conversion rates to CO_2 (full mineralization) using relative low energy, and a clean reagent– the electron.[2, 23, 24, 30-32] Many prominent researchers in the electrochemical degradation field, such as C. Comninellis, C.A. Martinez-Huitle, M. Panizza, and G. Cerisola have published extensively on proposed models describing the mechanism for anodic oxidation processes as being initiated by physisorbed or chemisorbed $^{\bullet}OH$ radicals generated from the electrolysis of water.[2, 32, 33]

To summarize the dominant mechanistic theory, electrochemical oxidation (or electrolytic treatment) is an emerging AOP that can completely mineralize aqueous organic compounds mediated by highly reactive hydroxyl radicals generated from the electrolysis of water (eq. 1). [34-36]

$$H_2O \rightarrow {}^{\cdot}OH + H^+ + e^- \quad (1)$$

In many instances, organic pollutants can be degraded by direct anodic oxidation as shown in equation 2 below, where an electron is transferred from the contaminant (RH) to the anode.[37, 38]

$$RH \rightarrow R^{\cdot} + e^- + H^+ \quad (2)$$

More specifically, the model proposes that the initial reaction of the anode (denoted as M) with water produces a physisorbed hydroxyl radical M(•OH) (equation 3). In the case of "non-active" electrodes, like BDD anodes, the •OH remains loosely sorbed and is readily available for oxidation reactions with any nearby organic molecules via hydrogen abstraction or addition across π bonds. The continual production of these physisorbed •OH are non-selective in their oxidation capacity and therefore full mineralization of organic pollutants (R) is more efficiently obtained (equation 4). The competing reaction to form molecular oxygen is shown in equation 5.

$$M + H_2O \rightarrow M(^{\bullet}OH) + H^+ + e^- \quad (3)$$

$$3\ M(^{\bullet}OH) + R \rightarrow M + CO_2 + H_2O + H^+ + e^- \quad (4)$$

$$M(^{\bullet}OH) \rightarrow M + \tfrac{1}{2}\ O_2 + H^+ + e^- \quad (5)$$

For surface "active anodes", like the Ti/IrO_2-Ta_2O_5 mesh electrodes used in the experiments presented here, the more dominant pathway is thought to be one in which a higher oxide (MO) of the metal oxide coating can be formed. This is more of a "chemisorbed •OH", and the literature generally describes this species as being more selective in its oxidation capacity and not as capable of leading to full mineralization of pollutants to CO_2.[30]

$$M(^{\bullet}OH) \rightarrow MO + H^+ + e^- \quad (6)$$

$$MO + R \rightarrow M + RO \quad (7)$$

$$MO \rightarrow M + \tfrac{1}{2}\ O_2 \quad (8)$$

Some batch reactor studies have shown successful degradation of 1,4-dioxane using electrochemical oxidation.[21, 39, 40] De Clercq, et al., was able to achieve 92% COD removal of 1,4-dioxane using solely electrochemical treatment on a boron-doped diamond anode and proposed that complete oxidation takes place due to electro-generated hydroxyl radicals.[40] Other investigations have demonstrated that electrochemical treatment could be combined with

photocatalysis or ozonation to oxidize recalcitrant 1,4-dioxane. Kushimoto, et al., combined electrolysis with ozonation using a two compartment reaction cell and a solid electrolyte to degrade 1,4-dioxane, and Yanagida, et al., utilized the adsorption and desorption effects of voltage switching to assist photocatalytic degradation of 1,4-dioxane.[41, 42] However, these electrochemical degradation studies primarily focused on wastewater and/or surface water treatment; very few studies have been related to electrochemical degradation technologies for groundwater applications.

The study presented here is the first to use flow-through electrochemical reactors to investigate the potential for treatment of 1,4-dioxane in groundwater. Figure 1.1 is a conceptual diagram of what permeable electrolytic barriers look like when installed in the ground.

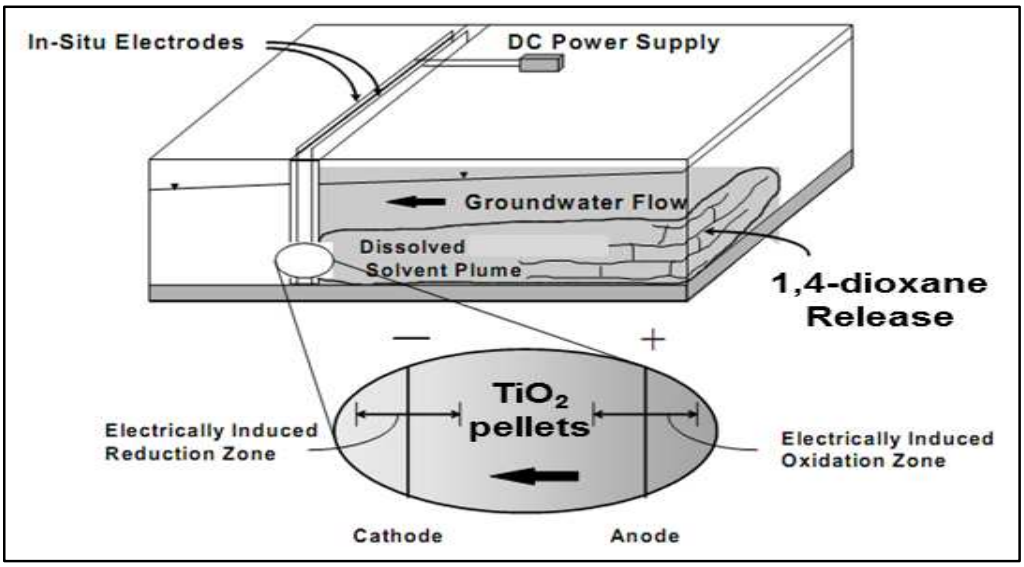

Figure 1.1 A conceptual diagram of an *in situ* permeable electrolytic reactor.

The reactor consists of parallel sets of closely spaced (e.g. 5-10 cm) permeable electrodes transverse to groundwater flow through a solvent plume. The application of a low DC voltage

difference between the electrodes induces aqueous oxidation reactions at the anode (positive) and reduction reactions at the cathode (negative). Field-scale permeable electrolytic barriers have been installed by the Center for Contaminant Hydrology (CCH) in the past. In one field application using up to 6.5 Volts, chlorinated solvents were treated at F.E. Warren Air Force Base in Cheyene, Wyoming. This study demonstrated that the electrical cost to power this technology was low, averaging \$0.013/m^2/day during 18 months of operation, all while reducing TCE flux concentrations by 90 to 95%.[43] A second field demonstration was performed by the CCH group to successfully degraded energetic compounds, like trinitrotoluene, at the Pueblo Chemical Depot in Colorado.[44] Photos in Figure 1.2 show the installation of mesh electrode barriers into the subsurface and the solar panel array that was used to supply all power needed for the reactor.

TiO_2 as a catalyst. We hypothesized that an inter-electrode catalyst will provide additional reactive surface area, in addition to the electrode surface, to enhance the oxidation rates of 1,4-dioxane. In preliminary studies conducted in the laboratory comparing possible inter-electrode catalysts, the highest organic pollutant removal efficiencies were achieved by titanium oxide (TiO_2) based catalysts compared to activated carbon and zeolite. The TiO_2 provides a catalytic surface within bulk volume between the electrodes, and have been immobilized through a pelletization fabrication process which prevented losses of catalytic material through the small openings in the mesh electrodes. The idea for using TiO_2 as an inter-electrode catalyst was inspired by its widespread use in photocatalytic degradation or organics in water– however, instead of high energy UV photons, the production of ·OH radicals and the energetics of the reactions will be driven electrochemically. Additional benefits of electrolytic treatments include tunability of its oxidizing potential via voltage control, ease of automation,

and environmental and cost benefits that come with not requiring the addition of strong chemical reagents.

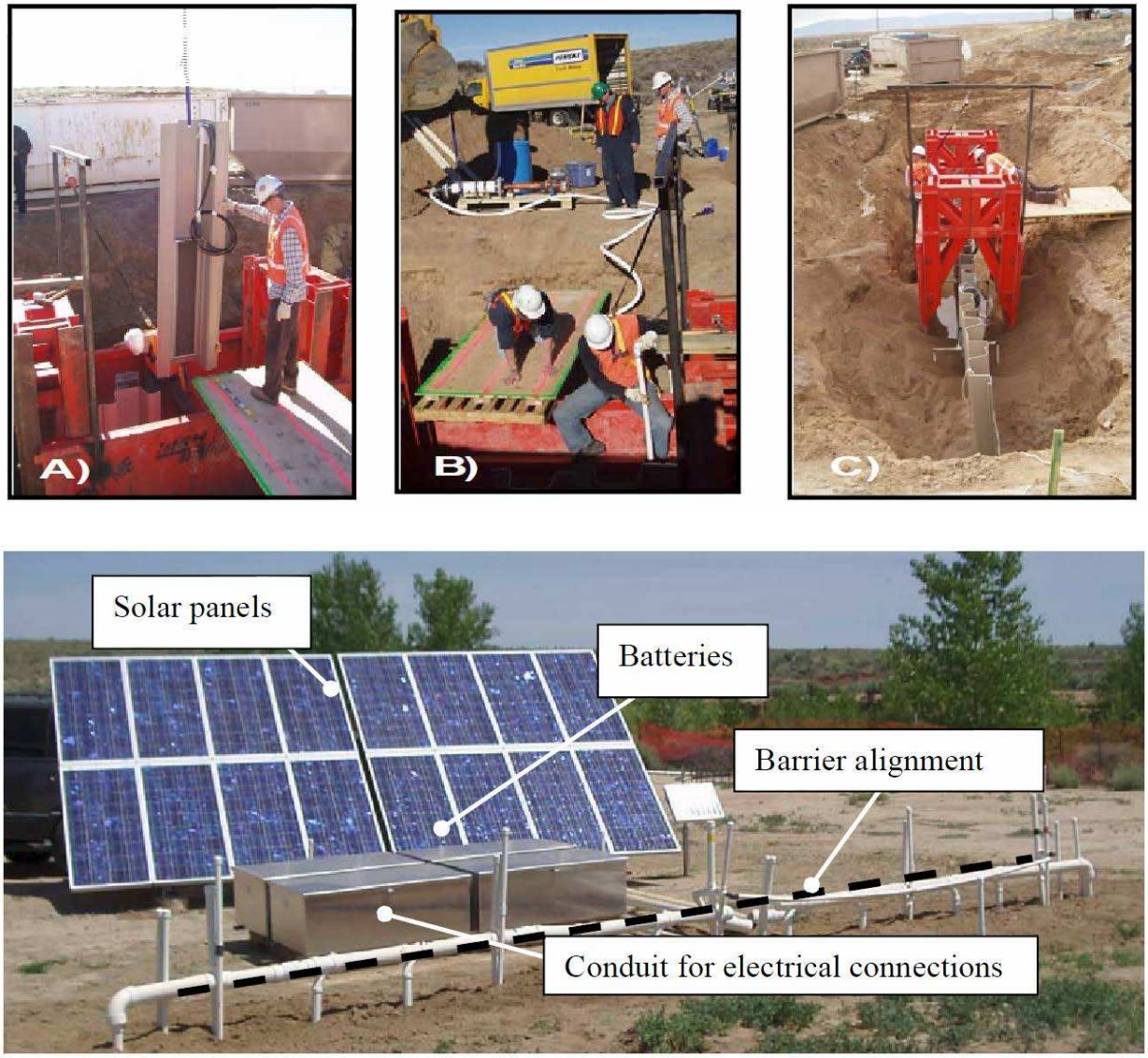

Figure 1.2 Installation photos of field demonstration of an *in situ* electrolytic barrier. A) Setting the mesh electrode panels inside the trench box, B) emplacing a cement/bentonite seal at the base of the barrier to limit underflow, C) sheet pile prior to backfill with native sands, and D) solar panels powering the permeable electrical barrier sustainably at the Pueblo Chemical Depot. Photos are used with permission of Sale, et al. (2010) SERDP-ESTCP Project ER-0519.[44]

Since our inter-electrode TiO_2 pellets are detached from the electrode, much like what is used in TiO_2 photocatalysis, we used literature in this area to help with possible mechanistic

clues. The semiconductor TiO_2 exists in two main crystalline phases: rutile and anatase, among which rutile is the thermodynamically stable state, while anatase is a metastable state.[45] Many studies have confirmed that the anatase phase of TiO_2 is usually superior as a photocatalytic material for water purification, and hazardous waste remediation.[45-47] Band gap excitation of the semiconductor TiO_2 is initiated by high energy UV light absorption, causing the excitation of an electron e^{-}* into the conduction band, leaving an oxidizing hole h^{+} in the valence band. This excitation step, especially the formation of highly oxidizing h^{+}, leads to the production of ·OH from adsorbed water molecules. The strong oxidizing power and low selectivity of these ·OH radicals allows for successful oxidation– and often full mineralization to CO_2 – of many different organic pollutants, even those considered highly recalcitrant, like 1,4-dioxane.[21, 48-50] When compared with other semiconductor materials with catalytic potential, TiO_2 is shown to be the most promising due to its high efficiency, low cost, photostability, and nontoxicity.[51, 52]

TiO_2 has also been used as an electrocatalyst to protect against corrosion of the underlying metal anode and enhance electron transfer reactions due to the ability of the semiconductor to quickly exchange protons and electrons along its lattice structure. Previous researchers have demonstrated that upon anodic polarization of the metallic anode, the excitation of electrons into the conduction band (to travel toward the metal anodic substrate) will leave holes (positive charge carriers) in the valence band capable of oxidizing adsorbed organic pollutants directly, or indirectly by producing •OH radicals from the oxidation of adsorbed H_2O molecules.[5354 53-56] The use of immobilized, inter-electrode TiO_2 pellets in our FTERs is aimed toward mitigating the mass transport limitations intrinsic to electrochemical reactors, which require direct contact of the electrode with organic pollutants in order to achieve electrochemical oxidation or reduction. The addition of detached TiO_2 pellets extends the reactive surface area to within the bulk

solution between electrodes, possibly even allowing for additional production of •OH radicals from the water molecules adsorbed to the electro-activated TiO_2 surfaces.

CHAPTER 2

ADVANCED ELECROCHEMICAL OXIDATION OF 1,4-DIOXANCE VIA DARK CATALYSIS BY NOVEL TITANIUM DIOXIDE (TiO_2) PELLETS[1]

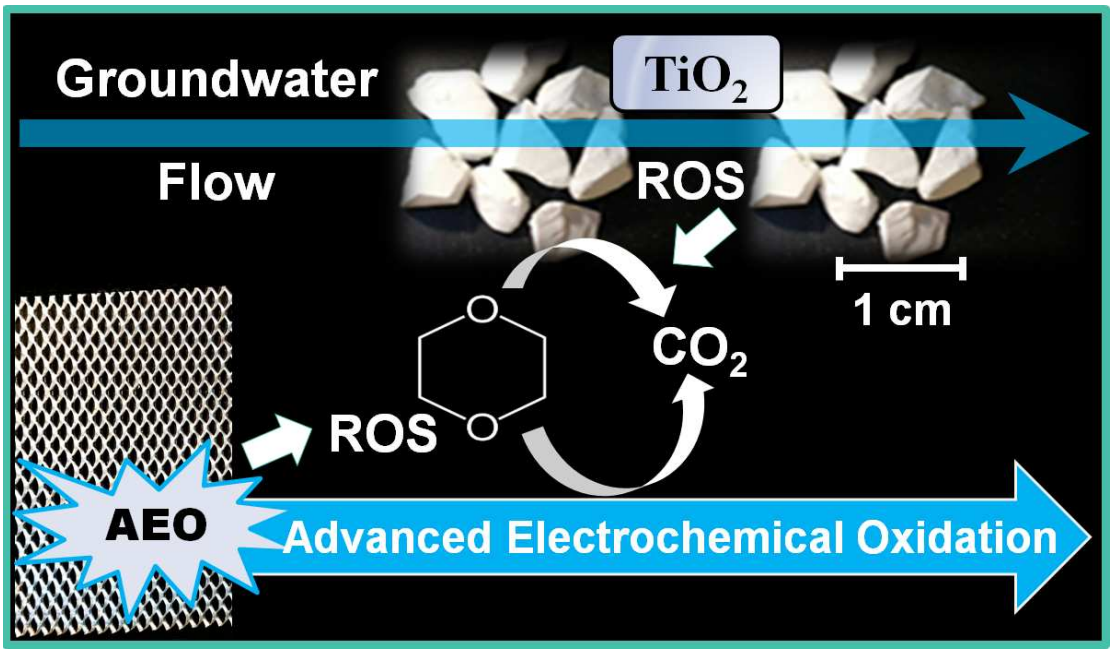

Conceptual Diagram

[1] Chapter 2 is taken from a manuscript of the same name recently accepted with revisions (to be completed by June 28, 2016) by Environmental Science & Technology with authors Jasmann, J.R., Borch, T., Sale, T., and Blotevogel, J. All sampling, sample preparation, analytical chemistry, and other work described was performed by the author of this dissertation.

CHAPTER SYNOPSIS

1,4-dioxane is an emerging groundwater contaminant with significant regulatory implications. Since it is resistant to traditional groundwater treatments, remediation of 1,4-dioxane is often limited to costly *ex situ* UV-based advanced oxidation. By varying applied voltage, electrical conductivity, seepage velocity, and influent contaminant concentration in flow-through reactors, we show that electrochemical oxidation is a viable technology for *in situ* and *ex situ* treatment of 1,4-dioxane under a wide range of environmental conditions. Using catalytic titanium dioxide (TiO_2) pellets, we demonstrate for the first time that this prominent catalyst can be activated in the dark even when electrically insulated from the electrodes. TiO_2-catalyzed reactors achieved efficiencies of greater than 97% degradation of 1,4-dioxane, up to 3.2 times higher than non-catalyzed electrolytic reactors. However, the greatest catalytic enhancement (70% degradation vs. no degradation without catalysis) was observed in low ionic strength water, where conventional electrochemical approaches notoriously fail. The TiO_2 pellet's dark-catalytic oxidation activity was confirmed on the pharmaceutical lamotrigine and the industrial solvent chlorobenzene, signifying that electrocatalytic treatment has tremendous potential as a transformative remediation technology for persistent organic pollutants in groundwater and other aqueous environments.

INTRODUCTION

1,4-Dioxane is a semi-volatile, cyclic ether historically used as a stabilizer in chlorinated solvents, and currently still used in the manufacturing of various commodities.[12, 57 58, 59] Due to accidental releases or inefficient removal with conventional wastewater treatment, 1,4-dioxane has been increasingly identified in surface water and groundwater.[13, 17] Its water miscibility and

low potential for sorption to soil promote the formation of large and dilute plumes. 1,4-Dioxane is not expected to rapidly biodegrade in the environment due to strong internal chemical bonding of its heterocyclic ether ring.[1, 13, 57, 58] Moreover, conventional groundwater treatments, such as sorption to activated carbon and air stripping, are extremely inefficient for 1,4-dioxane removal.[1, 57]

The most commonly employed remediation technologies for 1,4-dioxane are UV/H_2O_2, UV/O_3 or other advanced oxidation processes (AOPs)[19] involving hydroxyl radicals ($^{\bullet}OH$) as potent, non-selective oxidants.[21, 48, 60-62] However, the power requirements for continuous UV irradiation and consumption of chemical reagents (e.g., H_2O_2, O_3, ferrous iron) have been a critical limitation to full-scale (plume) treatment due to the high operation and maintenance costs.[18, 63] Furthermore, UV-based AOPs are limited to more costly *ex situ* applications such as pump and treat.[1] Thus, there remains a pressing need to develop low-energy, cost-effective removal technologies for 1,4-dioxane.

Advanced electrochemical oxidation (AEO), also referred to as electrolytic treatment, is an emerging AOP that can completely mineralize persistent organic pollutants (POPs) with direct electron transfer at the electrode surface and through mediated oxidation by electro-generated reactive oxygen species (ROS), such as $^{\bullet}OH$ radicals produced from the electrolysis of water.[30, 35, 64] Many water treatment studies have demonstrated high conversion rates of recalcitrant organic pollutants to CO_2 or readily biodegradable products using AEO processes, but have also acknowledged the intrinsic mass transport limitations associated with organic pollutants required to interact with the electrode surface.[27, 28, 65] Recent studies, using boron-doped diamond (BDD) electrodes, demonstrated that 1,4-dioxane can indeed be completely mineralized by anodic oxidation.[39, 40] The high cost of BDD electrodes, however, precludes their application in large-

scale operations at this point. In addition, many electrochemical studies are conducted in stirred batch reactors with elevated electrolyte concentrations that favor high mass transfer rates and current densities, creating increased contaminant degradation rates that may not transfer well to field applications. This is especially true for treatment of contaminated groundwater low in electrical conductivity, which remains a major challenge that has thus far only been overcome by resorting to the addition of chemical oxidants.[66]

To advance electrolytic treatment as a practical solution for field-scale application, we built flow-through electrochemical reactors (FTERs) to investigate the potential for treatment of groundwater contaminated with 1,4-dioxane under electrical conductivity and flow conditions simulating *in situ* implementation or aboveground reactors. These bench-scale FTERs are equipped with dimensionally stable Ti/IrO_2-Ta_2O_5 mesh electrodes that are cost-practical due to their widespread use in cathodic corrosion protection, resistant to fouling through periodic polarity reversals, and have been used successfully in permeable reactive barrier format for the electrochemical degradation of chlorinated solvents and energetic compounds in field applications at voltages of up to 17 V over extended periods of more than two years.[44, 67, 68]

Moreover, we explored whether contaminant degradation rates can be increased by placing a catalytic material in the inter-electrode space. Fabricating a stable pellet from titanium dioxide, which is widely known to promote photocatalytic degradation of recalcitrant organics in water,[22, 69] we show for the first time that in an electric field, TiO_2 is also catalytically active in the dark even when electrically insulated from direct electrode contact, i.e., without any potential applied to it.

The specific objectives of our study were to 1) evaluate the dark catalytic activity of the TiO_2 inter-electrode pellets, 2) elucidate the degradation pathway of electrocatalytic oxidation of

1,4-dioxane, and 3) determine effects of the major operational parameters of voltage, current density, seepage velocity, and both electrolyte and 1,4-dioxane concentration as a basis for technical planning for field implementation. Finally, to better recognize the future application potential for this catalyzed AEO technology, we evaluated the removal efficiency for two other POPs, namely the anti-epileptic drug lamotrigine and the industrial solvent chlorobenzene.

MATERIALS AND METHODS

Reagents. All chemicals (> 99% purity) were used as received. 20-L glass carboys were used to prepare Na_2SO_4 (EMD Chemicals) electrolyte solutions in deionized, ultra-purified water, spiked with 1,4-dioxane (Honeywell), chlorobenzene (JT Baker), or lamotrigine (trade name Lamictal, ENZO Life Sciences). A >99.6% anatase form of TiO_2 powder (Alfa Aesar) was used to fabricate catalyst pellets. 1,4-benzoquinone (Alfa Aesar) was used to assess the potential for electrochemical $^{\bullet}OH$ generation.

Mesh electrodes. Dimensionally stable, expanded mesh Ti/IrO_2-Ta_2O_5 electrodes (1.0 mm thick with 1.0 x 2.8 mm diamond-shaped openings) were used (Corrpro).

Fabrication and characterization of TiO_2 pellets. TiO_2 powder was molded into a mechanically stable pellet with dimensions 3.33 to 9.42 mm. The multi-step fabrication process involved pressure compaction into cylindrical discs, chiseling into loosely adhered pellets, and 4-hour sintering in ambient air at temperatures of 700 °C to 1,000 °C (Appendix A, Figure S2.1). Several techniques were used to characterize the TiO_2 pellets, including mechanical stability screening, scanning electron microscopy (SEM) imaging, BET specific surface area and porosimetry analysis, and synchrotron radiation-based X-ray diffraction (XRD) to determine fractional mass in anatase or rutile mineral phases (Appendix A).

Flow-through electrochemical reactors. The removal efficiency of 1,4-dioxane was investigated using FTERs constructed of clear PVC pipe (10 cm I.D. x 46 cm, Ryan Herco Products) with four circular mesh electrodes (10 cm O.D.) spaced 5.0 cm apart (Figure 2.1). The first and third electrodes were positively polarized anodes with the second and fourth acting as cathodes. Previous work has shown that an anode-cathode sequence (in the direction of flow) leads to higher contaminant removal than a cathode-anode sequence.[67] Each column was fitted with two Ag/AgCl redox reference electrodes (World Precision Instruments), sampling ports and multiple gas exhaust tubes to vent excess O_2 and H_2 gas produced during the electrolysis of water. The section of each FTER upstream of the initial anode was packed with quartz silica sand (20/35 mesh) to simulate porous aquifer material and enhance dispersive mixing of influent contaminant prior to contact with the first electrode. A permeable non-conductive geocomposite (HDPE geonet grid with polypropylene felt layer, GSE Environmental) was placed directly next to each anode to control movement of sediments and insulate the TiO_2 pellets from direct electrical conduction. The inter-electrode space was filled with TiO_2 pellets for the catalyzed FTER experiments or with inert, 6-mm diameter glass beads for the non-catalytic control experiments. While slight differences in porosity between TiO_2 pellets and glass beads may have led to different effective retention times at the same flow rate, we note that this would not invalidate comparison of degradation processes at the electrode surfaces, which under mass transport control occur within a ~1-μm diffuse zone around the electrodes,[70, 71] and thus remain unimpacted by variance in inter-electrode material porosity.

To simulate aquifer conditions, influent feedstock and FTERs were covered by black, opaque plastic to maintain dark conditions and exclude photo(cata)lytic degradation processes. Feedstock solutions contained 3.4 μM to 207 μM 1,4-dioxane in 10 mM Na_2SO_4 supporting

electrolyte (1,700 µS/cm). Na_2SO_4 is commonly used in electrochemical degradation studies since it is assumed to be less electrochemically reactive than other electrolytes, like Cl^- ions.[2, 72]

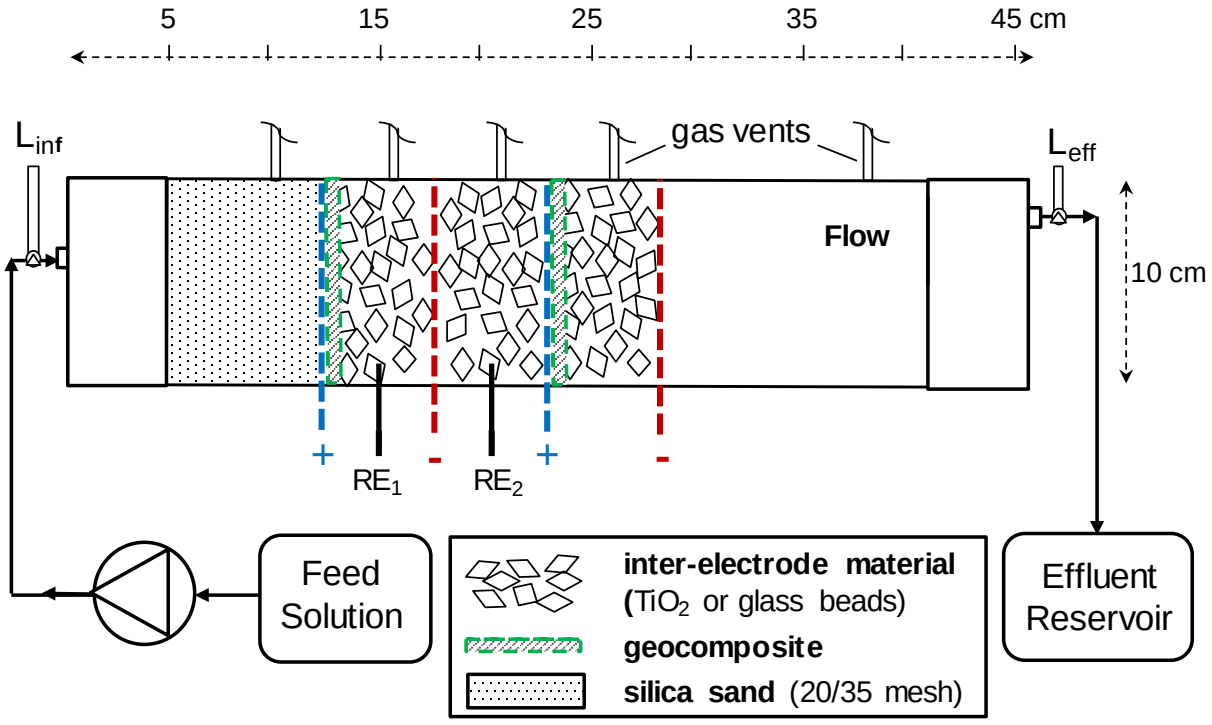

Figure 2.1 Schematic of flow-through electrochemical reactor, FTER (not to scale). L_{inf} and L_{eff} are sampling ports for liquid influent and effluent, respectively. RE are reference electrodes.

To minimize sorption, the feedstock was pumped through every reactor before each experiment until influent and effluent contaminant concentrations were equal. Once steady-state conditions were achieved at target voltage, a minimum of three influent and effluent samples were collected for chemical analysis for each contaminant. Daily measurements were made of pH, voltage potential and current between working electrodes. Control experiments without voltage applied showed 2.3 ± 0.4% and 3.7 ± 0.7% removal of 1,4-dioxane for the TiO_2-catalyzed and non-catalyzed column experiments, indicating negligible losses that could have been attributed to volatilization or adsorption to matrix materials.

To evaluate the degradation efficiency of other organic pollutants in comparison to 1,4-dioxane, smaller FTERs were constructed of 15 cm long acrylic pipe with 5.0 cm I.D. and a single pair of disc-shaped electrodes (18.25 cm^2) spaced with an inter-electrode gap of 2.5 cm (Figure S2.2). For the small-column FTER experiments, three aqueous feedstock solutions of 20 mM Na_2SO_4 (3,400 µS/cm) were prepared in 20-L glass carboys and spiked with 99 µM 1,4-dioxane, 41 µM lamotrigine, or 66 µM chlorobenzene. Sampling and measurements were performed in the same way as with the larger FTER experiments.

Analytical methods. Gas chromatography (Agilent 6890N GC) combined with mass spectrometry (Agilent 5973N MS) in full scan and selective ion mode was used to quantify 1,4-dioxane. The transformation products from 1,4-dioxane oxidation reactions were analyzed by reversed-phase liquid chromatography (Agilent 1100 LC) in combination with negative electrospray ionization time-of-flight mass spectrometry (Agilent G3250AA ESI^--TOF-MS). Lamotrigine (270 nm) and 1,4-benzoquinone (220 nm) were quantified by an Agilent 1200 series HPLC equipped with a UV-diode array detector. An Agilent 6890N GC followed by an electron capture device analysis was used to quantify chlorobenzene. Total organic carbon (TOC) was analyzed by Shimadzu TOC-L Analyzer. Details of the analytical methods are provided in the Appendix A.

RESULTS AND DISCUSSION

Catalyst characterization. Since anatase in its fine powder form would likely flush out of a flow-through reactor, it was initially molded into larger pellets. Mechanical stability tests (full results in Table S2.1) revealed that pellets sintered for four hours at 700 °C and 800 °C remained friable and prone to abrasion, making them unsuitable for a flow-through system.

However, the TiO_2 heat-treated at 880 °C and 1,000 °C achieved satisfactory cementing of the compacted TiO_2 powder into high-strength pellets. Synchrotron XRD data showed sharp diffraction peaks for all TiO_2 pellets analyzed (Figure S2.3**)**, indicative of high crystallinity. The fractions of anatase and rutile were determined from the intensities of the anatase A_{101} and rutile R_{110} diffraction peaks using the Spurr-Meyer equation[73] (Appendix A). Calculations determined that 98% remained in the anatase form for both the 700 °C and 880 °C treatments (800 °C pellets were not analyzed by XRD). Conversely, XRD measurements of TiO_2 sintered at 1,000 °C indicated 14% remained as anatase and 86% had transformed to the more thermodynamically stable rutile form.[45]

Based upon these screening results, only those TiO_2 pellets sintered at 880 °C were used in the FTER experiments. These pellets were further characterized by SEM and porosimetry analysis. SEM images at 7,000x and 30,000x magnification (Figure S2.3) showed homogenously sized spherical particles and uniform porosity across the surface of the TiO_2 pellets, which is consistent with other SEM images of anatase-based TiO_2 used for catalytic degradation of organic pollutants.[45, 47, 74] Results of porosimetry analysis on TiO_2 in the pellet form yielded a specific surface area of 8.15 ± 0.03 m^2/g, median pore diameter of 147 Å, and a relative porosity of 80% mesopore surface area (pore widths from 17 to 3,000 Å) to total surface area.

Catalyzed electrochemical degradation experiments. With the goal of using the inter-electrode space for additional degradation reactions to occur, and thus increase overall kinetics, catalytic TiO_2 pellets were packed between the electrodes (versus glass beads in the non-catalytic control). Flow-through experiments were conducted to evaluate the impact of four major operational parameters on the electro(cata)lytic degradation of 1,4-dioxane. As a point of reference from which to vary one parameter at a time, four “benchmark levels” were selected to

be representative of common aquifer conditions: 10 mM Na_2SO_4 supporting electrolyte (1,700 μS/cm), 30.6 cm/d mean linear seepage velocity, 3.4 μM (300 μg/L) 1,4-dioxane, and an imposed electrical potential of 8.0 V. The 8.0 V was experimentally determined to be an appropriate voltage for achieving near 50 - 70% 1,4-dioxane degradation under benchmark conditions, deliberately leaving capacity for increased degradation efficiencies when varying each operational parameter. The other varied parameters were chosen in ranges representative of conditions that may be present in 1,4-dioxane-contaminated groundwater. Voltage, rather than current (density), was chosen as the independent electrical variable to ensure a threshold voltage was maintained above the O_2 evolution potential of 1.8 V vs. NHE on Ti/IrO_2-Ta_2O_5 electrodes,[30] high enough to generate $^{\bullet}OH$ radicals and prevent fouling of the mesh electrodes by organic adhesions.[40] In electrolytic degradation experiments of 1,4-dioxane performed with starting pH values of 1.7, 7.0 and 12.4, Choi and co-workers demonstrated that initial pH did not have a significant effect on anodic oxidation rates of 1,4-dioxane.[39] Thus, pH was not varied in our experiments and instead the measured pH of 7.2 ± 1.0 in our unbuffered electrolyte and 1,4-dioxane feedstock was the influent pH value for all experiments.

Details of each experimental regime tested are summarized in Table S2.2 of the Appendix A, including current density, effluent pH, solution redox potential, overall electrochemical degradation efficiency, and the observed pseudo-first order rate constant (k_{obs}). The k_{obs} values were calculated using a rate expression specific to flow-through experiments:[75]

$$k_{\mathrm{obs}} = \frac{-\ln(C_{\mathrm{eff}}/C_{\mathrm{inf}})}{\mathrm{HRT}}$$

where C_{eff} is effluent and C_{inf} is influent 1,4-dioxane concentration and HRT is hydraulic residence time. The electrochemical degradation efficiencies, expressed as the percentage of 1,4-

dioxane degraded after a single pass through an FTER, are displayed in Figure 2.2 for ten different experimental regimes.

The results in Figure 2.2 reveal that 1,4-dioxane degradation efficiency was significantly higher in the presence of the catalytic TiO_2 pellet ($p \leq 0.010$, $\alpha = 0.05$) for all conditions tested. Previous electrochemical studies have reported dark catalytic activity of TiO_2, however, only when used as electrode or in direct contact with an electrode, i.e., when a potential was directly applied to it.[53, 54, 76, 77] In our experiments, however, the TiO_2 pellets were electrically insulated from the anodes, revealing a yet unreported activation mechanism. To further elucidate how TiO_2 is activated in the dark, we conducted FTER experiments comparing the performance of non-insulated and insulated TiO_2 pellets to a non-catalytic control. Figure S2.5 (Appendix A) shows that 1,4-dioxane degradation was catalyzed by inter-electrode TiO_2 pellets with the insulating geotextile layer (36% removal) and without the insulation (44%) when compared to 15% removal of 1,4-dioxane in the non-catalytic column. Thus, it was confirmed that direct electrode contact or application of a potential to the TiO_2 is not needed for its catalytic activation. The detailed effects of this novel mechanism on aqueous contaminant degradation are discussed below.

Effect of electrode potential. Figure 2.2(a) shows that there were no significant changes in 1,4-dioxane removal efficiency in the non-catalyzed FTERs when the voltage was increased from 8.0 to 11.0 to 14.0 V, displaying 49%, 45% and 46% degradation ($p \geq 0.20$, $\alpha = 0.05$). This is likely due to the reaction kinetics being controlled by mass transport to the electrode surface and not limited by ROS production.[78, 79] At all three voltages, the inter-electrode TiO_2 pellets improved the degradation efficiency, increasing relative removal of 1,4-dioxane by a factor of 1.4 - 1.8 compared to electrolytic removal in the absence of inter-electrode catalysts.

Additionally, stepwise improvements in degradation efficiency were observed in the catalyzed reactors as the voltage increased, although a statistically significant increase was only observable when going from 8.0 V (69% removal) to 14.0 V (81% removal) ($p = 0.0006$, $\alpha = 0.05$).

Furthermore, raising the voltage concurrently increased the current density from 3.5 to 5.3 to 8.3 ± 0.02 mA/cm^2 in catalyzed FTERs, creating appreciable increases in the pseudo-first order rate constant k_{obs} from 0.065 to 0.074 and 0.094 hr^{-1} respectively. In the non-catalyzed experiments, current densities increased from 1.5 to 2.2 to 3.3 ± 0.02 mA/cm^2, yet k_{obs} values remained relatively constant at 0.038, 0.033 and 0.034 hr^{-1}. This shows that the increased degradation rates in the TiO_2-catalyzed FTERs cannot be explained simply due to the increases seen in current density, serving as first line of evidence that the pellets operate under a different mechanism than the electrodes.

Effect of electrolyte concentration. Varying the supporting electrolyte concentrations from 3 to 10 to 30 mM Na_2SO_4 resulted in corresponding electrical conductivities of 570, 1,700, and 5,000 µS/cm. Current densities increased from 2.5 to 3.5 to 7.0 ± 0.02 mA/cm^2 in TiO_2-catalyzed FTERs, and from 1.1 to 1.5 to 3.4 ± 0.02 mA/cm^2 in non-catalyzed FTERs. The most substantial performance enhancement by the TiO_2 catalyst was observed at the lowest electrolyte concentration. Figure 2.2(b) shows that despite having a current density of 1.1 mA/cm^2 with 8.0 V applied, no 1,4-dioxane removal was achieved in the non-catalyzed FTER, i.e., with treatment at the electrodes only. However, when the inter-electrode TiO_2 was present, 70% of influent 1,4-dioxane was removed. These results highlight the great potential for TiO_2-catalyzed electrochemical technologies since the ability to achieve contaminant degradation in low ionic strength waters is known to be a critical limitation of electrochemical degradation processes.[66]

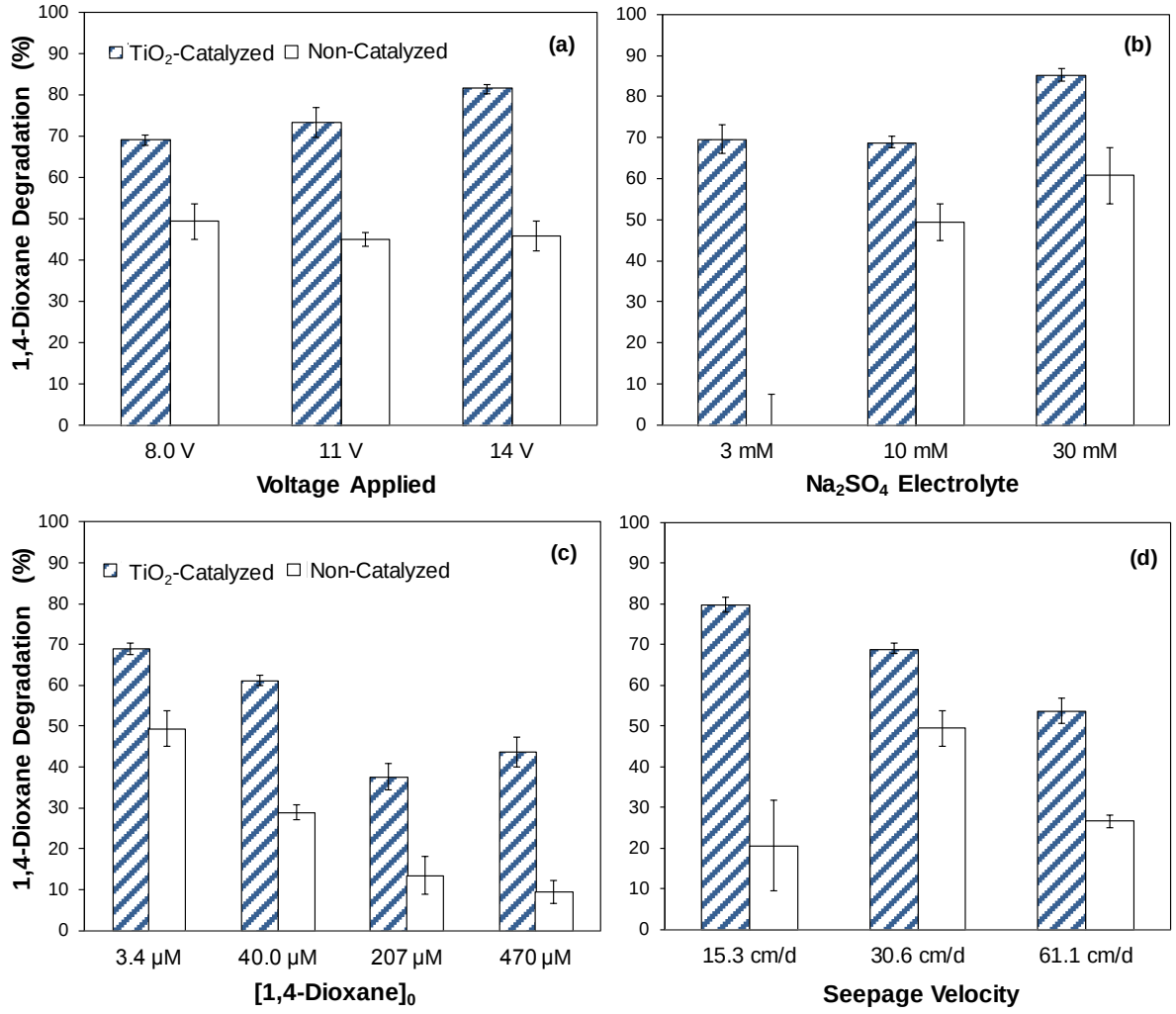

Figure 2.2 Degradation efficiencies of 1,4-dioxane in flow-through electrochemical reactors, showing the effects caused when varying one of four operation parameters at a time: (a) applied voltage, (b) Na_2SO_4 electrolyte concentration, (c) influent 1,4-dioxane concentration, and (d) mean seepage velocity. The other parameters within each experiment were at "benchmark levels": 3.4 µM 1,4-dioxane, 10 mM Na_2SO_4 electrolyte, 30.6 cm/day and 8.0 V applied. Error bars indicate standard deviation (n = 3) for samples taken during steady-state.

At higher electrolyte concentrations, both the catalyzed and non-catalyzed reactors showed increases in degradation efficiencies. Under 10 mM and 30 mM Na_2SO_4 electrolyte conditions, 1,4-dioxane removal efficiencies (and k_{obs}) of 69% (0.065 hr^{-1}) and 85% (0.107 hr^{-1}) were achieved in TiO_2-catalyzed FTERs versus 49% (0.038 hr^{-1}) and 61% (0.052 hr^{-1}) in non-catalyzed FTERs (Figure 2.2(b), Table S2.2). The k_{obs} values obtained here were the highest

compared to all other treatment schemes tested, showing the major impact conductivity has on electrolytic treatment efficacy.

Although lower electrolyte concentrations tended to produce decreased degradation rates as expected, the surprising contrast in degradation performance in the 3 mM Na_2SO_4 treatment provides further evidence that the catalytic mechanism of TiO_2 is independent of chemical processes directly at the electrode, and more strikingly, largely independent of electrolyte concentration within the range of conditions tested.

Effect of influent 1,4-dioxane concentration. Contaminant load effects were investigated with different initial 1,4-dioxane concentrations in FTERs. Results from the TiO_2-catalyzed FTERs in Figure 2.2(c) show a decline in relative removal efficiencies, 69%, 61%, 38%, and 44% corresponding to increases in initial 1,4-dioxane concentrations from 3.4 to 40.0 to 207 to 470 µM. Within non-catalyzed electrolytic columns, the same increases in influent 1,4-dioxane concentrations correlated to even greater reductions in performance, shifting from 49% 1,4-dioxane removal at the 3.4 µM level down to 13% and 9% removal when starting with 207 and 470 µM 1,4-dioxane, respectively. In absolute quantities, however, mass removal of 1,4-dioxane continued to increase with higher influent concentration in both reactors, ruling out the possibility of surface saturation or insufficient ROS production being the controlling process for the overall oxidation rates. This observation further supports previous reports of contaminant degradation in flow-through electrolytic systems being rate-controlled by molecular diffusion and not by reaction rate or ROS availability.[78, 79]

Effect of seepage velocity. In a mass transfer-limited system, a decline in degradation efficiency would be expected with faster flow rates. This is due to shorter hydraulic residence times, resulting in less opportunity for diffusion-driven collisions. In fact, Figure 2.2(d) shows

that as the mean seepage velocity doubled from 30.6 to 61.1 cm/d, 1,4-dioxane degradation decreased from 69% to 54% for TiO_2-catalyzed FTERs, and from 49% down to 27% in non-catalyzed FTERs. Interestingly, the non-catalyzed removal efficiency dropped by half as the flow velocity was doubled, while the catalyzed reactors exhibited only a 22% drop in removal efficiency with the doubled velocity. The inter-electrode TiO_2 diminished the detrimental impact associated with less residence time, providing additional evidence that TiO_2 offers a distinctive mechanism for organic contaminant degradation.

When feedstock flow was slowed to 15.3 cm/d in the TiO_2-catalyzed reactor, a substantially higher 1,4-dioxane removal efficiency of 80% was achieved. Conversely, the same 15.3 cm/d flow resulted in an unexpected decrease in performance to only 21% removal obtained in the non-catalyzed reactor. At slower velocities, surface tension interactions may allow for O_2 and H_2 gases, generated by water electrolysis, to remain at the electrode surface after exceeding their respective solubilities. Pronounced coverage of mesh electrodes by gas bubbles can hinder 1,4-dioxane adsorption and reduced hydraulic conductivity at certain mesh openings, leading to preferential flow paths through a reduced cross-sectional area, thus decreasing reactive contact time with electrode surfaces.[78, 79] Although the negative impact of low flow and gaseous inhibition is substantial in the non-catalyzed system, these conditions appear to have less impact in TiO_2-catalyzed systems where reactions involving TiO_2 pellets likely occur farther downstream from the localized gas bubble disturbance at the electrodes.

Extent of complete 1,4-dioxane mineralization. To assess the capacity to fully mineralize 1,4-dioxane to CO_2, total organic carbon (TOC) analysis was performed on triplicate influent and effluent samples from the TiO_2-catalyzed FTER experiment with 470 µM 1,4-dioxane feedstock (10 mM Na_2SO_4, 30.6 cm/d, 8.0 V). With this relatively high 1,4-dioxane

concentration feedstock, 44% of the initial 1,4-dioxane concentration was degraded (measured by GC/MS), but only 22% was fully mineralized to CO_2 (TOC analysis, Figure S2.4). Nevertheless, the percentage of full mineralization determined via TOC (CO_2 produced = $TOC_{effluent}$ - $TOC_{influent}$) is likely underestimated due to electrolytic reduction of CO_2 at the cathode, which is known to generate low-molecular weight organic compounds.[80]

Electrochemical degradation pathway of 1,4-dioxane. To examine the electrolytic degradation pathway for 1,4-dioxane, influent and effluent samples from the TiO_2-catalyzed FTER experiment performed with 207 µM 1,4-dioxane feed solution (10 mM Na_2SO_4, 30.6 cm/d, 8.0 V) were analyzed for transformation products using LC/ESI-TOF-MS, with mass spectra results tabulated in Table S2.4. In negative ESI mode, four organic acid intermediates were positively identified in the effluent: succinic acid (13), malic acid (14), mesoxalic acid (21), and glycolic acid (22). Glycolic acid has been reported in 1,4-dioxane oxidation pathways by other UV- or sonolysis-based AOPs.[42, 50, 81] To our knowledge, this is the first reported detection of the other three organic acids during 1,4-dioxane degradation.

Previous studies investigating the mechanism of oxidizing 1,4-dioxane by UV/H_2O_2 and sonolysis have determined the main oxidative species to be $^{\bullet}OH$ radicals in conjunction with dissolved O_2.[50, 81] It is reasonable to infer that the mechanism for electrochemical oxidation of 1,4-dioxane will be similar since the main oxidative species has been reported to be the electro-generated $^{\bullet}OH$ radical.[2, 30, 39, 55] To test whether $^{\bullet}OH$ radicals are involved in electrolytic 1,4-dioxane degradation, we conducted oxidation experiments with 1,4-benzoquinone (BQ) in a divided electrochemical batch cell, using a Nafion NRE-212 membrane impermeable for organic intermediates to divide the anodic and cathodic chambers (Appendix B, Figure S3.2). BQ is indicative of $^{\bullet}OH$ radical generation as it rapidly reacts with $^{\bullet}OH$ ($k_{\bullet OH, BQ} = 6.6 \times 10^9\ M^{-1}s^{-1}$),[82]

while being highly resistant to direct electrochemical oxidation.[83-85] Results indicated that BQ was oxidized in the divided anodic chamber, confirming that $^{\bullet}OH$ radicals are produced electrochemically (Chapter 3, Figure 3.3).

Hydroxyl radicals have been shown to rapidly oxidize 1,4-dioxane ($k_{^{\bullet}OH}$ = 1.1 – 2.35 x 10^9 $M^{-1}s^{-1}$) and its aldehyde and carboxylic acid intermediates.[86, 87] Furthermore, hydroperoxyl ($^{\bullet}OOH$) radicals may be an important reactive species in our flow-through system, capable of acting as either oxidant or reductant.[88] The formation of $^{\bullet}OOH$ is linked to the redox couple with the superoxide radical $^{\bullet}OOH$ / $O_2^{-\bullet}$ with standard reduction potentials (O_2 at 1 atm) of $E^0(O_2, H^+/ {}^{\bullet}OOH)$ = -0.05 V vs NHE and $E^0(O_2/ O_2^{-\bullet})$ = -0.33 V vs NHE.[89, 90] Therefore, dissolved O_2 can be reduced at the cathode to the strong reductant superoxide $O_2^{-\bullet}$ which is in constant equilibrium[91] with its protonated form $^{\bullet}OOH$:

$$O_2^{-\bullet} + H_2O \leftrightarrow {}^{\bullet}OOH + OH^- \ (pK_a = 4.88)$$

On the basis of (1) transformation products identified by LC/ESI-TOF-MS, (2) the evidence of $^{\bullet}OH$ radicals participating in the oxidation mechanism, and (3) previous reports in the literature,[50, 81] a pathway for electrochemical 1,4-dioxane degradation is proposed in Figure 2.3. Stable intermediates identified by this study are highlighted in solid boxes in Figure 2.3, while dashed boxes identify those molecular species identified as intermediates of 1,4-dioxane oxidation in the literature.[50, 81] All stable intermediates shown are considered to be less recalcitrant and less toxic than the 1,4-dioxane parent compound.

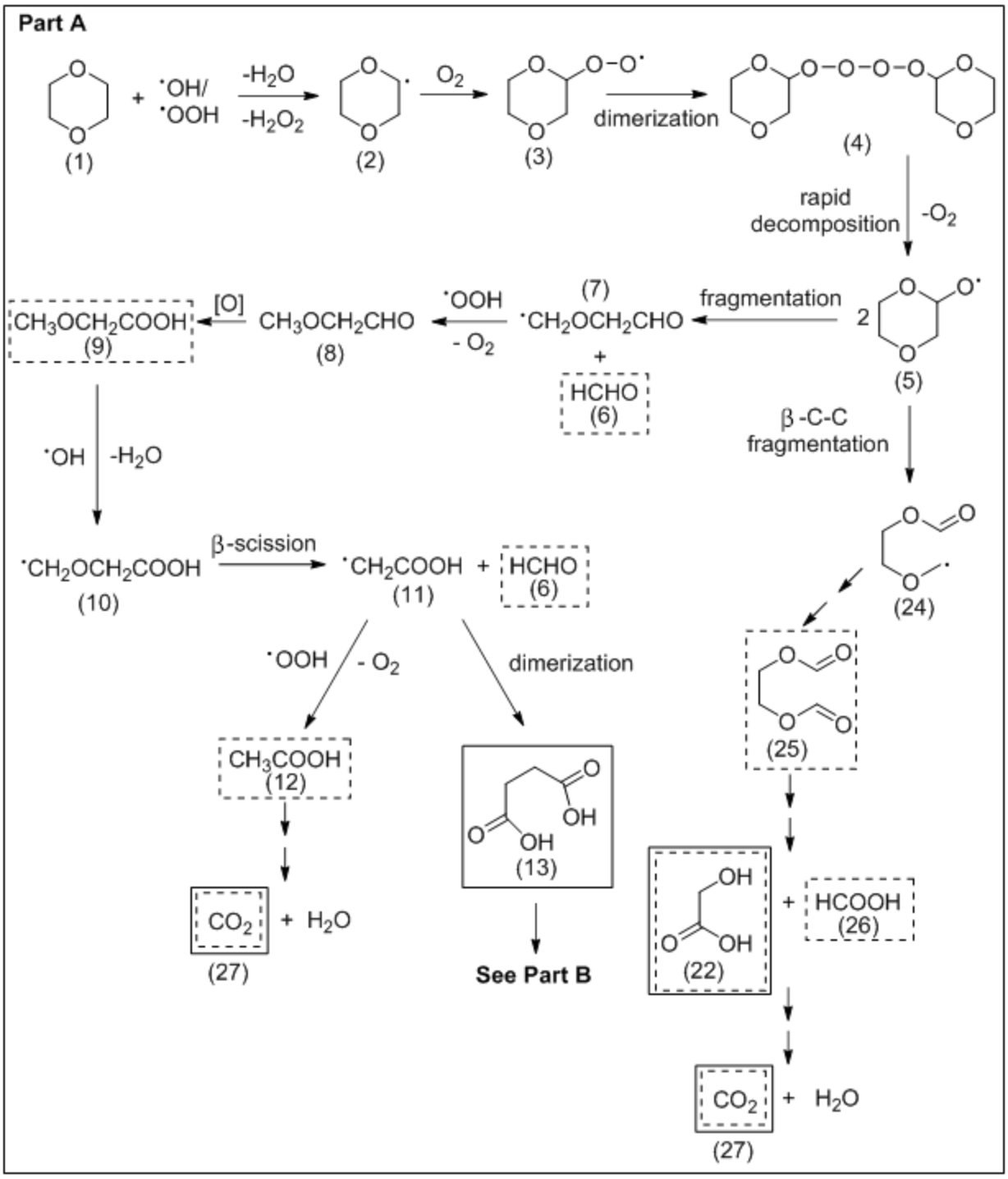
Part A
(1)
+ ·OH/ ·OOH
-H2O
-H2O2
(2)
O2
(3)
dimerization
(4)
rapid decomposition
-O2
2
(5)
fragmentation
(7)
·CH2OCH2CHO
+
HCHO
(6)
·OOH
- O2
CH3OCH2CHO
(8)
[O]
CH3OCH2COOH
(9)
·OH
-H2O
β-C-C fragmentation
(24)
(25)
·CH2OCH2COOH
(10)
β-scission
·CH2COOH
(11)
+ HCHO (6)
·OOH
- O2
dimerization
CH3COOH
(12)
CO2
+ H2O
(27)
(13)
See Part B
(22)
+ HCOOH
(26)
CO2
+ H2O
(27)

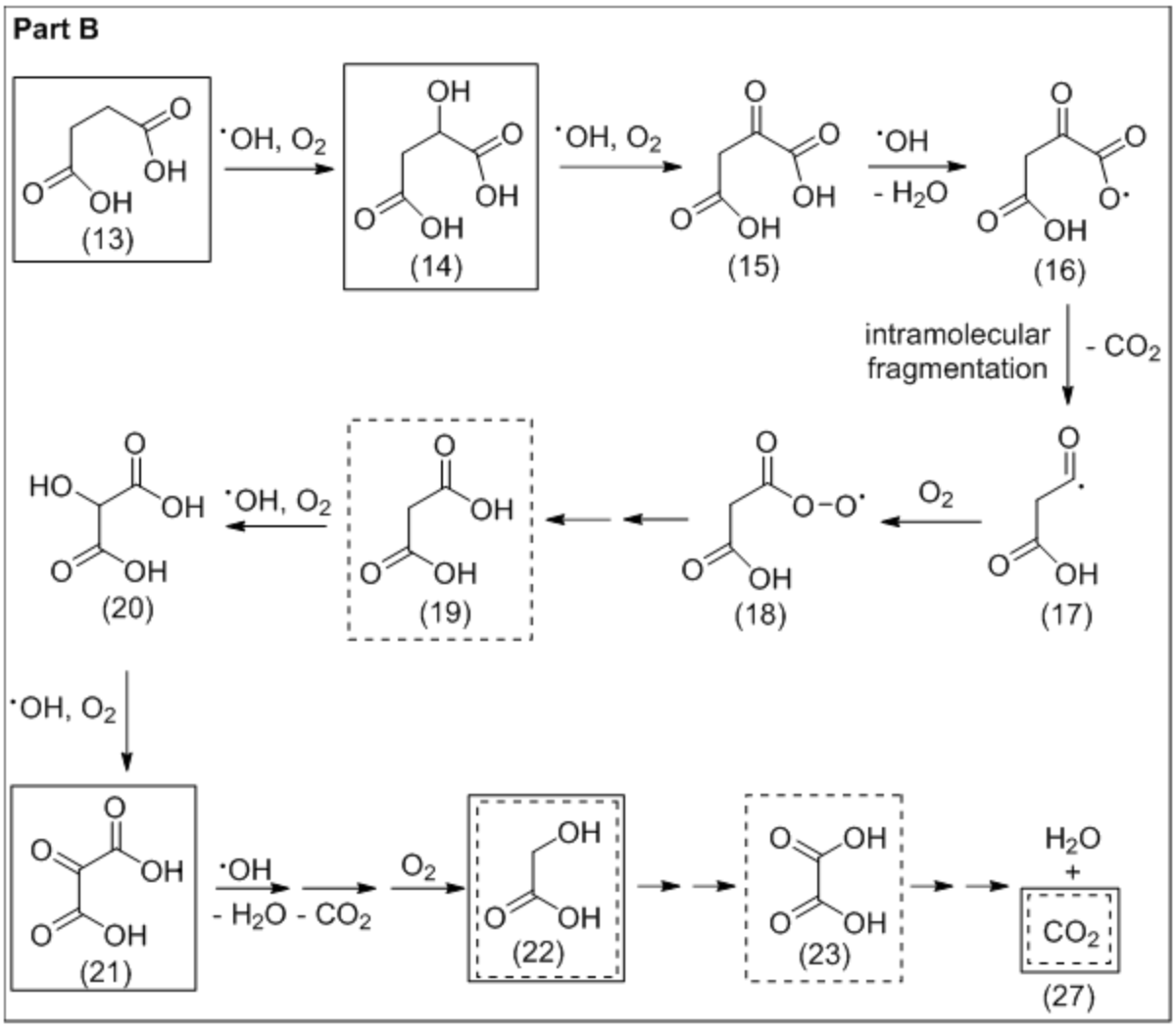

Figure 2.3 Proposed 1,4-dioxane oxidation pathway. Part A: Reaction pathway for the initial oxidation of 1,4-dioxane to CO_2 or the succinic acid (13) intermediate. Part B: Reaction pathway from succinic acid to CO_2. The major intermediates observed in this study are highlighted in solid boxes while dashed boxes indicate intermediates that have been reported in the literature to be formed by the oxidation of 1,4-dioxane.

In our electrocatalytic reactors, the initial oxidation step leading to cleavage of the diether ring is likely radical attack by ·OH on 1,4-dioxane (1), with H-abstraction from any of the carbons, leading to the 1,4-dioxanyl radical (2). Additionally, hydrogen abstraction of 1,4-dioxane by ·OOH radicals may lead to the same intermediate (2) and the production of H_2O_2. The 1,4-dioxanyl radicals react with O_2 by diffusion-controlled processes forming peroxyl

radicals (3). These peroxyl radicals generally undergo head-to-head termination reactions (bimolecular rate constants ~10^9 $M^{-1}s^{-1}$) to form the tetroxide intermediate (4), which rapidly decomposes to form α-oxyl radicals (5).[81, 92]

Upon formation, these α-oxyl radicals can undergo two primary types of reactions: (i) β-C-C splitting at the α′-C to form O=CH-O-CH_2CH_2-O-CH_2• (24) or (ii) an intramolecular fragmentation reaction. The β-C-C splitting path has been used to explain the formation of 1,2-ethanediol monoformate (not shown) leading to 1,2-ethanediol diformate (25), which is a stable intermediate previously reported in photocatalytic oxidation[42, 50, 81] and electrochemical oxidation[39] of 1,4-dioxane. Successive oxidation steps of 1,2-ethanediol diformate are capable of full mineralization to CO_2 (27) through glycolic acid (22) and formic acid (26) intermediates.[81, 92] Thus, the glycolic acid detected may be a result of this pathway.

Additionally, the intramolecular fragmentation pathway (ii) is capable of producing glycolic acid and the other three organic acids identified in our study. It involves oxyl oxygen abstracting hydrogen from the α′-C position followed by fragmentation to form formaldehyde (6) and the radical organic species O=$CHCH_2$-O-CH_2• (7). In accordance with the "methyl" group generation mechanism proposed previously, the carbon-centered radical (7) O=$CHCH_2$-O-CH_2• can then be reduced by •OOH radicals to produce methoxyacetaldehyde (8) O=$CHCH_2$-O-CH_3 (and release O_2), followed by further oxidation of methoxyacetaldehyde to methoxyacetic acid (9) $HOOCCH_2$-O-CH_3.[81] Methoxyacetic acid reacts rapidly with •OH radicals by H-abstraction to form •CH_2OCH_2COOH (10) followed by β-scission fragmentation into formaldehyde (6) and formylmethyl radical (11). The latter $HOOCCH_2$• radical (11) is reduced to acetic acid (12) by •OOH radicals or proceeds through a termination step by dimerization with a nearby $HOOCCH_2$• radical to form the stable intermediate succinic acid (13),[93, 94] one that was

detected in this study. The acetic acid (12) and formaldehyde (6) intermediates are expected to fully mineralize through successive oxidation reactions as their rate constants for reactions with $^{\bullet}OH$ radicals are as high as those for 1,4-dioxane.[50, 81]

The succinic acid (13) intermediate is then successively oxidized by $^{\bullet}OH$ / O_2 reactions through peroxyl radical intermediates to form malic acid (14) and then 2-oxosuccinic acid (15), an α–ketoacid susceptible to decarboxylation reactions in highly oxidizing environments.[93-95] Hydroxyl radical attack of a terminal hydroxyl group produces H_2O and leaves $HOOCCH_2COCOO^{\bullet}$ (16), an unstable oxyl radical which undergoes intramolecular fragmentation reactions to eliminate CO_2 (27). The resulting carbon radical species (17), in the presence of O_2, immediately forms a peroxyl radical (18) leading to malonic acid (19). Multistep $^{\bullet}OH/O_2$ mechanisms similar to those mentioned can be invoked to explain the formation of 2-hydroxymalonic acid (20), mesoxalic acid (21), glycolic acid (22) and oxalic acid (23), with (21) and (22) identified as intermediates in this study. The mineralization of oxalic acid to CO_2 (27) is a decomposition reaction mediated by hydroxyl radicals.[81, 92]

Implications for electrochemical oxidation of persistent organic pollutants. In this study, we only operated FTERs in a limited performance range to elucidate the relative impacts of operational parameters on the degradation of 1,4-dioxane. In full-scale applications, treatment can be further optimized toward achieving downstream 1,4-dioxane or water quality target levels by adding additional electrodes and TiO_2 pellets within the flow path to improve degradation efficiencies. To simulate the addition of more working electrodes, treated effluent from a single pass (2-anode treatment) through an 11.0 V FTER was passed through the treatment process a second time (4-anode treatment) and a third time (6-anode treatment). Figure 4 demonstrates the capacity for greater overall 1,4-dioxane removal with each sequential electrolytic treatment,

increasing from 45 to 72 to 84 % for the non-catalyzed FTERs and from 73 to 93 to 97 % for the TiO_2-catalyzed FTERs. With an increasing number of anodes, the rate of 1,4-dioxane degradation asymptotically approaches full removal due to continuously decreasing concentration gradients in this diffusion-controlled system, similar to the observed effects in Figure 2.2(c). Even if full 1,4-dioxane mineralization is not achieved, many of the produced organic acid and aldehyde transformation products are readily biodegradable once ring cleavage of 1,4-dioxane is achieved.[62, 96]

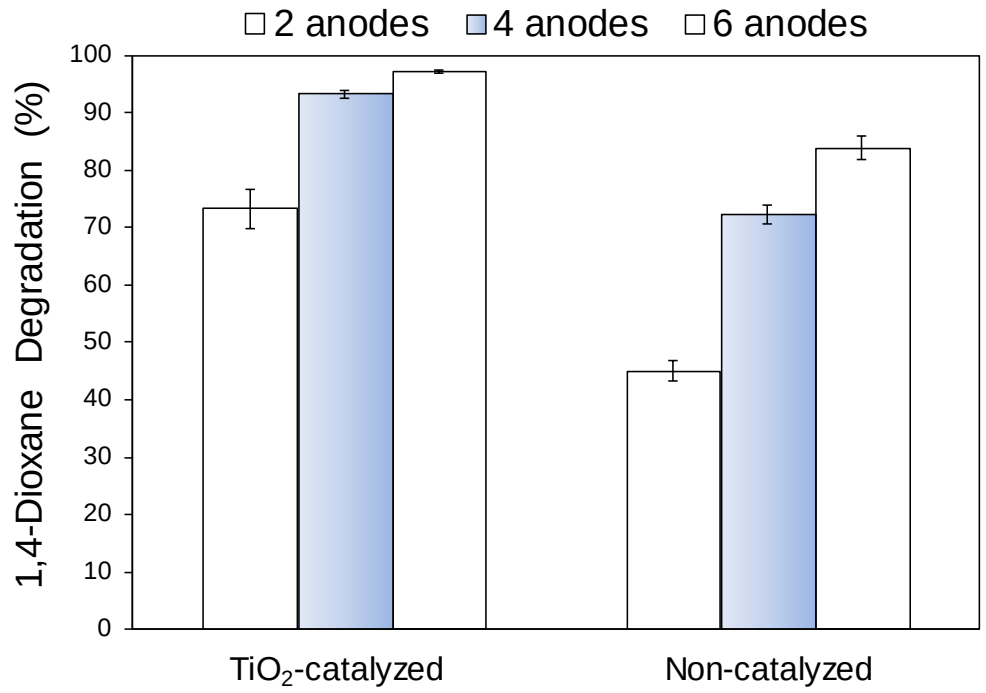

Figure 2.4 1,4-dioxane removal with increasing number of anodes. Degradation performance is represented as the percentage of the initial 3.4 µM 1,4-dioxane feedstock concentration degraded after treatment through each sequential reactor operated at 11.0 V (10 mM Na_2SO_4 electrolyte, 30.6 cm/d). Error bars indicate standard deviation (n = 3) for samples taken at steady-state.

Another advantage of AEO technologies is their applicability to degrading many different or mixed persistent organic pollutants in the environment.[2, 27, 97, 98] To explore the adaptability of flow-through electro(cata)lysis and further verify the TiO_2 pellet's catalytic activity in dark

conditions, removal efficiencies were evaluated for two other recalcitrant pollutants, lamotrigine[99] and chlorobenzene[100], in direct comparison to 1,4-dioxane using separate 5.0 cm I.D. FTERs (Figure S2.2) under identical operating conditions: 20 mM Na_2SO_4 electrolyte, 27.3 cm/d seepage velocity, and 8.0 V. Results from non-catalyzed electrolytic treatment shown in Figure 2.5 indicate contaminant removal efficiencies of 13%, 51% and 79% after electrolytic treatment of initial feedstock concentrations of 99 µM 1,4-dioxane, 41 µM lamotrigine, and 66 µM chlorobenzene, respectively. These results illustrate the selectivity that electrolytic treatment technologies have toward different organic molecules. The removal efficiency was much higher for the other two contaminants when compared to 1,4-dioxane, even though 1,4-dioxane was intentionally tested at elevated molar concentrations to induce greater diffusion gradients. Thus differences in mass transfer rates cannot explain the degradation differences observed. Benzene was not detected in the effluent of the chlorobenzene reactors, suggesting that oxidation at the lead anode was more likely even though electrolytic reduction is possible. The explanation for greater removal rates for lamotrigine and chlorobenzene is likely due to lower activation energies for initial electron transfer reactions and/or preferential adsorption/desorption characteristics between contaminants and the electrode or TiO_2 pellet surfaces.

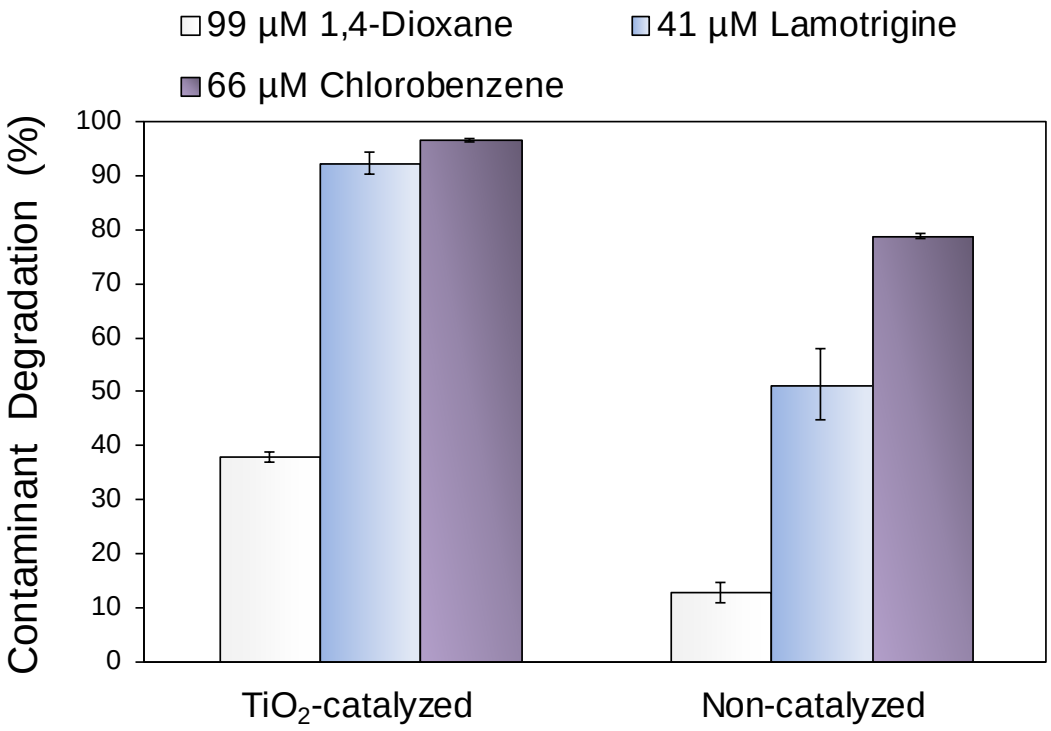

Figure 2.5 Degradation performance of FTERs for three persistent organic pollutants (POPs). All treatments were performed at 8.0 V applied, 20 mM Na_2SO_4, seepage velocity 27.3 cm/d. Performance is plotted as % of degradation of initial pollutant concentrations. Error bars indicate standard deviation (n = 3) for samples taken at steady-state.

When the same electrolytic treatments were performed in TiO_2-catalyzed FTERs, all three contaminants did show significant improvement in removal percentages ($p \leq 0.001$, α=0.05) with values of 38%, 92% and 97% respectively for 1,4-dioxane, lamotrigine, and chlorobenzene (Figure 2.5). Notably, the inter-electrode TiO_2 catalysts provided 3.2 times greater 1,4-dioxane removal when compared to electrolytic degradation on its own, in contrast to 1.8 and 1.2 times greater removal corresponding to TiO_2-catalyzed treatment of lamotrigine and chlorobenzene, respectively. This may indicate that successful large-scale treatment of certain contaminants may not require the addition of TiO_2 pellets in order to achieve high removal efficiencies. However, the catalytic degradation activity in the latter two may have been

underestimated due to near-complete removal, establishing a very low diffusion gradient in a system controlled by mass transport.

Our experiments demonstrate that flow-through electro(cata)lytic treatment is a viable option for successful degradation of 1,4-dioxane and other recalcitrant organic pollutants in aqueous environments.[2, 27, 97] Furthermore, we have revealed for the first time that TiO_2 can be electrochemically activated in the dark without direct electrode contact to become an efficient catalyst for organic contaminant oxidation. In a permeable reactive barrier or an aboveground reactor, significant improvements in contaminant degradation can be achieved using TiO_2 in the inter-electrode space instead of backfilling with unreactive material such as sand. In fact, catalytic enhancement by inter-electrode TiO_2 pellets was observed under all conditions tested, with the most notable 1,4-dioxane degradation improvement occurring low ionic strength water, where conventional electrochemical approaches typically fail.[66] The advantages of catalyzed AEO processes over standard UV-based AOPs include the potential for lower operational cost, no need to add chemical oxidants, and perhaps most notable, the ability to treat organic contaminants *in situ*.[30, 101, 102] However, the application of high voltages in complex environmental settings may entail the potential formation of disinfection by-products such as perchlorate and trihalomethanes,[55, 71, 103, 104] and therefore needs to be closely monitored.

Further investigations are needed to elucidate the mechanism of electrochemical activation of TiO_2 in dark conditions and to determine the activating and inhibitory effects that come with more complex water quality constituents. However, the results presented here illustrate that electro(cata)lytic oxidation is highly efficient at degrading 1,4-dioxane and other POPs under a wide range of environmental conditions.

CHAPTER 3

MECHANISTIC INSIGHTS INTO DARK CATALYSIS OF ORGANIC POLLUTANT OXIDATION USING NOVEL INTER-ELECTRODE TIO_2 CATALYSTS

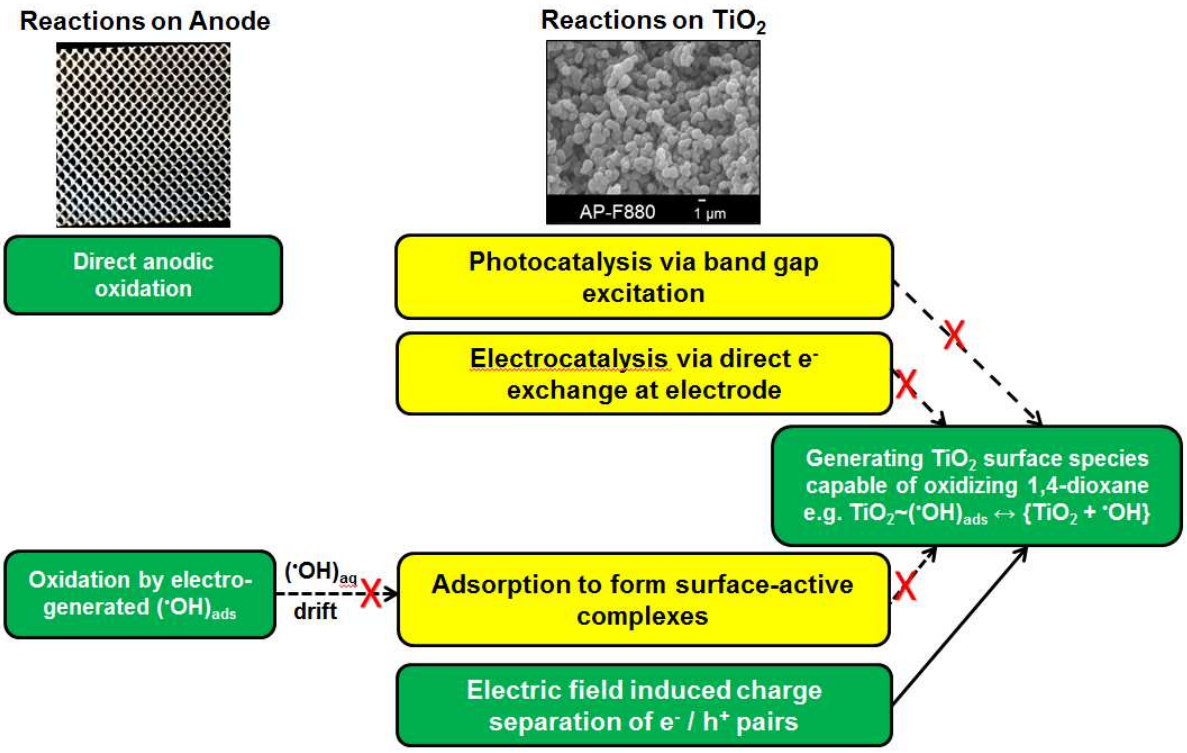

Conceptual Diagram of Possible Mechanism Pathways

CHAPTER SYNOPSIS

Recalcitrant contaminants in the aqueous environment often pose a major environmental problem. Semiconductor photocatalysis using titanium dioxide (TiO_2) has been shown to be effective at degrading a wide range of organic pollutants. Here, we demonstrate for the first time that electrically insulated, inter-electrode TiO_2 pellets can be electrochemically activated, in the absence of light, to degrade organic compounds. Novel TiO_2 pellets consisting of anatase, rutile, and mixed phase composites were fabricated by heating compacted TiO_2 powders in air at different temperatures ranging from 400°C up to 1000°C. The resulting composites were characterized by powder X-ray diffraction (PXRD), porosimetry (BET analysis), UV-Vis diffuse reflectance spectroscopy (DRS), and scanning electron microscopy (SEM). Characterization data indicate that TiO_2 pellets composed predominantly of the anatase polymorph had higher porosity, specific surface area, and higher bandgap energy. This study used flow-through column reactors to compare the electrocatalytic activity of different TiO_2 pellets for the degradation of the persistent aqueous pollutants, like 1,4-dioxane, lamotrigine, and chlorobenzene. The highest electrocatalytic activity was obtained in anatase phase TiO_2 for the degradation of all substances as compared to the rutile phase pellets and compared to electrolysis alone (non-catalyzed control columns). It is concluded that the higher electrocatalytic activity in anatase TiO_2 pellets is due to surface parameters like higher surface area, active crystalline faces, and beneficial electrostatic adsorption phenomenon rather than due to band gap excitation. The pollutant degradation results are also discussed on the basis of electron transfer phenomena in coordination with *in situ* electro-generated oxidants like hydroxyl radicals. Additionally, mechanistic probe molecules, like 1,4-benzoquinone, *tert*-butyl alcohol, and highly oxidized carbon tetrachloride were used in electrochemical batch reactors to further investigate dominant mechanistic drivers. It is also

suggested that electric-field induced propagation of electrons and holes within the semi-conductive TiO_2 pellets contributes to reactive oxygen species leading to enhanced redox chemistry at the surface.

INTRODUCTION

Titantium dioxide (TiO_2) is a stable, non-toxic, semiconducting material with extremely strong oxidizing power. Titanium dioxide is unmatched for its photocatalytic activity and stability when used for wastewater treatment.[22, 45] TiO_2 is also used as a stable, catalytic coating on electrodes to increase the efficiency of electron and proton transfer during redox reactions at the electrode surface.[53, 54] Since our inter-electrode TiO_2 pellets are electrically insulated from the electrode, much like what is used in TiO_2 photocatalysis, we used literature in this area to help with possible mechanistic clues. Many studies have confirmed that the anatase phase of TiO_2 is superior as a photocatalytic material for air and water purification, and hazardous waste remediation.[45-47] Band gap excitation of the semiconductor TiO_2 is initiated by high energy UV light absorption, causing the excitation of an electron e^{-}* into the conduction band, leaving an oxidizing hole h^{+} in the valence band. This excitation step, especially the h^{+} formation, leads to the hydrogen abstraction of adsorbed H_2O producing ·OH radicals. The strong oxidizing power and low selectivity of these ·OH radicals allows for successful oxidation– and often full mineralization to CO_2 – of many different organic pollutants, even those considered highly recalcitrant like 1,4-dioxane.[21, 48-50] When compared with other semiconductor materials with photocatalytic potential, TiO_2 is shown to be the most promising due to its high efficiency, low cost, photostability, and nontoxicity.[51, 52]

Although less common due to is relatively low electrical conductivity, TiO_2 is also used for its fast exchange of protons and electrons along its lattice structure and its capacity for ambipolar diffusion of positive and negative charge carriers. Kesselman, et al. reported in 1997 that Nb-doped TiO_2 electrodes were capable of generating hydroxyl radicals under an anodic bias, without the need for UV light.[53] Others have confirmed that once the metal anodic substrate is polarized the excitation of TiO_2 will lead to oxidizing holes in the valence band and electrons in the conduction band.[54] These anodic holes on TiO_2 coating can oxidize adsorbed pollutants directly, generate active $^{\bullet}OH$ radicals from adsorbed H_2O on the surface leading to indirect oxidation of nearby pollutants similar to what happens in photocatalysis.[53-56] Our objective is to expand upon this idea by not having TiO_2 coated onto the electrode surface, but instead adding electrically insulated, inter-electrode TiO_2 pellets, with to expand hydroxyl radical production and reactor surface sites into the bulk solution beyond the electrodes. The electrochemical generation of hydroxyl radicals and production of highly oxidized surface properties on inter-electrode TiO_2 pellets is a possible solution to one of the main limitations of electrolytic degradation being the need for contact between the organic reactant and the electrode surface.

Some limitations hindering wide scale use of TiO_2 in heterogeneous catalysis for the degradation of wastewater and contaminants include the need for practical immobilization schemes[105] and UV light requirements when used as a photocatalyst, and poor conductivity as an electrocatalyst.[47, 53, 106] We address the first concern by synthesizing immobilized, TiO_2 pellets which prevent advective losses in a flow-through treatment system, and also extends the reactive surfaces and into the bulk solutions rather than being limited to the surface of the electrode, as is the case with thin film coatings. We propose that the strong voltage bias produced at the

electrodes could be an alternative driver to activating TiO_2 rather than the use of UV photons, and this may be more energy efficient.

Extensive studies on electrochemical oxidation of organic-contaminated wastewater often propose that physisorbed hydroxyl radicals (M~˙OH) on the anode surface provide for the dominant destruction pathway. These M~˙OH radicals are formed upon the extraction of an electron and proton from water. Anodes with high over potentials for oxygen evolution, such as Ti/PbO_2, Ti/SnO_2, and BDD, are said to be "non-active" anodes, because they do not bind the oxygen atom of the M~˙OH covalently, leaving the nonselective radical to initiate oxidation of nearby organic pollutants, often leading to full mineralization. These active electrodes are limited in their commercial application at this time due to the release of toxic ions (e.g. $Pb^{+2/+4}$) in basic solutions,[2, 107] premature deactivation (e.g. short service life of Ti/SnO_2 or delamination of BDD anodes),[55, 108-110] or high cost (e.g. Ta/BDD).[2] The mesh Ti/IrO_2-Ta_2O_5 electrodes used in our study are dimensionally stable, even in corrosive environments,[2, 43, 44] however, they are known to be "active" anodes which implies that their reactivity can be more selective toward organic pollutants. Active anodes of noble metal oxides are capable of higher oxidation states and so the M~˙OH can be further oxidized to covalently bound species M=O, known as chemisorbed active oxygen. Evidence of this reaction is known by tracking the transfer of isotopically labeled ^{18}O from ^{18}O-enriched water into the metal oxide.[37, 111] Additional experiments showed that the electrochemical oxidation of formic acid at ^{18}O-enriched metal oxide in unlabeled water occurred through oxygen transfer shown by incorporation of ^{18}O into CO_2.[37] However, Bejan, et al. 2012 in the case of Ebonex Magneli phase Ti_4O_7 electrodes,[83] and prominent electrochemists Foti and Comninellis[112] and Panizza and Cerisola[2] in regards to other metal oxide-based anodes, have acknowledged that these anodes do not necessarily divide cleanly into active and inactive

categories. Thus, some proportion of electro-oxidation reactions at an "active" anode, like Ti/IrO_2-Ta_2O_5, could still proceed by hydroxyl radical addition and/or hydrogen abstraction reactions.[113, 114]

We built flow-through electrochemical reactors (FTERs) and electrolytic batch reactors to investigate the potential for electrochemically activation of TiO_2 used as a heterogeneous catalyst for enhanced treatment of water contaminated with persistent pollutants. These bench-scale electrolytic reactors are equipped with dimensionally stable Ti/IrO_2-Ta_2O_5 mesh electrodes that are cost-practical, resistant to fouling, and have been used successfully to degrade 1,4-dioxane, chlorinated solvents and energetic compounds in our previous work (Chapter 2).[44, 67, 68] 1,4-dioxane, lamotrigine (pharmaceutical), and chlorobenzene were the three persistent aqueous pollutants used a model contaminants for our tests.

In this study, we show that properties induced by an electric field in an aqueous solution are able to activate TiO_2 as a heterogeneous catalyst for efficient degradation of persistent organic pollutants. Different TiO_2 pellets were investigated for their catalytic activity and analyzed by porosimetry, microscopic and spectroscopic techniques. The specific objectives of our study were to 1) compare the catalytic activity of different inter-electrode TiO_2 pellets during electrolytic degradation of organic pollutants, 2) characterize important chemical and physical properties of our fabricated TiO_2 pellets, and 3) use electrolytic batch reactors and specific molecular probes to elucidate the possible mechanism for TiO_2 dark catalysis of electrically insulated TiO_2 pellets.

MATERIALS AND METHODS

Reagents and materials. All chemicals (> 99% purity) were used as received. 20-L glass carboys were used to prepare Na_2SO_4 (EMD Chemicals) electrolyte solutions in deionized,

ultra-purified water, spiked with 1,4-dioxane (Honeywell), chlorobenzene (JT Baker), or lamotrigine (trade name Lamictal, ENZO Life Sciences). Three precursor TiO_2 powder were used from Alfa Aesar (>99.6 anatase, fine powder, ≤ 44 μm), Huntsman (>99.5% anatase, coarse powder, particle size, ≥ 100 μm), and Evonik P25 (approximately 80:20 anatase to rutile composition, fine powder, particle size < 1 μm). Dimensionally stable, expanded mesh Ti/IrO_2-Ta_2O_5 electrodes (1.0 mm thick with 1.0 x 2.8 mm diamond-shaped openings) were used (Corrpro).

Catalyst synthesis. In order to immobilize the catalyst for continuous-flow system and also extend the reactive material beyond the surface of the electrode, TiO_2 powder was compacted and heat treated to form mechanically stable pellets sized to be within mesh sieve dimensions of 3.33 to 9.42 mm. Details of this process are provided in Chapter 2 and in a previous publication (Jasmann, et al. 2016). In brief, the multi-stage fabrication process involved pressure compaction and chiseling into loosely adhered pellets, followed by a 4-hour sintering process in ambient air at temperatures ranging from 400 °C to 1,000 °C. TiO_2 pellets produced from the three different precursor powders (and mixtures of them) were screened for mechanical stability and abrasion resistance after the 4 hour heat treatment. The pellet types selected as stable enough for flow-through water treatment systems, were further characterized by several analytical techniques.

Catalyst characterization. Synchrotron radiation-based Powder X-ray Diffraction (PXRD), which presents a much higher signal-to-noise ratio than laboratory PXRD, was used to estimate crystallinity, crystallite size, and percentage of anatase and rutile composition in finished catalyst pellets. Synchrotron PXRD was performed at beamline 11-3 of the Stanford Synchrotron Radiation Lightsource, with the wavelength of 0.0972413 nm (12.7 keV).

Diffraction intensity data were collected using step size of 0.002° and varying 2θ between 20° and 50°. Two-dimensional diffraction patterns were recorded by a Mar345 imaging plate system, with a sample-to-detector distance of 150 mm. Diffraction angle 2θ was calibrated with lanthanum hexaboride (LaB_6). One-dimensional PXRD profiles were integrated from selected concentric circles areas of the symmetrical 2-dimensional powder rings using the Fit2D program. Crystal structure parameters were refined using curve-fitting package (or graphical interface package) of Igor 6 Pro. The crystalline grain sizes were obtained from the commonly used Scherrer's equation $D = K\lambda / (\beta\cos\theta)$ with the crystal grain size D, shape correction constant K = 0.95 for a spherical particle, and FWHM of the related Bragg peaks β. The relative fraction of anatase to rutile was estimated from the Spurr-Meyer equation and the crystalline shape constant K = 0.7905 specific to TiO_2 crystals.

The morphologies of the sample were examined by scanning electron microscopy (SEM), using a JEOL JSM-6500F Model FE-SEM at 5 kV accelerating voltage. TiO_2 pellet samples were sputter-coated with Au prior to analysis.

Diffuse reflectance UV-Vis spectra were collected at ambient temperature on Cary 500 spectrophotometer, using potassium bromide as reference of maximum reflectance.

Nitrogen physisorption and porosity measurements were carried out at 77 K with a Micromeretics ASAP 2020 system to determine the textural properties. Specific surface areas were calculated according to the Brunauer-Emmett-Teller (BET) method [115, 116] (P/P_0 = 0.1-0.3). Total pore volume of the TiO_2 pellets was determined by nitrogen desorption at P/P_0 = 0.99. Barrett-Joyner-Halenda (BJH) analysis[117] was employed to characterize pore size distribution and using average values from both adsorption and desorption techniques. Prior to adsorption/desorption measurements, samples were outgassed at 573 K for 24 h and duplicate

samples were analyzed and reported values to within ± 0.05 relative standard deviation of original samples.

Electrocatalytic activity. To compare the catalytic activity of different TiO_2 pellets during the degradation of our model contaminants, FTERs were constructed of clear, 15-cm length acrylic pipe with 5.0 cm I.D. and a single pair of disc-shaped electrodes (18.25 cm^2) spaced with an inter-electrode gap of 2.5 cm (Fig. SI). To minimize sorption, the feedstock was pumped through every reactor before each experiment until influent and effluent contaminant concentrations were equal. Once steady-state conditions were achieved at target voltage, a minimum of three influent and effluent samples were collected for chemical analysis for each contaminant. Daily measurements were made of pH, solution redox potential and current between working electrodes.

Three aqueous feedstock solutions of 20 mM Na_2SO_4 (~3,400 µS/cm) supporting electrolyte were prepared in 20-L glass carboys and spiked with 99 µM 1,4-dioxane, 41 µM lamotrigine, or 66 µM chlorobenzene. Feedstock solution is flowed vertically through the column reactor at a seepage velocity of 27 cm/d passing through the positively charge mesh anode and then cathode. Each column was fitted with a Ag/AgCl reference electrode (World Precision Instruments) to measure solution redox potential and a gas exhaust tube to vent excess O_2 and H_2 gas produced during the electrolysis of water. The section of each FTER upstream of the initial anode was packed with quartz silica sand (20/35 mesh) to enhance dispersive mixing of influent contaminant prior to contact with the first electrode. A permeable geotextile, composed of polypropylene felt, was placed after the anode and before the cathode to control movement of sediments onto the inter-electrode TiO_2 pellets and electrically insulate the pellets from direct conduction with the anode. The inter-electrode space was filled with three different

TiO_2 pellets for the catalyst comparison experiments and with inert, 6-mm diameter glass beads for the non-catalytic control experiments. To exclude photocatalytic degradation processes, influent feedstock and FTERs were covered by black, opaque plastic to maintain dark conditions. Na_2SO_4 and $NaClO_4$ electrolytes were used in our study since they are commonly used in other electrochemical degradation studies.[2, 72]

Concentric cylinder electrochemical batch reactors were used for some of the mechanistic investigation. In some cases, an undivided electrochemical cell was used, while in others the anodic and cathodic compartments were separated by a Nafion NRE-212 membrane ($Rf[OCF_2CF(CF_3)_2]_nOCF_2CF_2SO_3H$, 0.05 mm thick, 0.92 meq/g exchange capacity, Alfa Aesar PN 45036). A conceptual diagram and description of these reactors are given in Figure S3.2.

Analysis of the three model contaminants follows methods described in Chapter 2 and in a previous publication (Jasmann, et al., 2016). In brief, an Agilent 6890N gas chromatograph and mass selective detector (GC/MSD) operated in full scan and selective ion modes was used to quantify 1,4-dioxane using calibration. Lamotrigine was quantified at 270 nm by an Agilent 1200 series HPLC equipped with a UV-diode array detector. An Agilent 6890N GC followed by an electron capture device was used to quantify chlorobenzene. Calibration with external standards was used to quantify all contaminants studied. Degradation efficiency was quantitative compared by the percentage of contaminant degraded (% Degradation = $100 \cdot (C_{eff}/C_{inf})$, $n \geq 3$).

RESULTS AND DISCUSSION

Catalyst characterization. Although TiO_2 slurries would provide the greatest amount of reactive surface area, the powder is difficult to collect for reuse in batch systems, and it is difficult to prevent advective losses in flow-through systems. Therefore, we sacrificed on the surface area to volume ratio in exchange for having an immobilized TiO_2 pellet with better

reusability capacity and greater longevity. Synchrotron PXRD data showed sharp diffraction peaks for all TiO_2 pellets analyzed (Fig. 1**)**, indicative of high crystallinity. The diffraction peaks for TiO_2 pellets made from Evonik P25 TiO_2, a commercial mixture of approximately 80% anatase and 20% rutile, show that the pellets fully transform to 100% rutile crystalline phase during 4-hour calcination process at all temperatures at 700 ºC and above (Fig. 3.1c). However, analysis of the trends in diffraction peaks for those pellets made from fine and coarse anatase powders showed that ≥ 98 % remained in the anatase form for both the 700 °C and 880 °C treatments. Conversely, after the 1,000 °C calcination treatment, the majority of the anatase in each type had transformed to the more thermodynamically stable rutile form.[45] To evaluate the mechanical stability of the finished catalyst, TiO_2 pellets were shaken in glass vials at 210 rpm to determine which pellets had the greatest percentage by mass remaining as intact pellets after 10 and 25 seconds of vigorous shaking. Details of the testing procedures were reported earlier in Chapter 2 and in a previous publication (Jasmann, et al. 2016). Only the TiO_2 pellets subjected to 4-hour heat treatments at 880 °C and 1,000 °C achieved satisfactory cementing of the compacted TiO_2 powder into high-strength pellets. Pellets sintered at 400 °C, 700 °C and 800 °C remained friable and prone to abrasion, making them unsuitable for our over-arching goal of inter-electrode catalysts for flow-through systems.

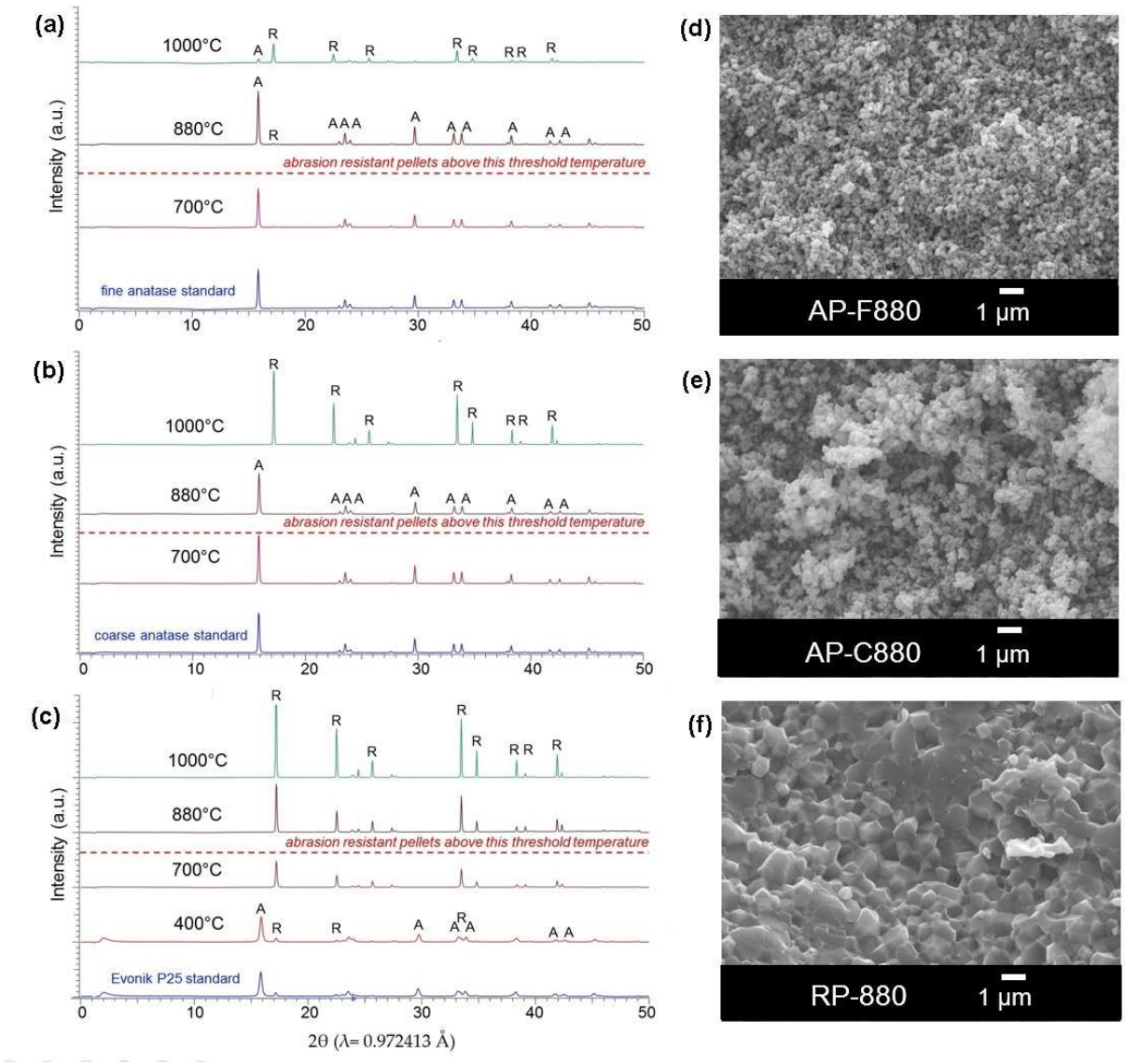

Figure 3.1 (a-c) Synchrotron PXRD diffractograms for each precursor TiO_2 powder after pellet compaction and heat treatment for 4 hours at various temperatures; d-f) SEM images of AP-F880, AP-C880, RP-880.

Based upon these screening results, three TiO_2 pellets sintered at 880 °C were used to investigate their catalytic activity in our flow-through and batch reactor experiments, and will be referred to as R-880, AP-F880 and AP-C880 from here forward. The P-X format uses P to refer to the final phase of the pellet RP for rutile, (MP for mixed phases seen later) and AP for anatase and X is the sintering temperature using during fabrication. To distinguish the pellets that

finished with high anatase percentage at 880 °C, AP-F880 is used for the one originating from the fine anatase powder and AP-C880 is used from the coarse anatase precursor.

These pellets were further characterized by SEM and porosimetry analysis. SEM images in Fig. 1 at 7,000x (and 30,000x magnification in Fig S3.3) showed homogenously sized spherical particles and uniform porosity across the surface of the AP-F880 and AP-C880 TiO_2 pellets, which is consistent with other SEM images of anatase-based TiO_2 used for catalytic degradation of organic pollutants.[45, 47, 74] The surface morphology of the RP-880 pellets was dramatically different, showing signs of crystallite union phenomena appearing to have shallower and more limited pore distribution. The RP-880 morphologies are expected to decrease the specific surface area and reduce the activity of these pellets compared with the others.

N_2 adsorption analysis at 77 K confirmed the qualitative observations made on SEM. Duplicate analyses of AP-F880 and AP-C880 pellets determined their specific surface areas to be 8.1 ± 0.05 m^2/g for both, while the EP-880 reported a much lower 0.016 ± 0.01 m^2/g. Due the concerns for this value, duplicates were repeated for EP-880 using Krypton as the physisorption gas and arrived at the same value. A detailed comparison of the properties of various samples as a function of precursor and calcination temperature is provided in Table 3S.1. Additional plots of UV-Vis diffuse reflectance, N_2 adsorption isotherms and porosity distribution can be found in Figure S3.3 and S3.4.

Scherrer equation was used to estimate average crystallite size for various composition of TiO_2 pellets with all ranging from 32 nm to 55 nm in size. As would be expected the AP-F880 and AP-C880 pellets had larger crystallite sizes of 45 and 51 nm, respectively compared to only 32 nm in the AP-C700 heated at a lower temperature. The impact of grain size can impact the surface-to-volume ratio of catalysts so this could partially explain the greater catalytic activity

observed by AP-C700. Hoffmann, et al., (1995) has reported that larger grain sizes also result in more density of states in and between the valence band and conduction band. The grain sizes observed in our TiO_2 pellets are on the larger side due to the long heating times allowing for more crystal growth. These larger sizes would imply greater density of states potentially allowing for higher probabilities of charge separation between electrons and holes in our pellets. Still others have found threshold sizes below 15 nm in grain size in which bulk properties switch such that anatase can become more stable than rutile and surface energies dramatically shift.[118] This is not considered with our TiO_2 pellets since results show them to be above this threshold.

Flow-through treatment: electrocatalytic behavior at steady state. The electrocatalytic activity of the TiO_2 pellets synthesized from different precursor materials at different sintering temperatures were initially evaluated by the percentage of 1,4-dioxane degradation achieved in FTER experiments. All flow-through reactors were operated under a constant 8.0 V at 22 ± 2 °C and were fed by influent of 91 µM 1,4-dioxane in 20 mM Na_2SO_4 (~3.8 mS/cm) electrolyte solution. Mesh geotextile material, composed of HDPE plastic and polypropylene felt was placed between the electrodes and the inter-electrode materials, as a barrier to sand transport, but also prevented direct electrical contact of the electrodes with the inter-electrode TiO_2 pellets. In the experiments labeled as AP-F880* in Figure 3.2, the geotextile was purposed lacking to determine whether direct electrode contact and thus conduction through the TiO_2 is required for catalyst activation. In an attempt to simulate seepage velocities that could be experienced in an *in situ* groundwater installation, flow rates of 0.23 mL/min were used, resulting in a seepage velocity of 27.4 cm/d through the porous media of the column reactors. Once steady state conditions were achieved (usually 3-5 pore volume exchanges), reactor

effluent was monitored for 1,4-dioxane degradation each day, along with current, redox potential, pH and conductivity.

The activity of five different TiO_2 pellets were compared against a non-catalytic FTER control column packed with inert glass beads rather than TiO_2 pellets. A schematic of these FTERs and photos are provided in Figure S3.1. Figure 3.2 shows RP-F880 and MP-C800 pellets degradation performance were only slightly better than electrolytic treatment without the TiO_2 catalyst. However, all of the predominantly anatase pellets provided enhancement of the degradation efficiency by 2 to 4 times that of the non-catalytic control, suggesting that the surface or electronic properties of anatase are better suited for electrocatalysis of organic pollutants. The observation of anatase phase TiO_2 outperforming rutile is generally supported in the literature describing photocatalytic and electro-photocatalytic degradation of pollutants,[45] with specific observations of higher concentrations of adsorbed radical species[119] and surface-bonded peroxo species[120] on anatase TiO_2, and other observations focusing on surface defect chemistry causing favorable reactivity.[121, 122] However, some researchers have found that rutile form on its own, or mixed with anatase (e.g. Evonik P25 TiO_2), can provide efficient pollutant degradation due to surface properties and since the rutile can act to inhibit facile recombination of electron/ hole pairs generated from band gap excitation.[45, 123-126] When using MP-F880 mixed phase inter-electrode TiO_2 pellets (final anatase-to-rutile composition of 93% anatase to 7% rutile), no significant improvement in performance was observed (Figure 3.2). This could indicate that e^- / h^+ recombination may be less important as a factor within electrochemical systems due to the constant electric field driving force in an electrochemical system.

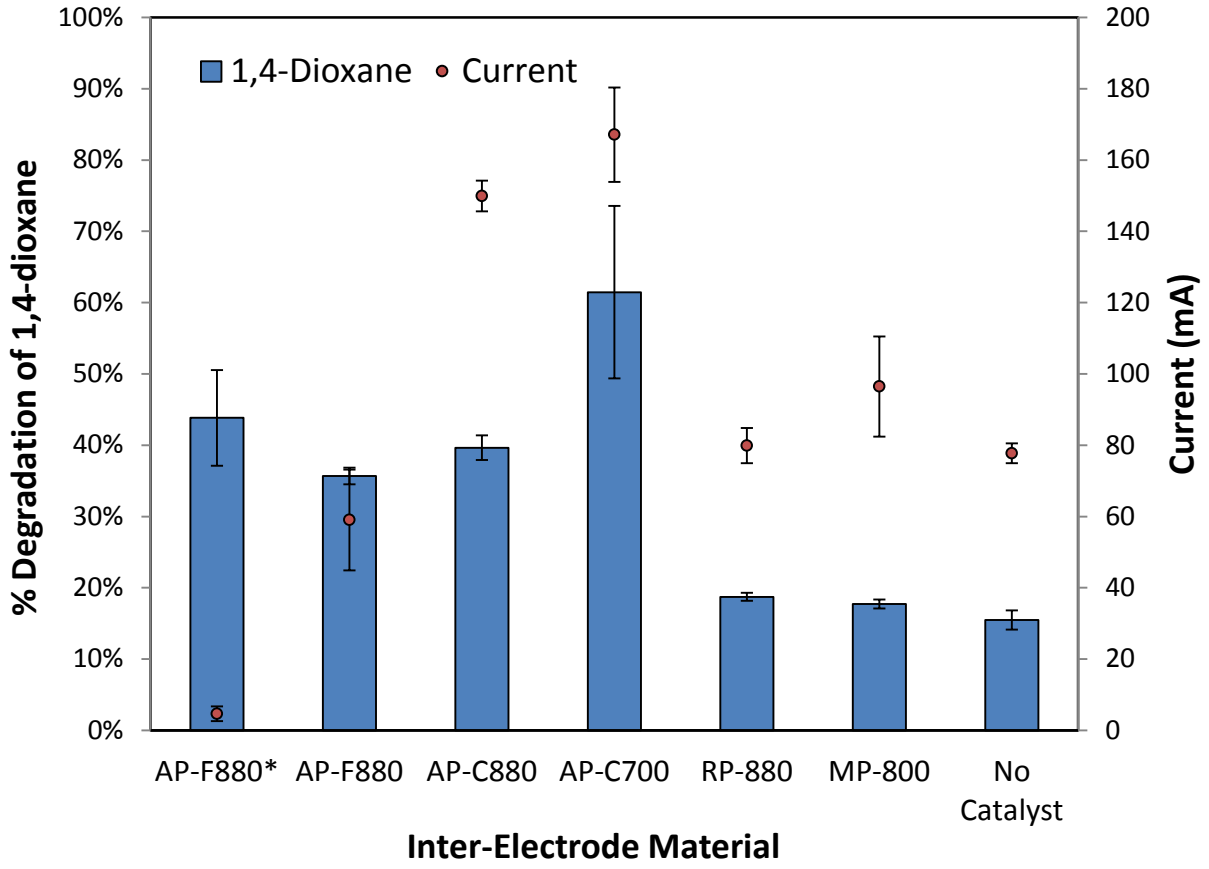

Figure 3.2 Comparison of the electrocatalytic activity of five different TiO_2 pellets was evaluated by the percentage of 1,4-dioxane degraded. The secondary y-axis plots the average steady state current for each column experiment. Experiments were performed using flow-through electrochemical reactors operating at 8.0 V at a seepage velocity of 27.3 cm/d, supplied by a 20mM Na_2SO_4 electrolyte feedstock spiked with 91 µM 1,4-dioxane. Effluent samples were monitored after steady-state conditions were achieved. Errors bars represent the standard deviation ($n \geq 3$). AP-F880* indicates that the AP-F880 pellets were used between electrodes but there was no geotextile in place to insulate the TiO_2 from touching the bordering electrodes. All other FTER experiments performed in the plot did have the insulating geotextile in place.

The greatest removal efficiency was achieved by AP-C700 (61% degradation) which could be explained by having the highest specific surface area and lowest average crystallite size of all the TiO_2 composites measured, along with its high percentage of anatase. The first two properties contribute to a higher surface area to volume ratio in this pellet, especially beneficial

when all catalysts in this study occupy a fixed volume between the electrodes. One downside to this pellet is in it having less mechanical stability, and thus more potential losses of catalytic material in flow-through systems, since the lower thermal treatment temperature left these pellets more friable than those heated at 880 °C. Despite all FTER experiments being operated at a constant 8.0V with the same ionic strength of solutions, the AP-C700 column also experienced the highest average current at 167 mA by a fairly large margin (Figure 3.2). However, while current (density) is usually a prime variable in kinetics of conventional (i.e., uncatalyzed) electrochemical processes, the results in Figure 3.2 imply that current and degradation rate are not proportionally correlated in the TiO_2-catalyzed electrolytic systems.

For example, the AP-C880 current is 90% that of AP-C700, but the degradation rate is only 66% of what AP-C700 achieved. Conversely, wide variances in current ranging from 4.7 to 150 mA in three TiO_2 pellets of similar composition, namely AP-F880*, AP-F880 and AP-C880, resulted in roughly the same amount of degradation, providing additional verification that these experimental conditions are not under current control. However, the differences in kinetics among the differently composed TiO_2 pellets are not due to mass transport limitations either, since all experiments have the same concentration of substrate 1,4-dioxane and the same advective flow rates. These observations provide further evidence that the characteristics of the catalytic pellets are more important predictors of kinetic activity than is the electrical current. More surprising results were observed when comparing the 1,4-dioxane degradation efficiency of AP-F880* TiO_2 (not having the insulating geotextile barrier between electrode and TiO2 pellets) vs. the AP-F880 TiO_2 reactors (which were completely insulated from both electrodes by geotextile). Figure 3.2 shows that the catalytic activity of the AP-F880 TiO_2 was similar in magnitude even when being insulated completely by the geotextile barrier. These results indicate

the potential for electro-activated TiO_2 to occur in the dark (not photocatalysis) even with insulated (not traditional electrocatalysis) from the polarized electrodes.

Redox potentials measured in the solution between the electrodes were consistently between 1.2 and 1.7 V vs SHE in all FTER experiments performed, with the exception of a very high 7.3 V consistently measured within the non-insulated AP-F880* FTER (Table S2). Electrical conductivities of effluent solutions displayed a small range of 4.1 to 5.6 mS/cm despite all treating the same influent solution. The non-buffered feedstock started with a pH of 7.0. After electro(cata)lytic treatment, the non-catalytic control ended at neutral pH, four of TiO_2-catalyzed experiments resulted in acidic effluent (pH 4.7 – 7), and the two others ended with highly alkaline effluents (pH 10 – 11). Redox chemistry at the electrodes, such as the splitting of water, can contribute to wide fluctuations in solution pH. Additionally, other advanced oxidation processes have demonstrated that acidic conditions can form as a result of organic pollutants being transformed into organic acid intermediates, and with ongoing mineralization to CO_2 the pH can shift back toward higher pH values. Table S2 provides more quantitative information on measurements of current, redox potential, pH, and conductivity.

In separate FTER, the activity of the three of the TiO_2 compositions (AP-F880, AP-H880, and RP-F880) were tested on other persistent pollutants: the pharmaceutical lamotrigine and the industrial solvent chlorobenzene. The AP-F880 and AP-H880 pellets still possessed the highest catalytic activity for degrading lamotrigine and chlorobenzene, with AP-F880 achieving removal efficiencies of 92% and 97%, respectively, a flow-through reactor (Figure S3.5).

Additional experiments were performed in batch reactors to further investigate possible contributors to variation in current. Using tray reactors open on the top to allow for easy addition and subtraction of inter-electrode materials, we were able to show that glass beads used in our

control reactors have a lower average porosity of 0.42 compared to 0.73 when TiO_2 pellets were used to fill the inter-electrode gap. This lower pore volume results in greater resistivity and therefore lower electrical current. Detailed information regarding porosity, pore volume and electrical current measurements are provided in Table S3. This is likely to be a partial contributor to the higher voltages often seen in TiO_2 FTERs compared to control FTERs with glass beads between the electrodes. However, this is still not sufficient to explain the significant current difference observed in FTER experiments between AP-F880*, AP-F880, AP-C880, and AP-C700 since their bulk densities and thus pore volumes should be close to the same.

Electrocatalytic behavior in electrochemical batch reactors. Since $^{\bullet}OH$ radicals have been proposed as the dominant oxidative species in electrochemical systems, it is important to confirm the production of OH radicals, whether these $^{\bullet}OH$ radicals are produced at the anode and/or through chemical reactions at the activated TiO_2 surface. The difficulty in providing evidence of electro-generated $^{\bullet}OH$ radicals is that many of the probe molecules used to elucidate mechanisms and other advanced oxidation processes happen to use probes that are themselves easily electrochemically oxidized. For example, any of the nitrone spin trap probes such as DMPO (5,5-dimethylpyrrolidine-*N*-oxide) are oxidized to radical cations more easily than water is oxidized to hydroxyl radicals.[127-129] This $DMPO^{\bullet+}$ can then be transformed by nucleophilic attack of water to form $(DMPO\text{-}OH)^{\bullet}$, generating an EPR (electron paramagnetic resonance) spectrum that could be falsely interpreted to be the targeted spin adduct $(DMPO\text{-}OH)^{\bullet}$ assumed to be formed from the trapping of the free radical from the $M\sim OH^{\bullet}$ moiety on the electrode surface.[83]

Seeking to use a molecule subject to radical attack but resistant to electrochemical activity, 1,4-benzoquinone (BQ) was chosen as an organic probe molecule for $^{\bullet}OH$ radicals

specific to electrochemical system. BQ has been determined to be indicative of •OH radical generation as it rapidly reacts with •OH ($k_{•OH, BQ} = 6.6 \times 10^9\ M^{-1}s^{-1}$),[82] while being highly resistant to direct electrochemical oxidation.[83-85, 130] However, since BQ can be easily reduced at the cathode to form 1,4-hydroquinone, the anode and cathode were separated by a Nafion NRE-212 membrane to prevent any cathodic reduction reactions. Figure S3.2 shows a schematic and photos of this divided cell batch reactor. BQ was only added to the 50 mM Na_2SO_4 electrolyte solution in the separated anodic chamber. The oxidation of BQ from the anodic chamber at a constant current of 300 mA, as seen in Figure 3.3, provides evidence that •OH radicals were electro-generated causing the oxidation of BQ. Further confirmation of BQ oxidation was provided since we did not detect the formation of the reduced product 1,4-hydroquinone in anodic chamber.

Electrochemical experiments were carried out at 300 mA constant current in 50 mM Na_2SO_4 electrolyte in Nafion NRE-212 membrane divided cells in order to avoid electrochemical reduction of BQ. Results in Figure 3.3 show that BQ was oxidized within the anode chamber, providing evidence for electro-generated hydroxyl radicals since BQ is resistant to direct electron transfer from the anode.

Involvement of hydroxyl radicals in oxidation mechanism. To provide evidence for •OH radicals being produced from the Ti/IrO_2-Ta_2O_5 electrodes involved in the oxidation mechanism for 1,4-dioxane and other organic molecules tested, a divided electrochemical batch reactor was built (Figure S5). 1,4-benzoquinone (BQ) is a model probe molecule used to demonstrate electrochemical production of •OH radicals.[83, 130] This is because the kinetics of •OH radical oxidation of BQ is very fast ($k_{•OH, BQ} = 6.6 \times 10^9\ M^{-1}s^{-1}$) [82], while it is highly resistant to direct anodic oxidation.[83-85]

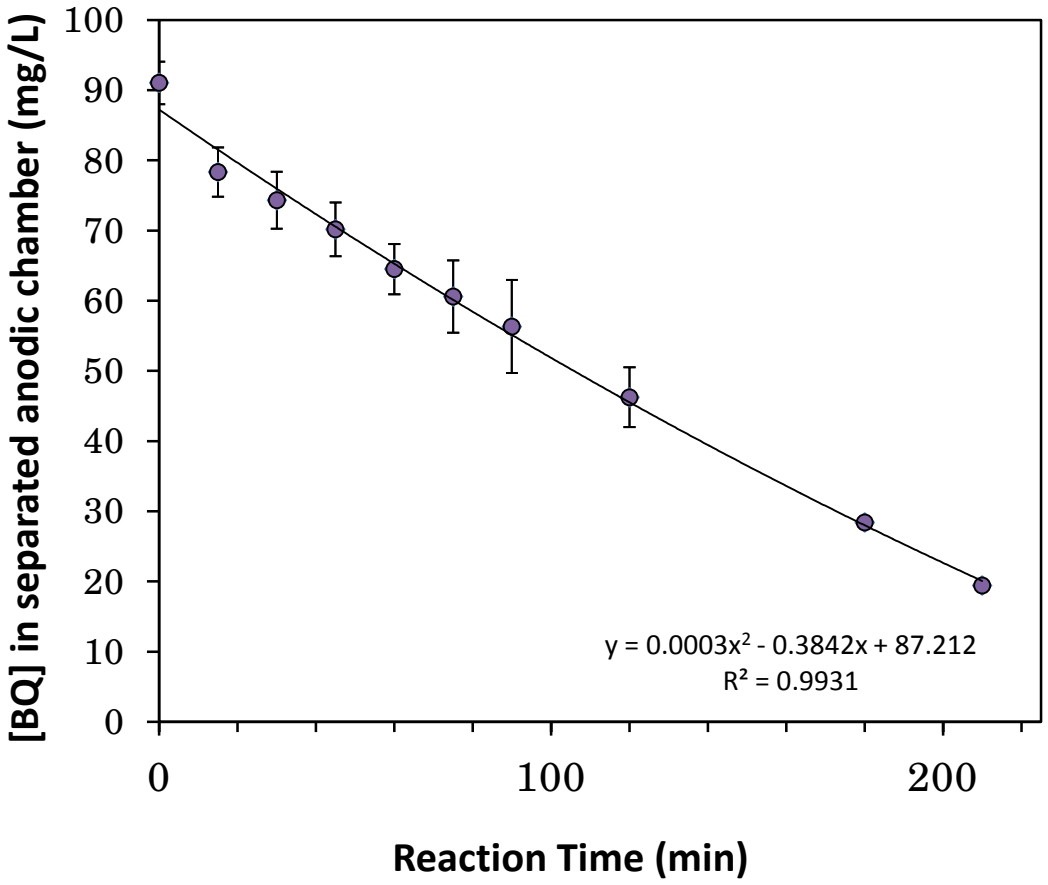

Figure 3.3 Concentration of 1,4-benzoquinone over time during electrochemical oxidation in the Nafion-separated anodic chamber at 300 mA constant current in 50 mM Na_2SO_4. Error bars indicate standard deviation (n = 4).

To confirm the contribution of hydroxyl radicals as a reactive species to 1,4-dioxane removal a competitive kinetics experiment was performed. The concentration of M~$^{\bullet}$OH or TiO_2~$^{\bullet}$OH is assumed to be high and at steady state, and two competing substrates are 1,4-dioxane and an effective $^{\bullet}$OH scavenger tert-butyl alcohol (TBA). The rate constant for TBA with $^{\bullet}$OH(aq) is very fast (k_{obs} = 5.2-6.0 x 10^8 $M^{-1}s^{-1}$)[131, 132] and so if placed concurrently at concentrations ~4,000 times higher than the molarity of 1,4-dioxane, much of the electro-generated hydroxyl radicals produced will necessarily react with TBA instead of 1,4-dioxane, causing an observable loss of expected degradation rates for 1,4-dioxane under these

conditions.[133] A single-cell electrochemical batch reactor (Figure S3.2) was used for all experiments in Figure 3.4, all having the same initial conditions of 10 µM 1,4-dioxane in 20 mM $NaClO_4$ electrolyte, with 140 g of AP-F880 TiO_2 packed between electrodes. Figure 3.4 shows a plot of these conditions monitored at 0 V in order to show that no significant losses in 1,4-dioxane occurred due to volatilization or adsorption over the 120 minute time period.

Under baseline conditions with 1.0 A applied in the absence of TBA, 45% of 1,4-dioxane was degraded after 60 minutes and 70% was degraded after 120 minutes (Figure 3.5). When in the presence of 40 mM TBA, and the same 10 µM of 1,4-dioxane under 1.0 A electrical bias roughly 16% of 1,4-dioxane was degraded after 120 minutes. This provides an additional line of evidence showing that $^{\bullet}OH$ is a major contributor to oxidizing recalcitrant 1,4-dioxane.

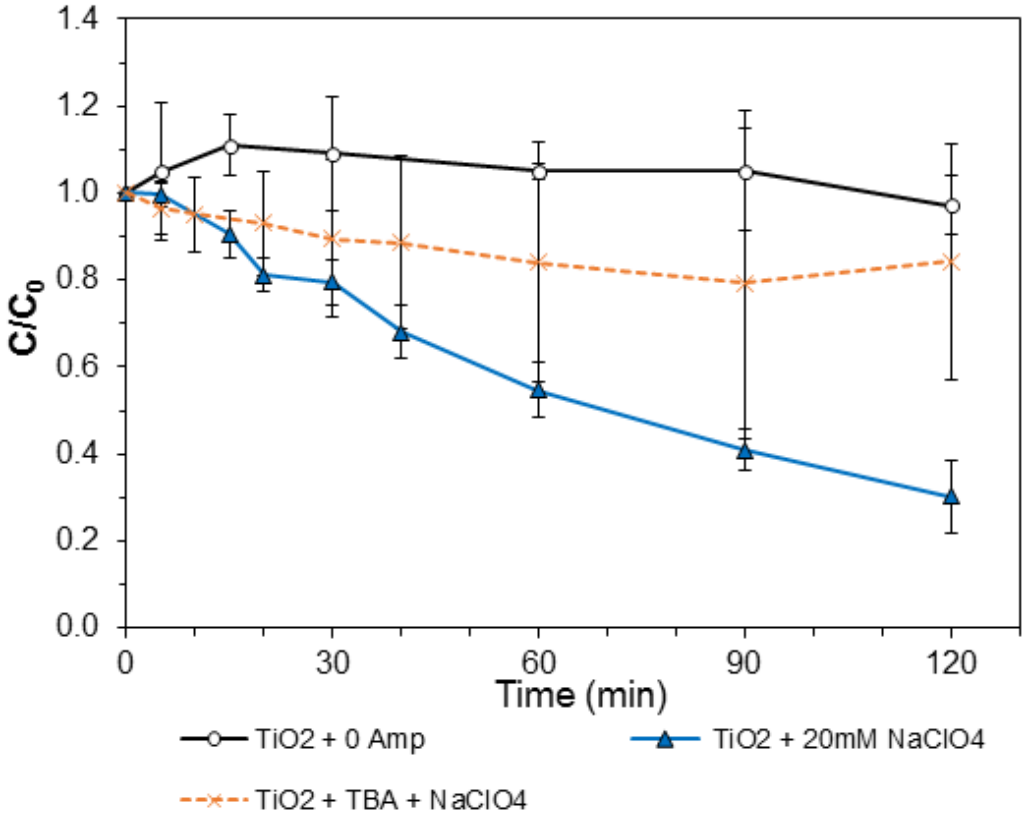

Figure 3.4 Relative concentration (C/C_0) of 10 µM 1,4-dioxane during degradation experiments at 1.0 Amp in 10 mM $NaClO_4$ electrolyte for competitive kinetics experiments comparing the degradation rate of 1,4-dioxane with TiO_2 as an inter-electrode material with and without the $^{\bullet}OH$ scavenger *tert*-butyl alcohol being present. A no-voltage control was also performed. Error bars represent the standard deviation (n = 3).

Involvement of band gap excitation in TiO_2 oxidation mechanism. The predominant mechanism for TiO_2 as a photocatalyst is bandgap excitation caused by the absorbance of photons of ultraviolet light. UV light provides the appropriate energy, allowing electron with in the valence band of TiO_2 to become energetically excited into the higher energy conduction band. A strongly oxidizing hole (h^+) remains in the valence band and is capable of oxidizing adsorbed water and many other organic pollutants adsorbed to the surface. Additionally, the excited electron can transfer onto adsorbed molecule, reducing them. Due to charge mobility within semiconductors like TiO_2, the excited electrons and oxidizing holes often recombine with

TiO_2, thus returning to ground state without any redox chemistry occurring. We postulated that it may be possible for the electric field to provide the necessary energy to promote electrons from the valence band to the conduction band within our TiO_2 pellets, forming h^+ capable of oxidizing 1,4-dioxane directly or producing hydroxyl radicals through extracting hydrogen from adsorbed water molecules.

To test our hypothesis, 100 µM of carbon tetrachloride (CCl_4) was spiked into 20 mM $NaClO_4$ electrolyte and added to the cathodic chamber of our divided electrochemical cell, with the anode only being filled with the electrolyte solution. Upon powering the electrodes with a constant current of 300 mA, CCl_4 was immediately reduced by electron transfer reactions at the cathode and concentrations dropped to less than 5% of the starting concentration within 2 minutes (Figure 3.5). The next experiments instead added the 100µM CCl_4 electrolyte into the anodic chamber of our divided electrochemical cell. The anodic chamber was also packed with TiO_2 pellets. Carbon tetrachloride is a molecule in a highly oxidized state, allowing for rapid reductive dechlorination at the cathode. However CCl_4 is incapable of being further oxidized electrochemically. Thus, our attempt to degrade CCl_4 in the anodic oxidizing chamber at 300 mA was with the assumption that the only possible pathway for degradation was if band gap excitation did occur, producing an energetic electron capable of reducing CCl_4. Results in Figure 3.5 indicate that CCl_4 was not degraded, implying that band gap excitation was not electrolytically activated. However, based on this experiment alone, we cannot completely exclude band gap excitation since the surrounding water may have acted as an excess pool of electron acceptors, diminishing the reducing effect on CCl_4. However, if band gap excitation was the initial step to obtaining the catalytic activity observed for the oxidation of 1,4-dioxane,

then it would be expected that the rutile-based pellets would have shown better catalytic activity due to their smaller band gap energy of 2.88 eV vs. ≥ 3 eV in the anatase pellets.

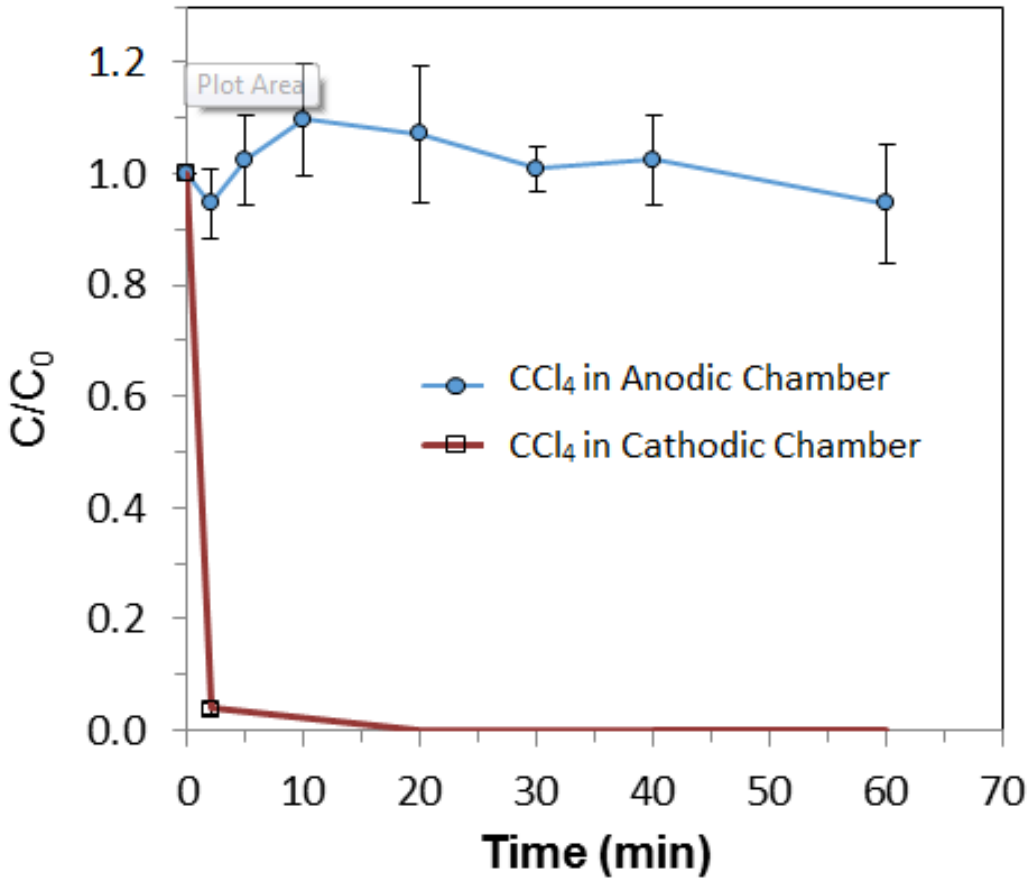

Figure 3.5 Relative concentration (C/C_0) of 100 µM CCl_4 over time while using 300 mA in a divided electrochemical cell. These plots are the averages (n=4) of two separate experiments: one with CCl_4 in the separated cathodic chamber and another with CCl_4 in the separated anodic chamber which also if filled with TiO_2 pellets. Error bars represent the standard deviation (n = 4).

Involvement of hydroxyl radicals on TiO_2 activity in absence of electric field. Once the importance of hydroxyl radicals was established, we wanted to better understand if our pellets were in some way electro-activated, or were the hydroxyl radicals simply interacting with the surface chemistry of our TiO_2 pellets along with co-adsorbed 1,4-dioxane on the surface,

forming some intermediate transition state, and diassociatively desorbing back into solution as reaction products. To determine whether the activity of the AP-F880 TiO_2 pellets would remain in the absence of an electric field (and light), Fenton's reagent solution, known to be able to degrade 1,4-dioxane,[21, 113, 134] was designed to produce large amounts of hydroxyl radicals without applying any voltage to the system.

Fenton's reagent is a solution of H_2O_2 with ferrous iron Fe^{2+} as a catalyst used to oxidize contaminants in water through the catalytic production of $^{\bullet}OH$ and $^{\bullet}OOH$ radicals. First, a control experiment was run with 10 µM 1,4-dioxane in the presence of 1.0 M H_2O_2 , which is also a strong oxidant, to determine if H_2O_2 alone was capable of oxidizing 1,4-dioxane. Results showed that 1,4-dioxane was not readily removed by H_2O_2 alone, at least during the 1 hour time period (Figure 3.6), confirming reports by others stating the same.[48, 62, 135] Next, 10 µM 1,4-dioxane was spiked into 0.1 mM $FeSO_4 \cdot 7H_2O$ in the absence of TiO_2 pellets, and the experiment was started as soon as H_2O_2 was added to achieve a final concentration of 0.20 mM H_2O_2. The results in Figure 3.6 show how quickly 1,4-dioxane was degraded by Fenton's reagent, achieving 90% and 95% removal in 2 and 5 minutes, respectively. The ability of ROS produced by Fenton's chemistry to rapidly oxidize 1,4-dioxane is in agreement with others who have researched this treatment.[134] Lastly, the same experiment was repeated, but this time with 140 g of AP-F880 TiO_2 pellets packed into the reactor vial. Approximately 17-20% removal was achieved in the first 5-10 minutes but then all 1,4-dioxane removal appeared to stop, confirmed by triplicate trials. It is unclear if the TiO_2 pellets simply created physical barriers to diffusion for homogeneous chemical reactions to occur, or if possibly the TiO_2 reacted in some way with the $^{\bullet}OH$ radicals or H_2O_2 to reduce their ability to perform the catalytic reproduction of reactive oxygen species. This experiment does help to confirm that without the electric field the powerful

oxidizing activity of the TiO_2 pellets was not possible. This is a strong indication that the mechanism at play is not simply surface adsorption lowering the activation energy of degradation reactions. It also is unlikely that the TiO_2 is only providing stabilization of $^{\bullet}OH$ radical complexation at the surface after $^{\bullet}OH$ drifts from where it is produced elsewhere.

In summary, we have demonstrated that inter-electrode TiO_2 pellets significantly enhance the electrolytic degradation efficiency of recalcitrant pollutants in flow-through systems, which is usually the preferred management strategy for wastewater and groundwater treatment. For the first time, the TiO_2 was electrochemically activated in the absence of light and without direct electrode contact in a packed bed material rather than being directly coated to the electrode surface. These novel TiO_2 pellets improve the electrocatalytic degradation efficiency of organic pollutants and provide a more sustainable approach due to the preservation and facile reuse of the pellets. Optimal conditions for fabrication of mechanical stable and catalytically active TiO_2 pellets included starting with high purity anatase powder pressure-compacted into pellets and sintered at 880 °C for 4 hr. The AP-F880 and AP-H880 pellets possess the highest catalytic activity for degrading the recalcitrant 1,4-dioxane and show the same trends when treating the pollutants lamotrigine and chlorobenzene.

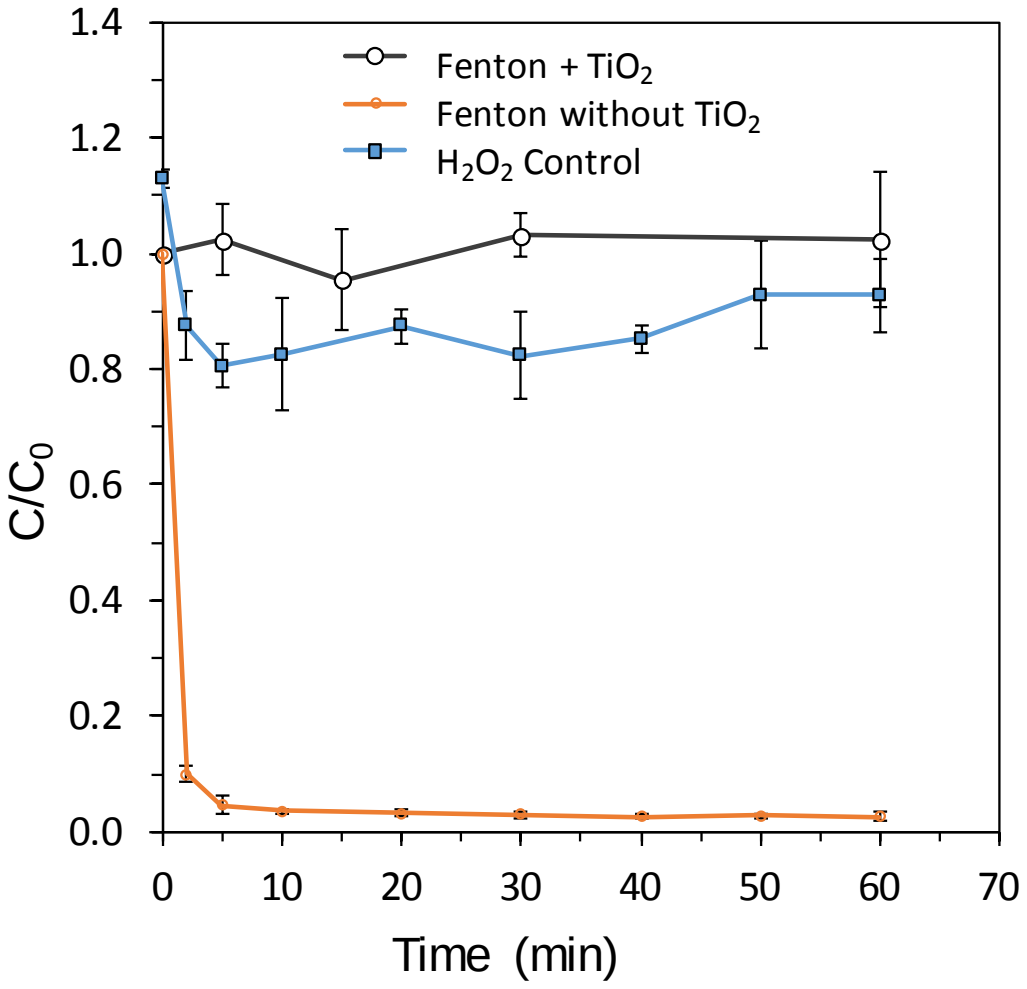

Figure 3.6 Relative concentration (C/C_0) of 10 µM 1,4-dioxane during treatment without voltage applied using Fenton's reagent (0.1 mM Fe^{+2} + 0.20 mM H_2O_2) with TiO_2 (140 g) and without TiO_2. A control experiment was performed with 1.0 H_2O_2 and no Fe^{+2} catalyst as well. Error bars represent the standard deviation (n = 3).

Mechanistic insights into dark catalysis of electrically insulated TiO_2. Based upon the results of batch reactor experiments, the dominant pathway appears to be the TiO_2 pellets being electroactivated at a distance by the electric field. We propose that the field effect is able to charge separate some portions of electrons into the conductance band and holes into the valence band. Charge separation along each TiO_2 pellet then can occur by diffusion of the most mobile charge carriers, the electron, leading to isolated holes capable of chemically oxidizing organic

molecules adsorbed to the TiO_2 surface. Additionally, these holes can oxidize adsorbed water to form [TiO_2 + $^{\bullet}OH$] species capable of oxidizing organic species also adsorbed.

We ruled out the possibility the activity simply being due to electrogenerated $^{\bullet}OH$ drifting to nearby TiO_2 pellets where the pollutant degradation could occur. The Fenton's experiment showed that without the electroactivation aspect, the activity of the TiO_2 was not there. Although there is agreement from most that hydroxyl radicals provide significant amount of the oxidizing power for electrolytic degradation processes, there is no consensus about the nature of M~$^{\bullet}OH$ as to whether reactions must happen at the electrode surface, or could detachment of $^{\bullet}OH(aq)$ potentially react with an organic molecule near the surface. However, it is generally accepted that due to the short half-life of $^{\bullet}OH$ radicals all, or most of their involvement, would need to happen within a few microns of the surface.[2, 55] Further evidence against the electrogenerated $^{\bullet}OH(aq)$ drift mechanism is provided by Kapalka, et al., estimating the profile of hydroxyl species adjacent to a BDD anode concurrent with the evolution of O_2 and suggested that there concentration falls to less than 10% of the value at the surface within 0.2 µm and essentially to zero by 1 µm.[70] This is eliminated because the geotextile insulator provides a gap of ~4 mm from electrode to the inter-electrode TiO_2.

Literature strongly supports that non-stoichiometry, i.e. TiO_{2-x}, and point defects within the lattice structure would have a substantial impact on catalytic properties as well.[136-138] These aspect are likely to be important, however, spectroscopic analyses of such surface properties were outside of the scope of this study. Future analysis of the oxidation state of Ti at the surface and surface hydroxyl abundance is warranted to better understand the fundamentals of catalyst chemistry which could lead to further optimization of its activity and range of applications an heterogeneous catalyst for electrochemical degradation. The ease-of-use and tunability of this

electrocatalytic treatment technology, along with the nontoxicity and stability of TiO_2 pellets, would warrant further investigation into field scale treatment only studies for polluted groundwater or wastewater streams, even if used in combination with other technologies.

CHAPTER 4

SYNERGISTIC TREATMENT OF MIXED 1,4-DIOXANE AND CHLORINATED SOLVENT CONTAMINATIONS BY ELECTROLYTIC STIMULATION OF *PSEUDONOCARDIA DIOXANIVORANS* CB1190[2]

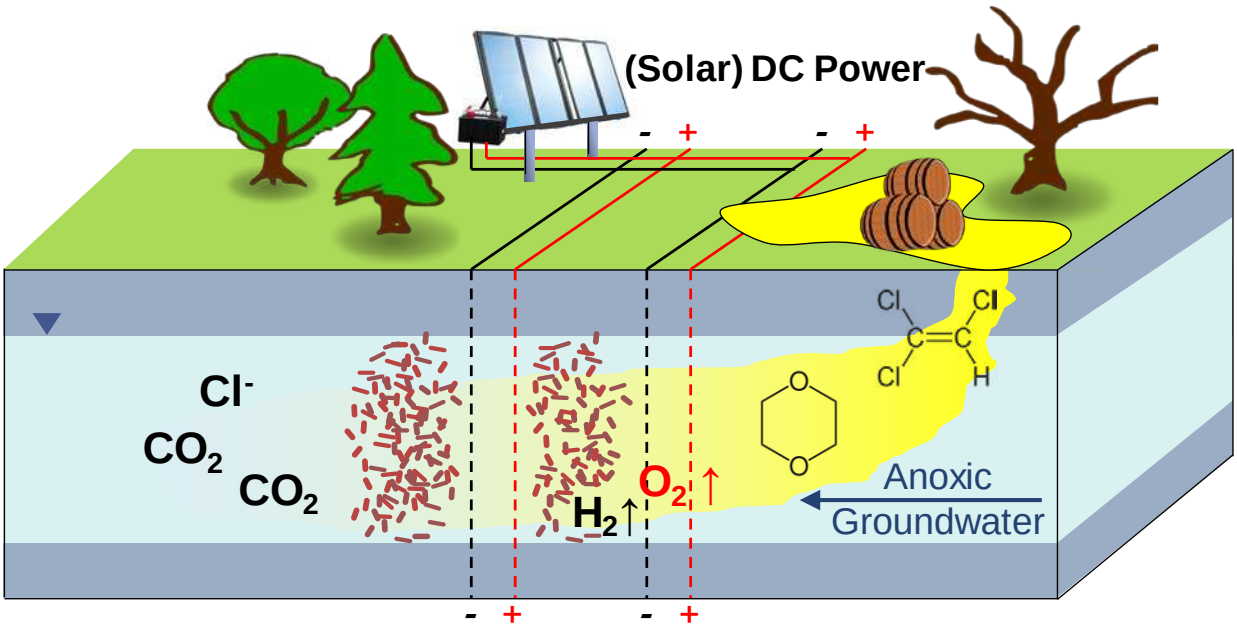

Conceptual Diagram

[2] Chapter 4 is taken from a manuscript that was recently submitted to *Environmental Science & Technology Letters* with authors: Jasmann, J.R., Gedalanga, P.B., Borch, T., Mahendra, S., and Blotevogel, J. All sampling, sample preparation, analytical chemistry, reactor construction and other work described was performed by me, except for the qPCR analysis which was performed by our collaborators in UCLA: P. Gedalanga and S. Mahendra – with DNA extraction assistance from Michelle Myers and Shu Zhang. The *Pseudonocardia dioxanivorans CB1190* culture was also sent to us from UCLA.

CHAPTER SYNOPSIS

Biodegradation of the persistent contaminant 1,4-dioxane in groundwater is often hindered by the absence of dissolved oxygen and the co-occurrence of microbially inhibiting chlorinated solvents. Using flow-through reactors with mesh electrodes, we show that electrolytic stimulation of *Pseudonocardia dioxanivorans* CB1190 leads to an over-additive treatment effect. At 3.0 V applied, 1,4-dioxane was oxidized three times faster than in unstimulated biodegradation controls, and twelve times faster than by electrolysis only. Quantitative PCR analyses revealed that microbial growth was generally promoted by anodic oxygen-generating reactions, yet at a higher voltage of 8.0 V, the planktonic cell abundance near the anode decreased due to unfavorable conditions. Slower 1,4-dioxane biodegradation rates were observed in the presence of trichloroethene, unless the voltage was high enough to sufficiently remove the inhibiting co-contaminant. Our results demonstrate that electrolytic stimulation is a viable synergistic approach for *in situ* treatment of 1,4-dioxane in mixed contaminant plumes.

INTRODUCTION

1,4-Dioxane is an emerging groundwater contaminant that is frequently observed at sites impacted by chlorinated volatile organic compounds due to its widespread use as solvent stabilizer.[12, 17, 139] Recent reports of contaminated site data from across the United States highlight the high probability of co-occurrence of 1,4-dioxane with trichloroethene (TCE) and 1,1,1-trichloroethane (TCA).[17, 140, 141] 1,4-Dioxane's miscibility in water and low sorption affinity to soil make it highly mobile in groundwater, often leading to large plume development.[142] Advanced oxidation processes (AOP) have shown success in mineralizing 1,4-dioxane, but their field implementability and high cost typically limit their use to *ex situ* treatment of comparatively small source zones and plumes.[62, 81, 143]

A limited number of laboratory studies have documented aerobic biodegradation of 1,4-dioxane either co-metabolically[5, 144, 145] or metabolically,[3, 4, 146] and one study demonstrated microbially driven Fenton-based degradation[147] of 1,4-dioxane. These studies suggest that *in situ* bioremediation of 1,4-dioxane is generally possible. However, two factors may limit the site-specific biodegradation potential for 1,4-dioxane: (1) anoxic groundwater conditions, and (2) inhibition by chlorinated solvents.[6, 148, 149] Mahendra et al. reported that both TCA and its abiotic breakdown product 1,1-dichloroethene (1,1-DCE) caused inhibition of the 1,4-dioxane-metabolizing strain *Pseudonocardia dioxanivorans* CB1190, with inhibition shown to be non-competitive and reversible.[6] Hand et al. provided evidence for TCE-inhibition of 1,4-dioxane biodegradation by two co-metabolizing bacteria, *Mycobacterium vaccae* JOB5 and *Rhodococcus jostii* RHA1.[148] Novel biomarkers and groundwater concentration data from 2000 to 2013 revealed evidence of natural 1,4-dioxane attenuation in plumes co-contaminated with TCE;[140, 150, 151] however, degradation rates were negatively correlated with chlorinated volatile organic compound concentrations and limited to aerobic regions of the aquifers. These studies suggest that in order for *in situ* biodegradation of 1,4-dioxane to become a widely used remediation strategy, some form of stimulation or augmentation is required, along with an economical treatment process for toxic co-contaminants such as TCE.[5, 152]

Permeable mesh electrodes installed perpendicular to groundwater flow[44] can produce dissolved molecular oxygen[30] through the electrolysis of water, creating favorable conditions for *in situ* aerobic biodegradation in previously anoxic aquifers.[153, 154] Furthermore, this electrochemical AOP is also capable of direct 1,4-dioxane oxidation[39, 40, 155] and oxidation/reduction of chlorinated solvents.[43, 68, 156] We thus hypothesized that the combination of electrolysis with biodegradation will lead to a synergistic treatment effect through electro-

generation of O_2 as electron acceptor while electrochemically removing microbially inhibiting co-contaminants such as TCE. Specific objectives were to determine optimum stimulation voltages and to elucidate potentially detrimental effects of applied potentials on microbial abundance using quantitative polymerase chain reaction (qPCR) analyses. Consequently, this is the first study to provide a fundamental basis for *in situ* electro-bioremediation as a synergistic treatment technology for 1,4-dioxane in mixed contaminant plumes.

MATERIALS AND METHODS

Flow-through column reactors. Flow-through experiments were performed using chemically disinfected 10-cm I.D. clear PVC column reactors, packed with 8/10 mesh quartz silica sand and two permeable, circular mesh electrodes (one anode, one cathode) installed perpendicular to flow (Appendix C, Figures S4.1-S4.2). Mesh Ti/IrO_2-Ta_2O_5 electrodes (Corrpro, Medina, OH) were selected based upon previous studies demonstrating their long service life and ability to degrade aqueous organic contaminants as *in situ* permeable electrolytic reactors.[43, 44] with a particular affinity to more chlorinated species due to favorable surface chemistry interactions.[67, 68, 114] Additionally Ti/IrO_2-Ta_2O_5, having a low overpotential for O_2 evolution of 0.25 V, is known to be a good catalytic surface for oxygen evolution reactions in water.[30, 64] For abiotic controls, column reactors were packed with sand after heat-sterilization at 232 °C for 18 hours. For biological controls and synergistic voltage/biological experiments, sand inoculated with active CB1190 cultures was transferred into column reactors once mid- to late-exponential growth phase was observed. These cultures were grown aerobically in ammonium mineral salts (AMS) medium[3] at 30 °C for 2-3 weeks with 50-200 mg/L 1,4-dioxane as sole energy and carbon source (Figure S4.3).

Contaminant analysis. Twenty-liter glass carboys were used for feedstock solutions of de-gassed AMS media spiked with 100 mg/L 1,4-dioxane (99.98%, Honeywell Burdick & Jackson), and an additional 5 mg/L TCE (99.5%, Alfa Aesar) for co-contaminant investigations. All flow-through sand column experiments were operated at 23 ± 2 °C and a flow rate of 1.07 mL/min (seepage velocity 46 cm/d). Aqueous contaminant concentrations were monitored at steady-state to minimize sorption effects (previous studies had shown that 1,4-dioxane sorption in these columns is negligible).[155] Filtered samples (0.45-µm nylon filters for 1,4-dioxane-only samples and 0.20-µm PTFE filters for samples containing TCE) were analyzed with an Agilent 6890N gas chromatograph and mass selective detector (GC/MSD) equipped with a Restek Rxi-624Sil MS column using 1,4-dioxane-d_8 isotopic dilution. Chlorinated ethenes were quantified by an Agilent 6890N GC equipped with an electron capture detector (GC/ECD).

Microbial analysis. At start and completion of flow-through experiments, 0.5-mL liquid samples and 0.5-g solid sand samples were collected into 2.0-mL microcentrifuge tubes and frozen at -20°C. Liquid sample aliquots were taken from influent, ports 1, 2, 3 and effluent, while sand samples were only collected from ports 1, 2 and 3 (Figure S4.1). Deoxyribonucleic acid (DNA) was extracted from sand and liquid phase samples using a bead beating method followed by phenol/chloroform purification. Briefly, liquid samples were centrifuged to pellet the biomass for 3 minutes at 13,200 x *g*. The supernatant was discarded and the pellet was subjected to total DNA extraction, while 0.25 mL of extraction buffer, 0.1 mL 10% SDS, and 1 mL saturated phenol was added to all tubes. Samples were heated at 65˚C for 2 minutes followed by bead beating for 2 minutes using a minibead beater-16 (Biospec Products, Bartlesville, OK). Lysed samples were incubated at 65˚C for 8 min followed by another round of bead beating for 2 min. Samples were centrifuged and the lysate was transferred to a sterile 1.7-mL microcentrifuge tube

for phenol/chloroform purification as previously described.[157] Nucleic acid extracts were resuspended in 100 µL of nuclease-free H_2O and stored at -80˚C until further analyses.

CB1190 populations were monitored using qPCR and primers targeting the (dxmB) genes coding for dioxane monooxygenase.[157] All qPCR reactions were performed in a total volume of 20 µL containing 1X Kapa Sybr Fast qPCR Master Mix (Kapa Biosystems, Wilmington, MA), 0.25 µM of each primer (IDTDNA, San Diego, CA), and 2 µL of template DNA. All reactions were performed on an Applied Biosystems StepOnePlus real-time PCR system (Life Technologies, Carlsbad, CA) as previously described[157] and were accompanied with a melt curve analysis to confirm the specificity of qPCR products.

RESULTS AND DISCUSSION

Stimulation of 1,4-dioxane degradation. To simulate an *in situ* field implementation of an electrolytic permeable reactive barrier (TOC Art), we used sand-packed flow-through columns equipped with two permeable mesh electrodes.[44] *P. dioxanivorans* CB1190 was used as model organism due to its growth-supporting metabolism of 1,4-dioxane.[4, 157, 158]

Figure 4.1 shows that in the absence of TCE, only 11.6 and 14.6 mg 1,4-dioxane were oxidized per hour per m^2 of mesh electrode surface area in the abiotic electrolytic flow-through reactors at 8.0 V and 3.0 V, respectively. These low abiotic removal rates are likely explained by saturation of electrode active sites and limited generation of reactive oxygen species (ROS).[55] In the biological control column (no voltage) with oxygen-depleted (degassed) feedstock, the CB1190 culture oxidized 1,4-dioxane at a rate of 53.2 $mg \cdot h^{-1} \cdot m^{-2}$. When both abiotic and biotic processes were combined, oxidation rates substantially increased in an over-additive manner to 101 $mg \cdot h^{-1} \cdot m^{-2}$ at 8.0 V and 169 $mg \cdot h^{-1} \cdot m^{-2}$ at 3.0 V. The observation of O_2 gas bubbles at the

anode led us to conclude that CB1190 were stimulated by increased electron acceptor levels.[153] Hence, by extending oxidation processes beyond the electrode surface, electro-biostimulation doubled to tripled 1,4-dioxane degradation rates when evaluated against the biological control, and increased rates by about an order of magnitude compared to electrochemical degradation only.

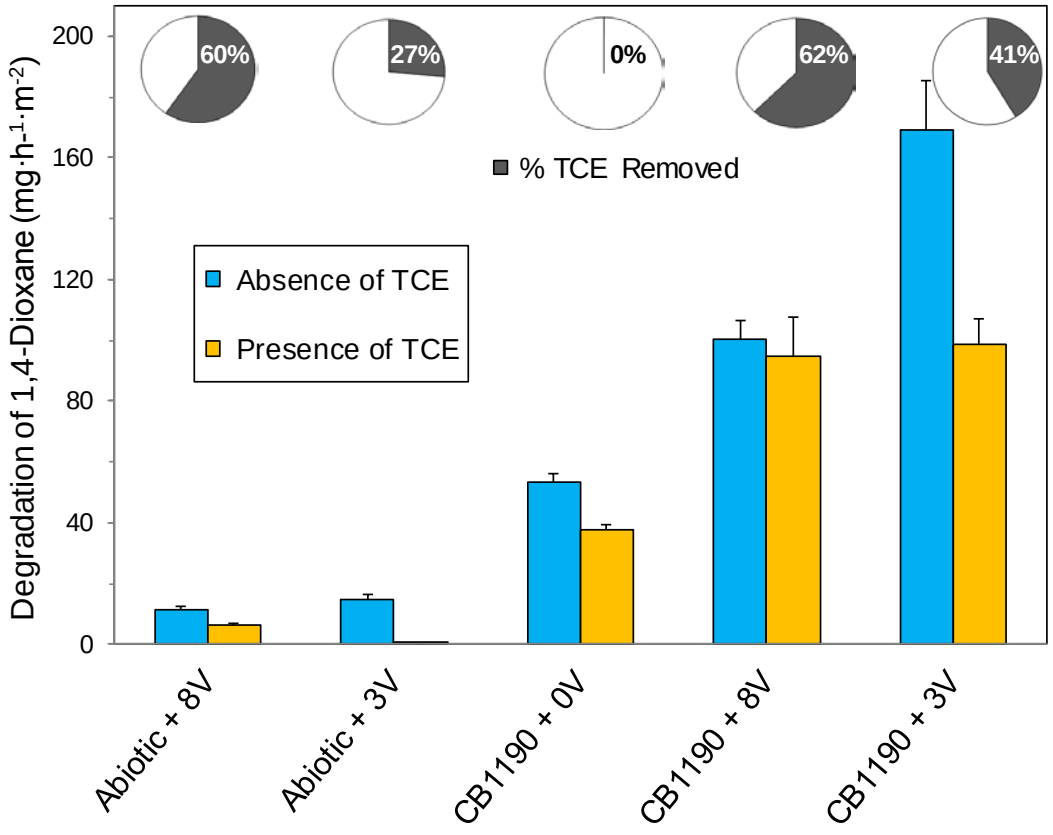

Figure 4.1 1,4-Dioxane degradation rates in flow-through sand reactors in the absence (blue) and presence (orange) of TCE co-contaminant. The percentage of TCE degraded during the mixed co-contaminant experiments is represented by the shaded region of the pie charts above each experiment. All feedstock solutions consisted of 100 mg/L 1,4-dioxane [and 5 mg/L TCE] in AMS nutrient media, treated at a seepage velocity of 46 cm/d. Error bars indicate standard deviation ($n \geq 3$).

The potential for adverse effects to microbes near the electrodes was investigated by analyzing liquid and solid (sand) aliquots along the horizontal flow path for *P. dioxanivorans* CB1190 abundance. Due to the electrolysis of water and dissolved aqueous chemical species, extreme pH and redox conditions may evolve in the vicinity of the electrodes. In addition, biologically destructive hydroxyl radicals[159] and highly oxidized chlorine species[103, 160] may be generated. Consequently, qPCR data can help elucidate preferential location(s) of microbial attachment or growth, leading to a better understanding of optimum spacing between multiple electrode pairs.

Upon inoculation of the sand columns for degrading 1,4-dioxane only, mean abundance values were 4.5×10^8 cells/mL for planktonic and 1.3×10^7 cells/g for sessile CB1190 present as biofilm (Figure 4.2(a,b)). After two weeks of flow-through operation in the biological control column without voltage, the planktonic CB1190 abundance along the sand column averaged 3.5×10^8 cells/mL, thus remaining very near the initial baseline count. To maintain this steady-state population, growth and reproduction must have occurred at rates sufficient enough to account for biomass losses of $>10^7$ cells/min (1.03×10^7 cells/mL × 1.07 mL/min flow) to the effluent triggered by hydraulic shear. Therefore, removal of 1,4-dioxane can be explained by biodegradation since column conditions in the degassed feedstock are sufficiently favorable for the microaerophilic *P. dioxanivorans* CB1190 to maintain steady growth on 1,4-dioxane.[4] Abiotic control experiments were also monitored with qPCR and provided in Appendix C (Figure S4.4).

At a low stimulation voltage of 3.0 V, average planktonic abundances of 1.5×10^8 cells/mL indicate that the conditions remained conducive to cellular growth (Figure 4.2(a)). At sample port 1 between the electrodes (located 2.5 cm downstream of the anode), planktonic cell

counts were slightly lower than without voltage applied, and biofilm cell counts were below detection limit. Here, the pH dropped to 4.7 (Figure S4.5), which is at the low end of the optimal range for CB1190 growth near pH 5-8.[3] The subsequent CB1190 population rebound 12.5 cm downstream of the anode reveals the "sweet spot" for bacterial abundance along the flow path. Here, immediately after the cathode, the pH returned to circumneutral (6.5) and short-lived reactive oxidizing species are potentially depleted. These localized maximum cell counts suggest that sloughing of biofilms may be an important source of 1,4-dioxane-degrading bacteria and could warrant further study into the predominance of the role played by these detached cells.[161]

When a higher electrolytic stimulation voltage of 8.0 V was used, a substantial decrease in planktonic abundance to 4.8×10^4 cells/mL was observed between the electrodes, along with biofilm levels dropping to below the detection limit (Figure 4.2(a,b)). A more acidic pH of 3.1, along with greater anodic production of reactive oxygen species associated with higher voltages,[55] apparently created less favorable conditions for microbial growth or survival. Although planktonic cells did rebound to 2.3×10^8 cells/mL 12.5 cm downstream from the anode, biofilm counts remained below detection limits for the remainder of the column. This CB1190 population decline likely explains why the 1,4-dioxane degradation rates were lower at a higher stimulation voltage.

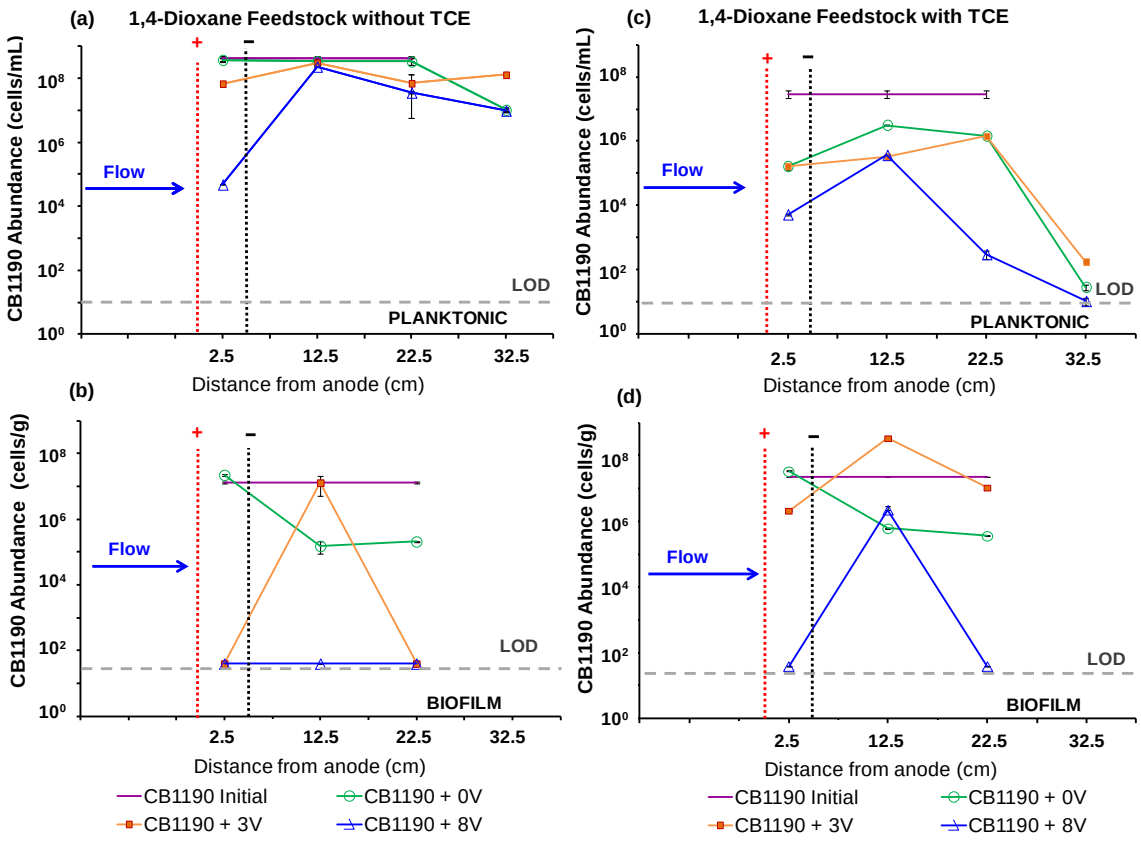

Figure 4.2 CB1190 abundance along the flow path for planktonic (a,c) and biofilm cells (b,d) in the absence (a,b) and presence (c,d) of TCE co-contaminant, plotted as a function of distance from the anode. Sampling ports 1, 2 and 3 correspond to 2.5, 12.5 and 22.5 cm, the column effluent is located at 32.5 cm. Any samples that were below the detection limit of the biofilm qPCR analysis were plotted at 4×10^{1} cells/g, which was the method detection limit. The error bars represent the average range of qPCR duplicates.

Co-contaminant impact on 1,4-dioxane degradation. In the presence of the common co-contaminant TCE, abiotic control experiments showed slightly lower 1,4-dioxane degradation rates of 6.4 $mg{\cdot}h^{-1}{\cdot}m^{-2}$ (8.0 V) and 0.06 $mg{\cdot}h^{-1}{\cdot}m^{-2}$ (3.0 V, Figure 4.1), suggesting that competition for active sites on the mesh electrode negatively impacted 1,4-dioxane removal. In these two reactors, 60% and 27%, respectively, of TCE was removed.[43, 68] No chlorinated reduction products of TCE were detected, implying that TCE was either oxidized or volatilized by ebullient oxygen and hydrogen gas bubbles.[162]

In the biological control column, TCE inhibition lowered 1,4-dioxane biodegradation rates from 53.2 to 37.5 $mg \cdot h^{-1} \cdot m^{-2}$(Figure 4.1). No TCE removal was observed, confirming previous reports that *P. dioxanivorans* CB1190 is not capable of biodegrading TCE.[6] 1,4-dioxane oxidation rates were highest again when both abiotic and biotic processes were combined, having rates of 94.5 $mg \cdot h^{-1} \cdot m^{-2}$ at 8.0 V and 98.4 $mg \cdot h^{-1} \cdot m^{-2}$ at 3.0 V. At the higher stimulation voltage (8.0 V), 62% of TCE was removed, apparently sufficient to eliminate adverse effects on biodegradation by CB1190 such that 1,4-dioxane removal rates were nearly equivalent to rates when TCE was not present. In contrast, despite the removal of 41% of the initial TCE load with 3.0 V applied, 1,4-dioxane biodegradation was still inhibited. However, it is critical to point out that even when TCE was present, the same trend of substantial enhancement in electro-biodegradation rates over the biological control rates was observed. Thus, aerobic biodegradation enhancement of 1,4-dioxane occurs both by concurrent removal of the inhibiting co-contaminant and electrochemical generation of molecular oxygen.

In the presence of TCE, qPCR analyses revealed that planktonic cell counts were generally orders of magnitude lower than when TCE was not added, reflecting the inhibiting effect of the chlorinated co-contaminant (Figures 2(c)). Nevertheless, the biological control and CB1190 + 3V were able to stabilize microbial populations at levels capable of maintaining 1,4-dioxane degradation. In this mixed contaminant scenario, mean biofilm abundance in the biological control (1.2×10^7 cells/g) and CB1190 + 3V (1.2×10^8 cells/g) columns were both consistently high, while CB1190 + 8V experienced extremely low biofilm counts (below detection limit) between the electrodes (2.5 cm) and at 22.5 cm downstream of the anode (Figure 2.2(d)). A substantial spike in sessile cell abundance at 12.5 cm downstream was experienced in both of the electro-biostimulation reactors, achieving 10^7-10^8 cells/g, lending further support to

our “sweet spot” hypothesis for optimum bacterial growth. The presence of biofilms can be explained by their greater ability to withstand pH changes and (short-lived) ROS.[163] Based upon the consistency of the location of peak sessile cell counts, it appears that biofilm formation is also being used as a strategy of colonization in a nutrient-dense and oxygen-rich area, where sloughing of cells can then occur, providing the majority of observable biodegradation.[163]

Technological implications. Our results clearly demonstrate that electrolytic stimulation of aerobic biodegradation is an effective, synergistic approach for the remediation of groundwater contaminated with 1,4-dioxane, even in mixed contaminant plumes. In the absence of a co-contaminant, where stimulation is mainly based on oxygen generation, low voltages only slightly above the oxygen evolution potential are preferable to limit generation of harsh conditions unfavorable for microbial growth. When microbially inhibiting co-contaminants such as TCE are present, higher voltages or more electrodes may be required in order to mineralize or transform them into less toxic or biodegradable intermediates. However, when 1,4-dioxane degradation rates at low and high voltage are similar, such as in this study, the lower voltage is preferable due to longer electrode lifetime, lower power cost, more uniform flow, and a lower potential for disinfection by-product formation.[55, 103, 160] Our data also suggest that microbial degradation activity is highest just downstream of the cathode, implying that when several electrode pairs are needed to reach site-specific remediation targets, spacing on the order of 10-20 cm should be used. Finally, it is conceivable that additional synergistic mechanisms exist, such as stimulation of other intrinsic microbes capable of degrading chlorinated solvents[164] or electrolytic transformation of a persistent parent compound into more readily biodegradable intermediates.[96, 156, 165, 166] The joint benefits of having tunable electrolysis to degrade recalcitrant pollutants while simultaneously stimulating intrinsic or augmented contaminant-degraders

strongly suggests that this technology can be used for the *in situ* treatment of mixed contaminant plumes.

CHAPTER 5

SUMMARY

Major findings. This body of work further builds and improves upon previous laboratory-scale and field-scale electrolytic treatment studies performed within the Center for Contaminant Hydrology here at Colorado State University.[44, 67, 68] For the first time, experiments were conducted to investigate catalytic enhancement strategies with electro-activated dark TiO_2 catalysis and electrochemical stimulation of microbial biodegradation processes. We demonstrated 1,4-dioxane can be efficiently degraded using flow-through electrochemical reactors, instead of stirred batch reactors, in order to simulate conditions more applicable to field scale remediation (Chapter 2). It was determined an electrical potential of 8V was effective for catalyzed electrochemical oxidation of 1,4-dioxane, with only minor improvements in efficiency observed at 11.0 V and 14.0 V. Thus, for field applications, higher voltages would not be worth the added energy consumption and decrease in faradaic current efficiency. The decreased degradation current efficiency is due to the FTER system being rate-controlled by contaminant transport phenomena (diffusion mainly) and not current (Chapter 2).

Significant improvements in 1,4-dioxane degradation rates were observed under all conditions tested when using inter-electrode TiO_2 pellets as a catalyst, typically achieving 2 to 5 times more pollutant removal (Chapter 2 and Table S2.2). More than 97% of 1,4-dioxane was removed by TiO_2-catalyzed FTERs after 6 anodes at 11.0V with a seepage velocity of 30.6 cm/d. The most notable catalytic improvement in 1,4-dioxane degradation efficiency occurred in low ionic strength water (70% degradation vs. no degradation without catalysis), where conventional

electrochemical approaches typically fail,[66] thus expanding application possibilities to aquifers with low total dissolved solids.

Moreover, we revealed for the first time that electrically insulated, inter-electrode TiO_2 can be electrochemically activated in the dark to catalyze the oxidation of organic contaminants. Mechanistic aspects of this process were further explored in Chapter 3. These TiO_2 pellets mitigate mass transport limitations by using TiO_2 pellets to extend reactive surfaces to the bulk solution between electrodes. FTER experiments with various types of TiO_2 pellets indicated that anatase form pellets showed greatest catalytic impact on the degradation of 1,4-dioxane (Chapter 3). Research by others has shown that anatase, especially the [1 0 1] crystalline face, has surface chemistry properties conducive to the formation of activated surface complexes with H_2O and/or organic pollutants adsorbed to the surface, and often outperforms the rutile phase as a heterogeneous catalyst.[45] These anatase pellets had higher specific surface area and more widely distributed porosity than the rutile pellets, likely contributing to their improvement performance. Batch reactor experiments showed that the dominant mechanism for the activation of the inter-electrode TiO_2 pellets is unique to previous reported photocatalytic and electrocatalytic mechanism (Chapter 3). We propose that the electric field is able to mobilize electrons from the valence band of TiO_2 into the conductance band, leaving behind positively charged holes in the valence band. These holes have very strong oxidation power (2.7 V vs. SHE) and are capable of chemically oxidizing organic molecules adsorbed to the TiO_2 surface. Additionally, these holes can oxidize adsorbed water to form [TiO_2 + $^{\bullet}OH$] species capable of oxidizing organic species also adsorbed.

Our results demonstrate that electrolytic stimulation is also an effective, synergistic approach for treating 1,4-dioxane-contaminated waters, even in mixed contaminant plumes.

When both electrolytic and microbial processes were combined, 1,4-dioxane oxidation rates substantially increased in an over-additive manner to 101 $mg \cdot h^{-1} \cdot m^{-2}$ at 8.0 V and 169 $mg \cdot h^{-1} \cdot m^{-2}$ at 3.0 V, compared to only 11.6 $mg \cdot h^{-1} \cdot m^{-2}$ for abiotic 8.0 V treatment and 53.2 $mg \cdot h^{-1} \cdot m^{-2}$ with 0 V using biodegradation alone (Chapter 4). The qPCR analysis helped to elucidate a "sweet spot" for microbial growth at about 12.5 cm downstream of the anode in our FTER experiments. Thus, this would also be the area of greatest biodegradation rates of 1,4-dioxane as the primary carbon and energy source. Higher dissolved O_2 concentrations were measured in the electrochemically stimulated FTERs (Table S4.1) adding support to the claim of more favorable aerobic conditions being produced downstream (downgradient) from the electrodes. When chlorinated co-contaminants such as TCE are present, higher voltages or more electrodes may be required to mineralize these microbial degradation inhibitors, or at least transform them into less toxic and more easily biodegradable intermediates (Chapter 4). None of the reduced transformation products (e.g. 1,1-DCE, vinyl chloride) were detected in the effluent of our FTER experiments. Based upon dominant pathways observed in electrochemical degradation of chlorinated solvents in previous work,[133, 156] and due to the anode being the lead electrode in our FTER experiments, it is plausible that oxidized, and more easily biodegradable, intermediates were formed.

When 1,4-dioxane degradation rates at low and high voltage are similar, such as in this study, the lower voltage is preferable due to longer electrode lifetime, lower power cost, more uniform flow, and a lower potential for toxic by-product formation.[55, 103, 160] The joint benefits of having tunable electrolysis to degrade recalcitrant pollutants while simultaneously providing electrolytic stimulation of intrinsic or augmented contaminant-degraders makes this technology very promising for the *in situ* treatment of mixed contaminant plumes, and pilot scale testing should be pursued.

Advantages and limitations. Some clear advantages of our two catalyzed AEO treatment processes exist over standard UV-based AOPs including the potential for *in situ* remediation of groundwater, the benefit of not needing to supplement with expensive chemical oxidants, and better economic & environmental footprint based upon cost comparisons performed in the literature.[23, 43, 96, 102] However, recent reviews highlight important challenges and knowledge gaps slowing down the widespread use of electrochemical oxidation for wastewater and groundwater treatment: (a) mass transfer limitations due to the intrinsic requirement for adsorption of target pollutants with electrode surfaces, (b) incomplete knowledge of matrix effects and disinfection by-product (DBP) formation, and (c) limited studies on the environmental footprint and economic costs of AEO treatments compared to other AOPs under environmentally relevant conditions. [55, 63, 103]

The scope of this dissertation is not able to solve all of these challenges, however many of these limitations and knowledge gaps were in mind during experimental design phase and continue to be a focus as this research moves forward into field scale reactors and testing in more complex matrices. For example, our flow-through electrochemical reactors attempted to address the mass transfer challenges by using an inter-electrode TiO_2 catalyst to fill the inter-electrode space usually back-filled with inert material and quantify the effects of operational parameters most important to field scale applications. In recognizing the need to lower costs (with less power and electrode material requirements) and reduce the potential negative chlorinated byproducts formed, we showed that low voltage settings (3.0 V) on one pair of electrodes was enough to degrade co-contaminant TCE and electro-stimulate *Pseudonocardia dioxanivorans* bacteria to aerobically biodegrade 1,4-dioxane. However, there is still a need to do more systematic testing of complex matrices, with chloride ions present capable of producing toxic

chlorinated hydrocarbon byproducts, or having bicarbonate present which is known to be an efficient •OH scavenger.[167]

This research was always performed with the intent to develop a field scale technology capable of providing a remediation solution to 1,4-dioxane-contaminated groundwater. As part of this aim, a separate treatability study was performed on original site groundwater from a former 1,4-dioxane production plant in the Netherlands which has 1,4-dioxane concentrations around 1,000 mg/L. Non-catalyzed FTERs were used to treat the groundwater influent at 11.0V and flowing at 15 cm/d (to match groundwater seepage velocity at the site). High degradation efficiencies were obtained, with a single pass through 2 anodes resulting in 84% removal of the initial 928 mg/L 1,4-dioxane, with most of that becoming fully mineralized to CO_2 based upon Shimadzu TOC analysis (Figure 5.1). Continuing the treatment through 2 more anodes achieved 97% removal. This high removal efficiency is likely due to this saline groundwater having a high conductivity of > 4,000 μS/cm which was shown to greatly impact electrolytic oxidation performance in our laboratory studies (Chapter 2). These results opened up the opportunity to build six larger electrochemical column reactors (30.5 cm I.D. x 46 cm L) shown in Figure 5.2 which are now in operation on site as a pilot study to measure 1,4-dioxane degradation, monitor for DBPs[160], and provide a side-by-side comparison of removal efficiency and economic costs with UV/AOP treatment operating in parallel.[55] These field scale reactors were built and implemented by Jens Blotevogel, and figure 5.2 shows how sand packing does allow for a very uniform distribution of red dye (a visual analogy for pollutants in the water), helping to confirm that assuming quasi-plug flow in our reactors is an acceptable approach. Results from this pilot study are beyond the scope of my dissertation, but the quantitative comparison to UV/AOP

treatment will be provide invaluable insight into the relative advantages and disadvantages of the AEO system.

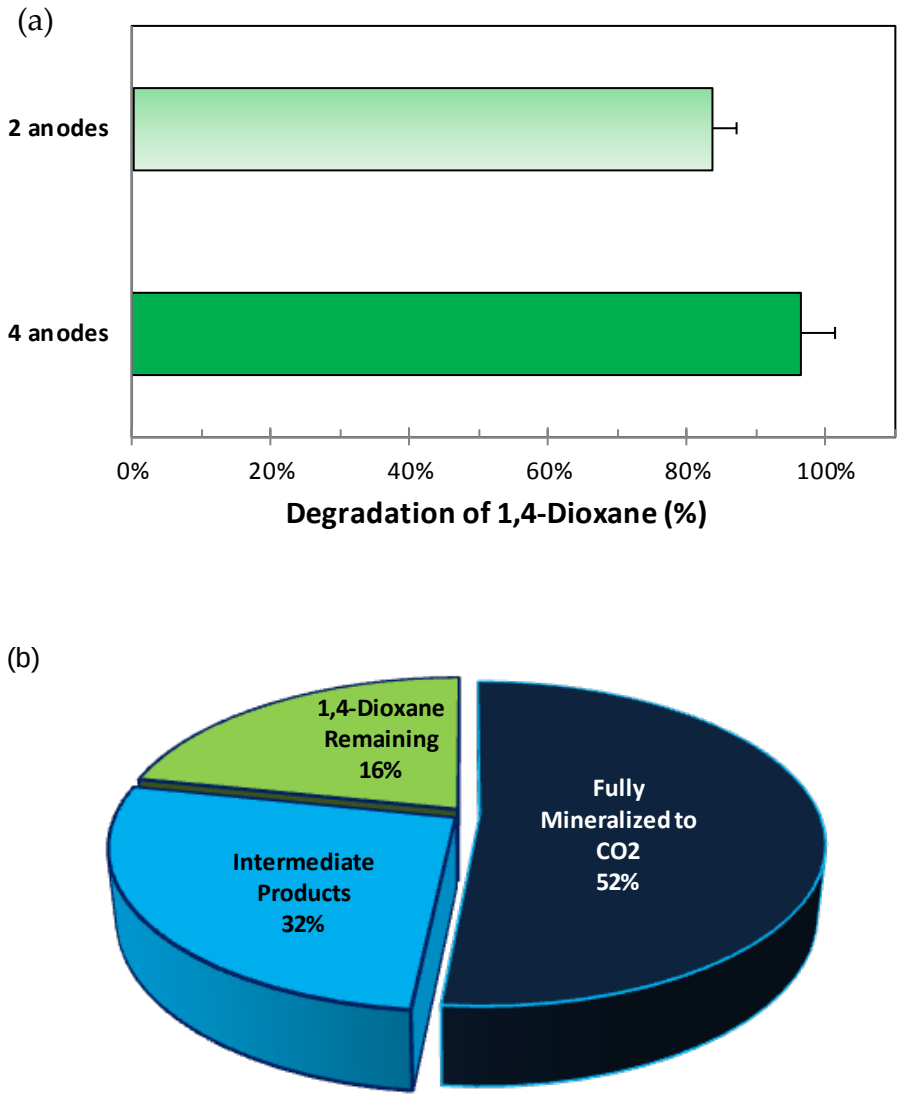

Figure 5.1 (a) Degradation of 1,4-dioxane (%) in original groundwater from an industrial site in the Netherlands after sequential AEO treatments in two FTERs operated at 11.0 V and seepage velocity of 15cm/d. Error bars represent standard deviation, n = 3. (b) Relative distribution of the 84% of 1,4-dioxane removed to either CO_2 or other organic intermediate products. A partial description of the groundwater composition included: 928 mg/L 1,4-dioxane, 1.1mg/L dissolved Fe^{+2}, 89 mg/L chlorides, with a pH of 7.8 and specific conductivity of 4.4 mS/cm.

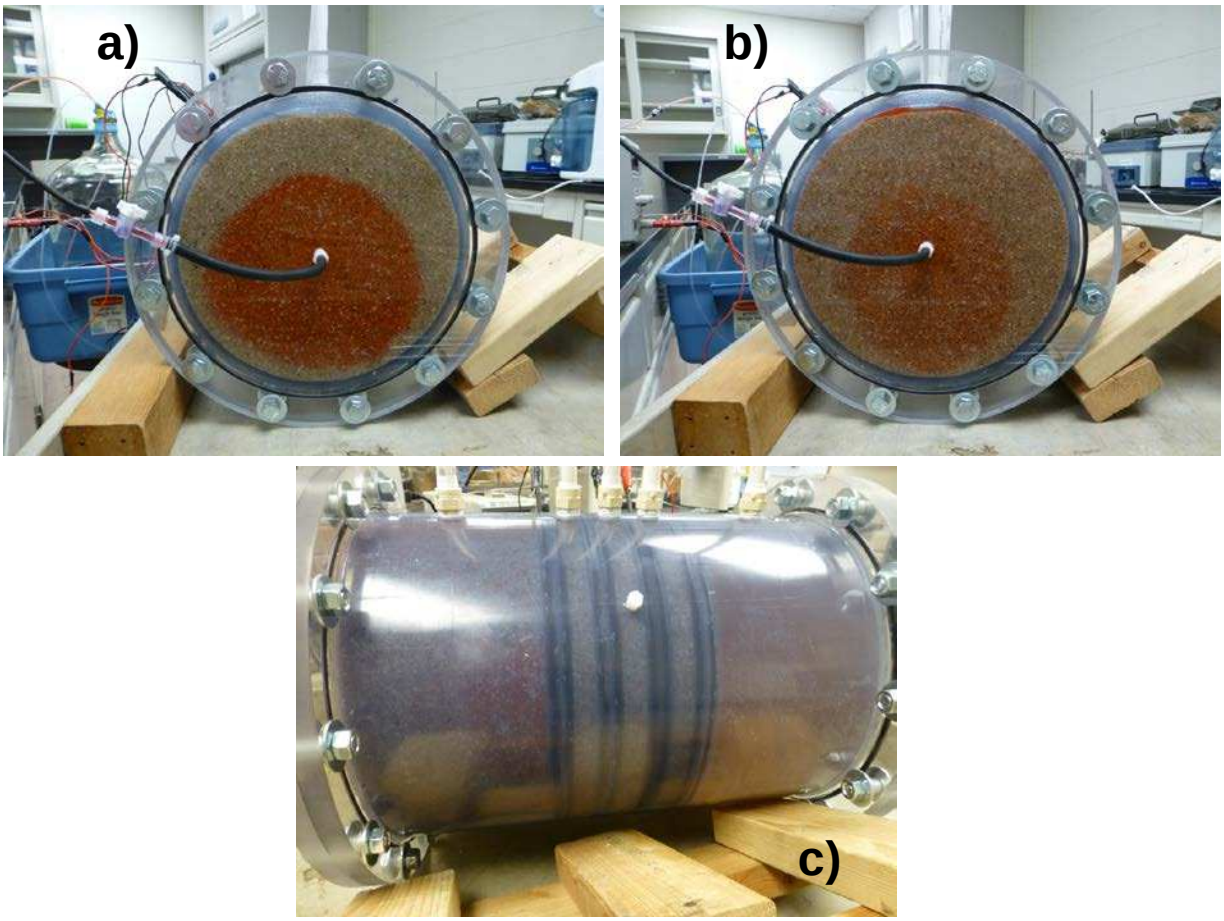

Figure 5.2 (a) Photo showing red food dye tracer test 4 h after start: The influent dye spreads out right at the entrance to the column reactor. Some density effects of the dye tracer are apparent. (b) Photo 20 h after start, showing the dye is spread out over the entire cross section with the primary injection halo still visible. (c) Side view photo 20 h after start, showing the red dye tracer is almost uniformly (though not perfectly) distributed throughout the entire volume before reaching the initial anode. This red food dye tracer test was performed by Jens Blotevogel in a large 30.5-cm I.D. FTER.

Future work. These results described here suggest that AEO treatment of recalcitrant aqueous pollutants is a promising field of research and plenty of opportunities and interesting questions remain for future Ph.D. dissertations. Briefly, here are three future directions in which productive research could be found:

- Diversify the analytical techniques to better understand the underlying processes
- Investigate AEO treatment in more complex mixtures and in field scale applications

- Explore “non-active” electrodes and AEO transferability to other contaminants

Due to limitations of time and funding, certain analytical techniques were outside the scope of this project. However, further investigations are needed to better understand the mechanism of electrochemical activation of TiO_2 in dark conditions. Analysis of the TiO_2 catalyst with X-ray photoelectron spectroscopy (XPS) could be used to quantitatively determine elemental composition, binding energies, and chemical/electronic state of surface elements of catalyst or possible elements contaminating the surface. This would help to better understand whether reduced Ti^{+3} and oxygen vacancies are prevalent. *In situ* Fourier transform infrared spectroscopy (FTIR) would help define functional groups bonded to the surface and their relative oxidation states, especially important for knowing the abundance of hydroxyl species. New probing molecules could be explored with well-defined degradation branching ratios depending on whether they are degraded by $(^{\bullet}OH)_{aq}$, direct anodic oxidation, or by TiO_2 hole mediated reactions.

With appropriate light absorbing contaminants, glass electrochemical chambers connected to a potentiostat and capable of *in situ* IR or UV-Vis spectroscopy would allow real-time monitoring of electrochemical changes in coordination with chemical transformations quantified by changes in absorbance. Another cutting-edge technique for real-time monitoring of electrochemical transformation products was tested in collaboration with Patrick Brophy of the Delphine Farmer group. On-line analysis of the headspace in a sealed electrochemical batch reactor monitored the organic acid transformation products of 1,4-dioxane degradation using high resolution time-of-flight, chemical ionization mass spectrometry (HR-TOF-CIMS), a novel analytical technique explained in more detail in Brophy and Farmer 2015.[168] The preliminary mass defect plots obtained are shown in Appendix E. These plots reveal the potential for rapidly

observing differences in product formation from 1,4-dioxane degraded in three different systems: Fenton's reagent without current, electrochemical degradation at 1.0 Amp both with and without catalytic TiO_2 pellets. Moreover, this technique can obtain these mass spectra data from complex aqueous samples without any pre-separation chromatography, pre-concentration or sample preparation. With better control of variables and potential interferences, non-targeted mass spectra data like this could be very useful when combined with complementary data from other analytical techniques.

The investigation into matrix effects, DBP formation, and quantitative comparison of performance are all being addressed in the ongoing pilot study described earlier. However, it is well known that the selectivity and electrochemical activity of specific electrode types can dramatically impact degradation efficiency with different targeted organic pollutants,[2, 32, 64, 114] thus other electrode material influences should be explored. Two new FTERs with mesh Ti/SnO_2 and Ti/RuO_2 electrodes were built for preliminary comparisons against the Ti/IrO_2-Ta_2O_5 electrodes used for all other experiments in this dissertation. 1,4-dioxane degradation results are shown in Figure 5.3 for FTERs operating with 8.0 V applied to two pairs of electrodes (3 different types, without inter-electrode TiO_2 pellets added) and a having seepage velocity of 27 cm/d (0.9 ft/d). The same influent feedstock of 3.4 μM 1,4-dioxane in 10 mM Na_2SO_4 electrolyte was used for all experiments. The 1,4-dioxaen degradation efficiency was greatest with the "non-active" Ti/SnO_2 (92% degraded), followed by Ti/RuO_2 (74%) and then Ti/IrO_2-Ta_2O_5 + TiO_2 pellets (69%) and Ti/IrO_2-Ta_2O_5 alone (52%). The low current for Ti/SnO_2 provides evidence for this material having an extremely efficient faradaic current efficiency. This means that larger relative amounts of the total current participates directly or indirectly (through adsorbed $^{\bullet}OH$ radicals) in the degradation reactions, rather than the competing oxygen evolution

reaction. Plots of current vs. degradation efficiency (Figure 5.4) and solution redox potential (Figure 5.5) do not show a linear response and do not even show a consistent positive correlation. This confirms trends discovered in earlier experiments showing that current density and % degradation of organic pollutants are not directly correlated (Chapter 3).

Based upon these results, it would appear that the exploration of non-active electrode materials (like Ti/SnO_2) could be promising since these are known to be better at achieving complete mineralization due to their high oxygen evolution reaction overpotential, however there are trade-offs with cost, longevity and environmental risk that need to be considered. Negative trade-offs for three of the most commonly studied non-active anodes include high cost (and no permeable mesh form available) for BDD anodes, reduced electrochemical lifetimes are problematic for SnO_2 anodes, and the risk of low levels of toxic lead release by PbO_2 anodes.[2, 30] Thus, when moving forward SEM (for surface morphology) and XPS (for elemental composition and redox states) should be used to characterize the electrode materials (i.e. Ti/SnO_2, Ti/RuO_2, and Ti/IrO_2-Ta_2O_5) before and after use to improve the assessment of service life.[110]

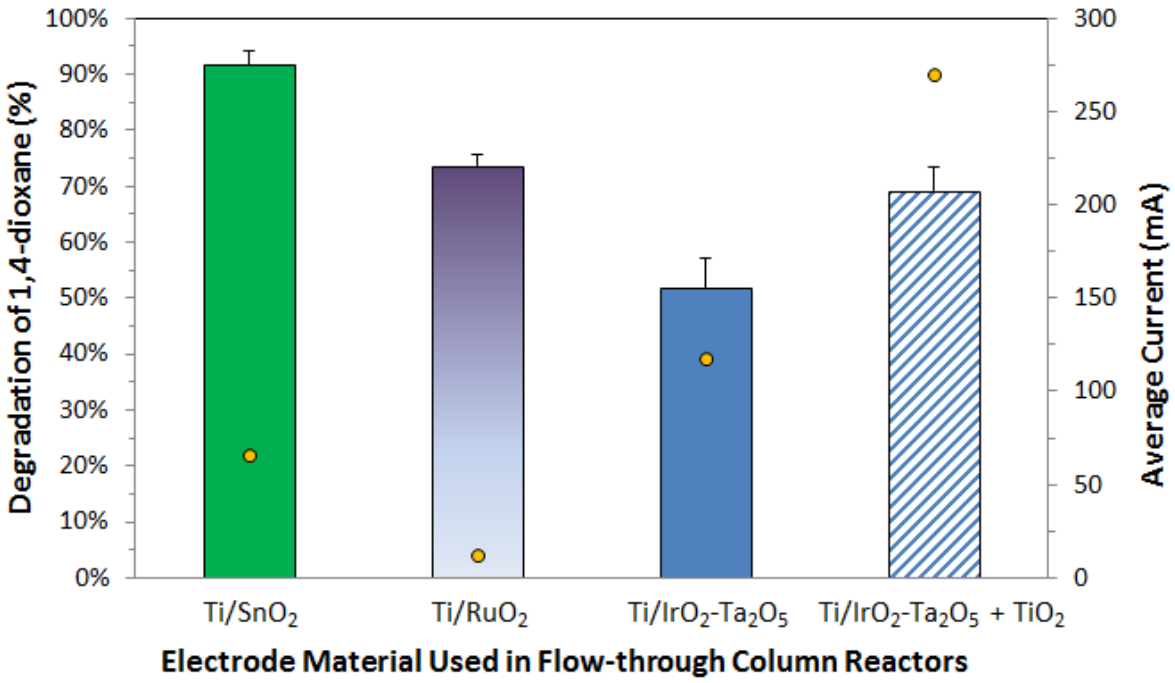

Figure 5.3 Electrocatalytic activity (% degradation) compared among three mesh electrodes tested without the use of inter-electrode TiO_2 pellets: Ti/SnO_2, Ti/RuO_2, and Ti/IrO_2-Ta_2O_5 electrodes. FTER data from Chapter 2 of Ti/IrO_2-Ta_2O_5 with inter-electrode TiO_2 pellets was also plotted for comparison. The secondary y-axis plots the average steady state current for each column experiment. Experiments were performed using flow-through electrochemical reactors operating at 8.0 V and a seepage velocity of 27.3 cm/d, supplied by a 20mM Na_2SO_4 electrolyte feedstock spiked with 3.4 µM 1,4-dioxane. Effluent samples were monitored after steady-state conditions were achieved. Errors bars represent the standard deviation ($n \geq 3$).

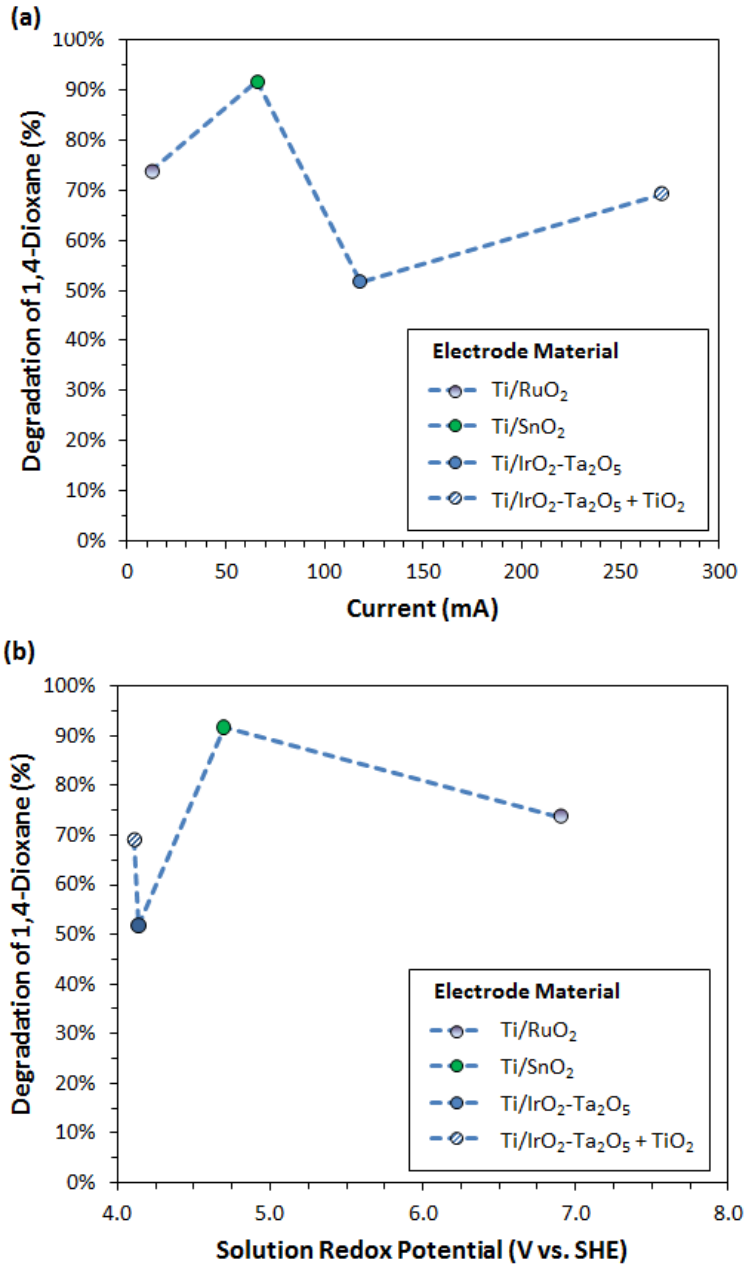

Figure 5.4 Impact of (a) average current and (b) solution redox potential on electrocatalytic activity (% degradation) of three mesh electrodes: Ti/SnO_2, Ti/RuO_2, and Ti/IrO_2-Ta_2O_5 electrodes. FTER data from Chapter 2 of Ti/IrO_2-Ta_2O_5 with inter-electrode TiO_2 pellets was also plotted for comparison. Experiments were performed using flow-through electrochemical reactors operating at 8.0 V and a seepage velocity of 27.3 cm/d, supplied by a 20mM Na_2SO_4 electrolyte feedstock spiked with 3.4 µM 1,4-dioxane. Effluent samples were monitored after steady-state conditions were achieved.

On the basis of the successful degradation seen with 1,4-dioxane, lamotrigine and chlorobenzene (Chapter 2), it is worthwhile to explore other possible niche applications of AEO treatment. For example, possible treatment applications could be explored for lamotrigine or other pharmaceuticals. There may be opportunities in wastewater treatment or point-of-use treatment for pharmaceutical residuals that remain bio-active (neuroactive, endocrine disrupting, etc.) after conventional wastewater treatment either to protect environmental health of the streams or the health of human populations downstream who use this as their source water for drinking water. There are also AEO opportunities to investigate continuing with recalcitrant pollutants associated with groundwater, like perfluorooctanoic acids (PFOA) and perfluorooctanesulfonic acids (PFOS). The PFOA and PFOS chemicals are still used today as important surfactants in aqueous film forming foams (AFFFs). Their use in flame-retardants for fire training at military bases, airports, and industrial sites has led to large amount of groundwater contamination with these PFCs which are difficult to treat. Studies in the literature have shown that many PFCs are resistant to conventional treatment and hydroxyl radical attack mechanisms, but have found that electrochemical treatment may be one of the few effective strategies.[27]

REFERENCES

(1) Mohr, T. K. *Solvent Stabilizers*. Santa Clara Valley Water District of California: San Jose, CA, 2001.
(2) Panizza, M.; Cerisola, G. Direct and Mediated Anodic Oxidation of Organic Pollutants. *Chemical Reviews* **2009,** *109*, (12), 6541-6569.
(3) Parales, R. E.; Adamus, J. E.; White, N.; May, H. D. Degradation of 1,4-Dioxane by an Actinomycete in Pure Culture. *Applied and Environmental Microbiology* **1994,** *60*, (12), 4527-4530.
(4) Mahendra, S.; Alvarez-Cohen, L. Pseudonocardia Dioxanivorans Sp Nov., a Novel Actinomycete That Grows on 1,4-Dioxane. *International Journal of Systematic and Evolutionary Microbiology* **2005,** *55*, 593-598.
(5) Mahendra, S.; Alvarez-Cohen, L. Kinetics of 1,4-Dioxane Biodegradation by Monooxygenase-Expressing Bacteria. *Environmental Science & Technology* **2006,** *40*, (17), 5435-5442.
(6) Mahendra, S.; Grostern, A.; Alvarez-Cohen, L. The Impact of Chlorinated Solvent Co-Contaminants on the Biodegradation Kinetics of 1,4-Dioxane. *Chemosphere* **2013,** *91*, (1), 88-92.
(7) Torrice, M. How Lead Ended up in Flint's Water. *Chemical & Engineering News* **2016,** *94*, (7), 26-29.
(8) Bicknell, D. J. Gelman Sciences, Inc. Exceedance of Deq Proposed Volatilization to Indoor Air Dioxane Criterion in the West Park Area of Ann Arbor, Michigan: Presents an Imminent & Substantial Endangerment to Public Health. *Global Environmental Alliance, LLC. [media.mlive.com/annarbornews_impact/other/Bicknell_052016.pdf] Last viewed June 2016*
(9) <Wong_2008_Cleaning_Chlorinated_Cmpnds_with_Paau_Catalyst.Pdf>.
(10) Schnoor, J. L. Re-Emergence of Emerging Contaminants. *Environmental Science & Technology* **2014,** *48*, (19), 11019-11020.
(11) <Berge_2009.Pdf>.
(12) Mohr, T. K.; Stickney, J. A.; DiGuiseppi, W. H. *Environmental Investigation and Remediation: 1, 4-Dioxane and Other Solvent Stabilizers*. CRC Press: Boca Raton, FL, 2010.
(13) Stepien, D. K.; Diehl, P.; Helm, J.; Thorns, A.; Puttmann, W. Fate of 1,4-Dioxane in the Aquatic Environment: From Sewage to Drinking Water. *Water Res* **2014,** *48*, 406-419.
(14) Edil, T. B. A Review of Aqueous-Phase VOC Transport in Modern Landfill Liners. *Waste Management* **2003,** *23*, (7), 561-571.
(15) <Gagne_1980_Ferrocene_Internal_Standard_Electrochem_Measurements.Pdf>.
(16) Kano, H.; Umeda, Y.; Kasai, T.; Sasaki, T.; Matsumoto, M.; Yamazaki, K.; Nagano, K.; Arito, H.; Fukushima, S. Carcinogenicity Studies of 1, 4-Dioxane Administered in Drinking-Water to Rats and Mice for 2years. *Food and chemical toxicology* **2009,** *47*, (11), 2776-2784.
(17) Adamson, D. T.; Mahendra, S.; Walker, K. L.; Rauch, S. R.; Sengupta, S.; Newell, C. J. A Multisite Survey to Identify the Scale of the 1,4-Dioxane Problem at Contaminated Groundwater Sites. *Environmental Science & Technology Letters* **2014,** *1*, (5), 254-258.

(18) Zenker, M. J.; Borden, R. C.; Barlaz, M. A. Occurrence and Treatment of 1,4-Dioxane in Aqueous Environments. *Environmental Engineering Science* **2003,** *20*, (5), 423-432.
(19) Glaze, W. H.; Kang, J. W.; Chapin, D. H. The Chemistry of Water-Treatment Processes Involving Ozone, Hydrogen-Peroxide and Ultraviolet-Radiation. *Ozone-Science & Engineering* **1987,** *9*, (4), 335-352.
(20) Takahashi, N.; Hibino, T.; Torii, H.; Shibata, S.; Tasaka, S.; Yoneya, J.; Matsuda, M.; Ogasawara, H.; Sugimoto, K.; Fujioka, T. Evaluation of O-3/Uv and O-3/H2o2 as Practical Advanced Oxidation Processes for Degradation of 1,4-Dioxane. *Ozone-Science & Engineering* **2013,** *35*, (5), 331-337.
(21) Chitra, S.; Paramasivan, K.; Cheralathan, M.; Sinha, P. K. Degradation of 1,4-Dioxane Using Advanced Oxidation Processes. *Environmental Science and Pollution Research* **2012,** *19*, (3), 871-878.
(22) Chong, M. N.; Jin, B.; Chow, C. W. K.; Saint, C. Recent Developments in Photocatalytic Water Treatment Technology: A Review. *Water Research* **2010,** *44*, (10), 2997-3027.
(23) Chatzisymeon, E.; Foteinis, S.; Mantzavinos, D.; Tsoutsos, T. Life Cycle Assessment of Advanced Oxidation Processes for Olive Mill Wastewater Treatment. *Journal of Cleaner Production* **2013,** *54*, 229-234.
(24) Solano, A. M. S.; Rocha, J. H. B.; Fernandes, N. S.; Da Silva, D. R.; Martinez-Huitle, C. A. Direct and Indirect Electrochemical Oxidation Process for Decolourisation Treatment of Synthetic Wastewaters Containing Dye. *Oxidation Communications* **2011,** *34*, (1), 218-229.
(25) Lyons, M. E. G.; Doyle, R. L.; Fernandez, D.; Godwin, I. J.; Browne, M. P.; Rovetta, A. The Mechanism and Kinetics of Electrochemical Water Oxidation at Oxidized Metal and Metal Oxide Electrodes. Part 2. The Surfaquo Group Mechanism: A Mini Review. *Electrochemistry Communications* **2014,** *45*, 56-59.
(26) Wang, B.; Kong, W. P.; Ma, H. Z. Electrochemical Treatment of Paper Mill Wastewater Using Three-Dimensional Electrodes with Ti/Co/Sno2-Sb2o5 Anode. *J Hazard Mater* **2007,** *146*, (1-2), 295-301.
(27) Schaefer, C. E.; Andaya, C.; Urtiaga, A.; McKenzie, E. R.; Higgins, C. P. Electrochemical Treatment of Perfluorooctanoic Acid (PFOA) and Perfluorooctane Sulfonic Acid (PFOS) in Groundwater Impacted by Aqueous Film Forming Foams (AFFFs). *Journal of Hazardous Materials* **2015,** *295*, 170-175.
(28) Panizza, M.; Bocca, C.; Cerisola, G. Electrochemical Treatment of Wastewater Containing Polyaromatic Organic Pollutants. *Water Res* **2000,** *34*, (9), 2601-2605.
(29) Panizza, M.; Barbucci, A.; Ricotti, R.; Cerisola, G. Electrochemical Degradation of Methylene Blue. *Separation and Purification Technology* **2007,** *54*, (3), 382-387.
(30) Martinez-Huitle, C. A.; Andrade, L. S. Electrocatalysis in Wastewater Treatment: Recent Mechanism Advances. *Quimica Nova* **2011,** *34*, (5), 850-858.
(31) Scialdone, O. Electrochemical Oxidation of Organic Pollutants in Water at Metal Oxide Electrodes: A Simple Theoretical Model Including Direct and Indirect Oxidation Processes at the Anodic Surface. *Electrochimica Acta* **2009,** *54*, (26), 6140-6147.
(32) Comninellis, C. Electrocatalysis in the Electrochemical Conversion/Combustion of Organic Pollutants for Waste-Water Treatment. *Electrochimica Acta* **1994,** *39*, (11-12), 1857-1862.

(33) Martinez-Huitle, C. A.; Ferro, S. Electrochemical Oxidation of Organic Pollutants for the Wastewater Treatment: Direct and Indirect Processes. *Chemical Society Reviews* **2006,** *35*, (12), 1324-1340.
(34) Duo, I.; Levy-Clement, C.; Fujishima, A.; Comninellis, C. Electron Transfer Kinetics on Boron-Doped Diamond Part I: Influence of Anodic Treatment. *Journal of Applied Electrochemistry* **2004,** *34*, (9), 935-943.
(35) Fierro, S.; Nagel, T.; Baltruschat, H.; Comninellis, C. Investigation of the Oxygen Evolution Reaction on Ti/Iro2 Electrodes Using Isotope Labelling and on-Line Mass Spectrometryle. *Electrochemistry Communications* **2007,** *9*, (8), 1969-1974.
(36) Kong, D. S.; Wu, J. X. An Electrochemical Study on the Anodic Oxygen Evolution on Oxide Film Covered Titanium. *Journal of the Electrochemical Society* **2008,** *155*, (1), C32-C40.
(37) Fierro, S.; Nagel, T.; Baltruschat, H.; Comninellis, C. Investigation of Formic Acid Oxidation on Ti/Iro(2) Electrodes Using Isotope Labeling and Online Mass Spectrometry. *Electrochemical and Solid State Letters* **2008,** *11*, (7), E20-E23.
(38) Panizza, M.; Kapalka, A.; Comninellis, C. Oxidation of Organic Pollutants on Bdd Anodes Using Modulated Current Electrolysis. *Electrochimica Acta* **2008,** *53*, (5), 2289-2295.
(39) Choi, J. Y.; Lee, Y. J.; Shin, J.; Yang, J. W. Anodic Oxidation of 1,4-Dioxane on Boron-Doped Diamond Electrodes for Wastewater Treatment. *J Hazard Mater* **2010,** *179*, (1-3), 762-768.
(40) De Clercq, J.; Van de Steene, E.; Verbeken, K.; Verhaege, M. Electrochemical Oxidation of 1,4-Dioxane at Boron-Doped Diamond Electrode. *Journal of Chemical Technology and Biotechnology* **2010,** *85*, (8), 1162-1167.
(41) Yanagida, S.; Nakajima, A.; Kameshima, Y.; Okada, K. Voltage Swing Interval Effects on Photocatalytic Decomposition of 1,4-Dioxane in Aqueous Media Using TiO_2 -Coated Stainless Mesh. *Journal of the Ceramic Society of Japan* **2008,** *116*, (1350), 181-186.
(42) Yanagida, S.; Nakajima, A.; Kameshima, Y.; Okada, K. Effect of Applying Voltage on Photocatalytic Destruction of 1,4-Dioxane in Aqueous System. *Catalysis Communications* **2006,** *7*, (12), 1042-1046.
(43) Sale, T.; Petersen, M.; Gilbert, D. *Electrically Induced Redox Barriers for Treatment of Groundwater*; ESTCP Final Report CU-0112. U.S. Department of Defense: 2005.
(44) Sale, T.; Olson, M.; Gilbert, D.; Petersen, M. *Field Demonstration/Validation of Electrolytic Barriers for Energetic Compounds at Pueblo Chemical Depot*; ESTCP ER-0519. U.S. Department of Defense: 2010.
(45) Hanaor, D. A. H.; Sorrell, C. C. Review of the Anatase to Rutile Phase Transformation. *Journal of Materials Science* **2011,** *46*, (4), 855-874.
(46) Hoffmann, M. R.; Martin, S. T.; Choi, W.; Bahnemann, D. W. Environmental Applications of Semiconductor Photocatalysis. *Chemical reviews* **1995,** *95*, (1), 69-96.
(47) Tayade, R. J.; Surolia, P. K.; Kulkarni, R. G.; Jasra, R. V. Photocatalytic Degradation of Dyes and Organic Contaminants in Water Using Nanocrystalline Anatase and Rutile TiO_2. *Science and Technology of Advanced Materials* **2007,** *8*, (6), 455-462.
(48) Maurino, V.; Calza, P.; Minero, C.; Pelizzetti, E.; Vincenti, M. Light-Assisted 1,4-Dioxane Degradation. *Chemosphere* **1997,** *35*, (11), 2675-2688.

(49) Hill, R. R.; Jeffs, G. E.; Roberts, D. R. Photocatalytic Degradation of 1,4-Dioxane in Aqueous Solution. *Journal of Photochemistry and Photobiology a-Chemistry* **1997,** *108*, (1), 55-58.
(50) Beckett, M. A.; Hua, I. Elucidation of the 1,4-Dioxane Decomposition Pathway at Discrete Ultrasonic Frequencies. *Environmental Science & Technology* **2000,** *34*, (18), 3944-3953.
(51) Yanagida, S.; Nakajima, A.; Kameshima, Y.; Okada, K. Photocatalytic Destruction of 1,4-Dioxane in Aqueous System by Surface-Roughened Tio(2) Coating on Stainless Mesh. In *Electrophoretic Deposition: Fundamentals and Applications Iii*, Boccaccini, A. R.; VanDerBiest, O.; Clasen, R.; Uchikoshi, T., Eds. 2009; Vol. 412, pp 137-141.
(52) Ravelli, D.; Dondi, D.; Fagnoni, M.; Albini, A. Photocatalysis. A Multi-Faceted Concept for Green Chemistry. *Chemical Society Reviews* **2009,** *38*, (7), 1999-2011.
(53) Kesselman, J. M.; Weres, O.; Lewis, N. S.; Hoffmann, M. R. Electrochemical Production of Hydroxyl Radical at Polycrystalline Nb-Doped TiO_2 Electrodes and Estimation of the Partitioning between Hydroxyl Radical and Direct Hole Oxidation Pathways. *Journal of Physical Chemistry B* **1997,** *101*, (14), 2637-2643.
(54) Zhang, A. Y.; Long, L. L.; Liu, C.; Li, W. W.; Yu, H. Q. Electrochemical Degradation of Refractory Pollutants Using TiO_2 Single Crystals Exposed by High-Energy {001} Facets. *Water Research* **2014,** *66*, 273-282.
(55) Chaplin, B. P. Critical Review of Electrochemical Advanced Oxidation Processes for Water Treatment Applications. *Environmental Science-Processes & Impacts* **2014,** *16*, (6), 1182-1203.
(56) Lawless, D.; Serpone, N.; Meisel, D. Role of Hydroxyl Radicals and Trapped Holes in Photocatalysis. A Pulse Radiolysis Study. *The Journal of Physical Chemistry* **1991,** *95*, (13), 5166-5170.
(57) Agency for Toxic Substances and Disease Registry (ATSDR). Toxicological Profile for 1,4-Dioxane. April 2012. (Http://Www. ATSDR.CDC.Gov/Toxprofiles/Tp187.Pdf).
(58) U.S. Environmental Protection Agency. Emerging Contaminant Fact Sheet--1,4-Dioxane. Office of Solid Waste and Emergency Response. EPA -505-F-09-006, 2009.
(59) U.S. Environmental Protection Agency. The Third Unregulated Contaminant Monitoring Rule (Ucmr 3): Data Summary. Office of Water. EPA -815-S-16-002, April 2016.
(60) Coleman, H. M.; Vimonses, V.; Leslie, G.; Amal, R. Degradation of 1,4-Dioxane in Water Using TiO_2 Based Photocatalytic and H2o2/Uv Processes. *J Hazard Mater* **2007,** *146*, (3), 496-501.
(61) Suh, J. H.; Mohseni, M. A Study on the Relationship between Biodegradability Enhancement and Oxidation of 1,4-Dioxane Using Ozone and Hydrogen Peroxide. *Water Research* **2004,** *38*, (10), 2596-2604.
(62) Adams, C. D.; Scanlan, P. A.; Secrist, N. D. Oxidation and Biodegradability Enhancement of 1,4-Dioxane Using Hydrogen-Peroxide and Ozone. *Environmental Science & Technology* **1994,** *28*, (11), 1812-1818.
(63) Barazesh, J. M.; Hennebel, T.; Jasper, J. T.; Sedlak, D. L. Modular Advanced Oxidation Process Enabled by Cathodic Hydrogen Peroxide Production. *Environmental Science & Technology* **2015,** *49*, (12), 7391-7399.
(64) Comninellis, C.; Kapalka, A.; Malato, S.; Parsons, S. A.; Poulios, L.; Mantzavinos, D. Advanced Oxidation Processes for Water Treatment: Advances and Trends for R&D. *Journal of Chemical Technology and Biotechnology* **2008,** *83*, (6), 769-776.

(65) Rajeshwar, K.; Ibanez, J. G.; Swain, G. M. Electrochemistry and the Environment. *Journal of Applied Electrochemistry* **1994,** *24*, (11), 1077-1091.
(66) Kishimoto, N.; Nakagawa, T.; Asano, M.; Abe, M.; Yamada, M.; Ono, Y. Ozonation Combined with Electrolysis of 1,4-Dioxane Using a Two-Compartment Electrolytic Flow Cell with Solid Electrolyte. *Water Res* **2008,** *42*, (1-2), 379-385.
(67) Gilbert, D. M.; Sale, T. C. Sequential Electrolytic Oxidation and Reduction of Aqueous Phase Energetic Compounds. *Environmental Science & Technology* **2005,** *39*, (23), 9270-9277.
(68) Petersen, M. A.; Sale, T. C.; Reardon, K. F. Electrolytic Trichloroethene Degradation Using Mixed Metal Oxide Coated Titanium Mesh Electrodes. *Chemosphere* **2007,** *67*, (8), 1573-1581.
(69) Zhang, Y. Z.; Xiong, X. Y.; Han, Y.; Zhang, X. H.; Shen, F.; Deng, S. H.; Xiao, H.; Yang, X. Y.; Yang, G.; Peng, H. Photoelectrocatalytic Degradation of Recalcitrant Organic Pollutants Using TiO_2 Film Electrodes: An Overview. *Chemosphere* **2012,** *88*, (2), 145-154.
(70) Kapalka, A.; Foti, G.; Comninellis, C. Investigations of Electrochemical Oxygen Transfer Reaction on Boron-Doped Diamond Electrodes. *Electrochimica Acta* **2007,** *53*, (4), 1954-1961.
(71) Donaghue, A.; Chaplin, B. P. Effect of Select Organic Compounds on Perchlorate Formation at Boron-Doped Diamond Film Anodes. *Environmental Science & Technology* **2013,** *47*, (21), 12391-12399.
(72) Fernandes, A.; Morao, A.; Magrinho, M.; Lopes, A.; Goncalves, I. Electrochemical Degradation of C. I. Acid Orange 7. *Dyes and Pigments* **2004,** *61*, (3), 287-296.
(73) Spurr, R. A.; Myers, H. Quantitative Analysis of Anatase-Rutile Mixtures with an X-Ray Diffractometer. *Analytical Chemistry* **1957,** *29*, (5), 760-762.
(74) Byrne, H. E.; Kostedt, W. L.; Stokke, J. M.; Mazyck, D. W. Characterization of Hf-Catalyzed Silica Gels Doped with Degussa P25 Titanium Dioxide. *Journal of Non-Crystalline Solids* **2009,** *355*, (9), 525-530.
(75) Carbonaro, S.; Sugihara, M. N.; Strathmann, T. J. Continuous-Flow Photocatalytic Treatment of Pharmaceutical Micropollutants: Activity, Inhibition, and Deactivation of TiO_2 Photocatalysts in Wastewater Effluent. *Applied Catalysis B-Environmental* **2013,** *129*, 1-12.
(76) Beck, F.; Gabriel, W. Heterogenous Redox Catalysis on Ti/ TiO_2 Cathodes--Reduction of Nitrobenzene. *Angewandte Chemie-International Edition* **1985,** *24*, (9), 771-772.
(77) Geng, P.; Su, J. Y.; Miles, C.; Comninellis, C.; Chen, G. H. Highly-Ordered Magneli Ti4o7 Nanotube Arrays as Effective Anodic Material for Electro-Oxidation. *Electrochimica Acta* **2015,** *153*, 316-324.
(78) Shah, A.; Jorne, J. Mass-Transfer under Combined Gas Evolution and Forced-Convection. *Journal of the Electrochemical Society* **1989,** *136*, (1), 153-158.
(79) Petersen, M. A.; Reardon, K. F. Effect of Gas Evolution on Mixing and Conversion in a Flow-through Electrochemical Reactor. *Aiche Journal* **2009,** *55*, (9), 2468-2476.
(80) Kortlever, R.; Shen, J.; Schouten, K. J. P.; Calle-Vallejo, F.; Koper, M. T. M. Catalysts and Reaction Pathways for the Electrochemical Reduction of Carbon Dioxide. *Journal of Physical Chemistry Letters* **2015,** *6*, (20), 4073-4082.

(81) Stefan, M. I.; Bolton, J. R. Mechanism of the Degradation of 1,4-Dioxane in Dilute Aqueous Solution Using the Uv Hydrogen Peroxide Process. *Environmental Science & Technology* **1998,** *32*, (11), 1588-1595.
(82) Schuchmann, M. N.; Bothe, E.; von Sonntag, J.; von Sonntag, C. Reaction of Oh Radicals with Benzoquinone in Aqueous Solutions. A Pulse Radiolysis Study. *Journal of the Chemical Society, Perkin Transactions 2* **1998**, (4), 791-796.
(83) Bejan, D.; Guinea, E.; Bunce, N. J. On the Nature of the Hydroxyl Radicals Produced at Boron-Doped Diamond and Ebonex® Anodes. *Electrochimica Acta* **2012,** *69*, 275-281.
(84) Bejan, D.; Malcolm, J. D.; Morrison, L.; Bunce, N. J. Mechanistic Investigation of the Conductive Ceramic Ebonex® as an Anode Material. *Electrochimica Acta* **2009,** *54*, (23), 5548-5556.
(85) Waterston, K.; Wang, J. W.; Bejan, D.; Bunce, N. J. Electrochemical Waste Water Treatment: Electrooxidation of Acetaminophen. *Journal of Applied Electrochemistry* **2006,** *36*, (2), 227-232.
(86) Thomas, J. K. Rates of Reaction of the Hydroxyl Radical. *Transactions of the Faraday Society* **1965,** *61*, (0), 702-707.
(87) Anbar, M.; Meyerste.D; Neta, P. Reactivity of Aliphatic Compounds Towards Hydroxyl Radicals. *Journal of the Chemical Society B-Physical Organic* **1966**, (8), 742-747.
(88) Vonsonntag, C.; Schuchmann, H. P. The Elucidation of Peroxyl Radical Reactions in Aqueous-Solution with the Help of Radiation-Chemical Methods. *Angewandte Chemie-International Edition in English* **1991,** *30*, (10), 1229-1253.
(89) Huie, R. E. In *Progress and Problems in Atmospheric Chemistry*, Barker, J. R., Ed. World Scientific: Singapore, 1995; pp 374-419.
(90) Oturan, M. A. An Ecologically Effective Water Treatment Technique Using Electrochemically Generated Hydroxyl Radicals for in Situ Destruction of Organic Pollutants: Application to Herbicide 2,4-D. *Journal of Applied Electrochemistry* **2000,** *30*, (4), 475-482.
(91) Bielski, B. H.; Cabelli, D. E.; Arudi, R. L.; Ross, A. B. Reactivity of Ho2/O− 2 Radicals in Aqueous Solution. *Journal of Physical and Chemical Reference Data* **1985,** *14*, (4), 1041-1100.
(92) Schuchmann, M. N.; Vonsonntag, C. Hydroxyl Radical Induced Oxidation of Diethyl Ether in Oxygenated Aqueous Solution - a Product and Pulse Radiolysis Study. *Journal of Physical Chemistry* **1982,** *86*, (11), 1995-2000.
(93) Schuchmann, M. N.; Schuchmann, H. P.; Hess, M.; Vonsonntag, C. O2.- Addition to Ketomalonate Leads to Decarboxylation: A Chain Reaction in Oxygenated Aqueous Solution. *Journal of the American Chemical Society* **1991,** *113*, (18), 6934-6937.
(94) Andreozzi, R. Paracetamol Oxidation from Aqueous Solutions by Means of Ozonation and H 2 O 2/Uv System. *Water research* **2003,** *37*, (5), 993-1004.
(95) Leitner, N. K. V.; Dore, M. Mechanism of the Reaction between Hydroxyl Radicals and Glycolic, Glyoxylic, Acetic and Oxalic Acids in Aqueous Solution: Consequence on Hydrogen Peroxide Consumption in the H2o2/Uv and O-3/H2o2 Systems. *Water Research* **1997,** *31*, (6), 1383-1397.
(96) Barndok, H.; Hermosilla, D.; Cortijo, L.; Torres, E.; Blanco, A. Electrooxidation of Industrial Wastewater Containing 1,4-Dioxane in the Presence of Different Salts. *Environmental Science and Pollution Research* **2014,** *21*, (8), 5701-5712.

(97) Abdessalem, A. K.; Oturan, M. A.; Oturan, N.; Bellakhal, N.; Dachraoui, M. Treatment of an Aqueous Pesticides Mixture Solution by Direct and Indirect Electrochemical Advanced Oxidation Processes. *International Journal of Environmental Analytical Chemistry* **2010,** *90*, (3-6), 468-477.
(98) Oturan, N.; van Hullebusch, E. D.; Zhang, H.; Mazeas, L.; Budzinski, H.; Le Menach, K.; Oturan, M. A. Occurrence and Removal of Organic Micropollutants in Landfill Leachates Treated by Electrochemical Advanced Oxidation Processes. *Environmental Science & Technology* **2015,** *49*, (20), 12187-12196.
(99) Young, R. B.; Chefetz, B.; Liu, A. J.; Desyaterik, Y.; Borch, T. Direct Photodegradation of Lamotrigine (an Antiepileptic) in Simulated Sunlight - Ph Influenced Rates and Products. *Environmental Science-Processes & Impacts* **2014,** *16*, (4), 848-857.
(100) Sennour, R.; Mimane, G.; Benghalem, A.; Taleb, S. Removal of the Persistent Pollutant Chlorobenzene by Adsorption onto Activated Montmorillonite. *Applied Clay Science* **2009,** *43*, (3-4), 503-506.
(101) Chen, X. M.; Chen, G. H.; Yue, P. L. Anodic Oxidation of Dyes at Novel Ti/B-Diamond Electrodes. *Chemical Engineering Science* **2003,** *58*, (3-6), 995-1001.
(102) Canizares, P.; Paz, R.; Saez, C.; Rodrigo, M. A. Costs of the Electrochemical Oxidation of Wastewaters: A Comparison with Ozonation and Fenton Oxidation Processes. *Journal of Environmental Management* **2009,** *90*, (1), 410-420.
(103) Radjenovic, J.; Sedlak, D. L. Challenges and Opportunities for Electrochemical Processes as Next-Generation Technologies for the Treatment of Contaminated Water. *Environmental Science & Technology* **2015,** *49*, (19), 11292-11302.
(104) Bagastyo, A. Y.; Radjenovic, J.; Mu, Y.; Rozendal, R. A.; Batstone, D. J.; Rabaey, K. Electrochemical Oxidation of Reverse Osmosis Concentrate on Mixed Metal Oxide (Mmo) Titanium Coated Electrodes. *Water research* **2011,** *45*, (16), 4951-4959.
(105) Hamdy, M. S.; Saputera, W. H.; Groenen, E. J.; Mul, G. A Novel Tio 2 Composite for Photocatalytic Wastewater Treatment. *Journal of catalysis* **2014,** *310*, 75-83.
(106) Dong, S. Y.; Feng, J. L.; Fan, M. H.; Pi, Y. Q.; Hu, L. M.; Han, X.; Liu, M. L.; Sun, J. Y.; Sun, J. H. Recent Developments in Heterogeneous Photocatalytic Water Treatment Using Visible Light-Responsive Photocatalysts: A Review. *Rsc Advances* **2015,** *5*, (19), 14610-14630.
(107) Bock, C.; MacDougall, B. The Anodic Oxidation of P-Benzoquinone and Maleic Acid. *Journal of the Electrochemical Society* **1999,** *146*, (8), 2925-2932.
(108) Lipp, L.; Pletcher, D. The Preparation and Characterization of Tin Dioxide Coated Titanium Electrodes. *Electrochimica Acta* **1997,** *42*, (7), 1091-1099.
(109) Correa-Lozano, B.; Comninellis, C.; De Battisti, A. Service Life of Ti/Sno2–Sb2o5 Anodes. *Journal of Applied Electrochemistry* **1997,** *27*, (8), 970-974.
(110) Chaplin, B. P.; Wyle, I.; Zeng, H.; Carlisle, J. A.; Farrell, J. Characterization of the Performance and Failure Mechanisms of Boron-Doped Ultrananocrystalline Diamond Electrodes. *Journal of Applied Electrochemistry* **2011,** *41*, (11), 1329-1340.
(111) Rosental, K. I.; Veselovsky, V. I. The Use of the O-18 Isotope as a Label in Studying the Electrochemical Evolution of Oxygen on a Pt Electrode. *Doklady Akademii Nauk Sssr* **1956,** *111*, (3), 637-639.
(112) Fóti, G.; Comninellis, C. *Modern Aspects of Electrochemistry*. Kluwer Academic/Plenum Publishers: New York, 2004; Vol. 37, p.87.

(113) Pignatello, J. J.; Oliveros, E.; MacKay, A. Advanced Oxidation Processes for Organic Contaminant Destruction Based on the Fenton Reaction and Related Chemistry. *Critical Reviews in Environmental Science and Technology* **2006,** *36*, (1), 1-84.
(114) Rodgers, J. D.; Jedral, W.; Bunce, N. I. Electrochemical Oxidation of Chlorinated Phenols. *Environmental Science & Technology* **1999,** *33*, (9), 1453-1457.
(115) Brunauer, S.; Emmett, P. H.; Teller, E. Adsorption of Gases in Multimolecular Layers. *Journal of the American Chemical Society* **1938,** *60*, 309-319.
(116) Brunauer, S.; Deming, L. S.; Deming, W. E.; Teller, E. On a Theory of the Van Der Waals Adsorption of Gases. *Journal of the American Chemical Society* **1940,** *62*, 1723-1732.
(117) Barrett, E. P.; Joyner, L. G.; Halenda, P. P. The Determination of Pore Volume and Area Distributions in Porous Substances .1. Computations from Nitrogen Isotherms. *Journal of the American Chemical Society* **1951,** *73*, (1), 373-380.
(118) Navrotsky, A. Energetics of Nanoparticle Oxides: Interplay between Surface Energy and Polymorphism†. *Geochemical Transactions* **2003,** *4*, (1), 1-4.
(119) Sclafani, A.; Herrmann, J. Comparison of the Photoelectronic and Photocatalytic Activities of Various Anatase and Rutile Forms of Titania in Pure Liquid Organic Phases and in Aqueous Solutions. *The Journal of Physical Chemistry* **1996,** *100*, (32), 13655-13661.
(120) Augustynski, J. The Role of the Surface Intermediates in the Photoelectrochemical Behaviour of Anatase and Rutile Tio 2. *Electrochimica Acta* **1993,** *38*, (1), 43-46.
(121) Bak, T.; Nowotny, J.; Nowotny, M. K.; Sheppard, L. R. Reactivity at the Oxygen/Titania Interface and the Related Charge Transfer. *Ionics* **2006,** *12*, (4-5), 247-251.
(122) Nowotny, M. K.; Sheppard, L. R.; Bak, T.; Nowotny, J. Defect Chemistry of Titanium Dioxide. Application of Defect Engineering in Processing of TiO_2 -Based Photocatalysts. *Journal of Physical Chemistry C* **2008,** *112*, (14), 5275-5300.
(123) Bak, T.; Nowotny, J. Reactivity of Rutile with Oxygen and Hydrogen and Related Charge Transfer. *Journal of Physical Chemistry C* **2011,** *115*, (31), 15345-15354.
(124) Bak, T.; Nowotny, J.; Sucher, N. J.; Wachsman, E. Effect of Crystal Imperfections on Reactivity and Photoreactivity of TiO_2 (Rutile) with Oxygen, Water, and Bacteria. *Journal of Physical Chemistry C* **2011,** *115*, (32), 15711-15738.
(125) Kitazawa, S. I.; Choi, Y.; Yamamoto, S.; Yamaki, T. Rutile and Anatase Mixed Crystal TiO_2 Thin Films Prepared by Pulsed Laser Deposition. *Thin Solid Films* **2006,** *515*, (4), 1901-1904.
(126) Imanishi, A.; Okamura, T.; Ohashi, N.; Nakamura, R.; Nakato, Y. Mechanism of Water Photooxidation Reaction at Atomically Flat TiO_2 (Rutile) (110) and (100) Surfaces: Dependence on Solution Ph. *Journal of the American Chemical Society* **2007,** *129*, (37), 11569-11578.
(127) Janzen, E. G.; Wang, Y. Y.; Shetty, R. V. Spin Trapping with Alpha-Pyridyl 1-Oxide N-Tert-Butyl Nitrones in Aqueous-Solutions - Unique Electron-Spin Resonance-Spectrum for Hydroxyl Radical Adduct. *Journal of the American Chemical Society* **1978,** *100*, (9), 2923-2925.
(128) McIntire, G. L.; Blount, H. N.; Stronks, H. J.; Shetty, R. V.; Janzen, E. G. Spin Trapping in Electrochemistry .2. Aqueous and Non-Aqueous Electrochemical Characterizations of Spin Traps. *Journal of Physical Chemistry* **1980,** *84*, (8), 916-921.

(129) Eberson, L. Inverted Spin Trapping - Reactions between the Radical Cation of Alpha-Phenyl-N-Tert-Butylnitrone and Ionic and Neutral Nucleophiles. *Journal of the Chemical Society-Perkin Transactions 2* **1992**, (10), 1807-1813.
(130) Zaky, A. M.; Chaplin, B. P. Porous Substoichiometric TiO_2 Anodes as Reactive Electrochemical Membranes for Water Treatment. *Environmental Science & Technology* **2013,** *47*, (12), 6554-6563.
(131) Buxton, G. V. Critical Review of Rate Constants for Reactions of Hydrated Electrons, Hydrogen Atoms and Hydroxyl Radicals (· Oh/· O− in Aqueous Solution. *Journal of physical and chemical reference data* **1988,** *17*, (2), 513.
(132) Clifton, C. L.; Huie, R. E. Rate Constants for Hydrogen Abstraction Reactions of the Sulfate Radical, So4- - Alcohols. *International Journal of Chemical Kinetics* **1989,** *21*, (8), 677-687.
(133) Xu, M.; Gu, X.; Lu, S.; Qiu, Z.; Sui, Q. Role of Reactive Oxygen Species for 1, 1, 1-Trichloroethane Degradation in a Thermally Activated Persulfate System. *Industrial & Engineering Chemistry Research* **2014,** *53*, (3), 1056-1063.
(134) Kishimoto, N.; Sugimura, E. Feasibility of an Electrochemically Assisted Fenton Method Using Fe2+/Hocl System as an Advanced Oxidation Process. *Water Science and Technology* **2010,** *62*, (10), 2321-2329.
(135) Hoigné, J.; Bader, H. Rate Constants of Reactions of Ozone with Organic and Inorganic Compounds in Water—I: Non-Dissociating Organic Compounds. *Water Research* **1983,** *17*, (2), 173-183.
(136) Bak, T.; Bogdanoff, P.; Fiechter, S.; Nowotny, J. Defect Engineering of Titanium Dioxide: Full Defect Disorder. *Advances in Applied Ceramics* **2012,** *111*, (1-2), 62-71.
(137) Bak, T.; Chu, D. W.; Francis, A. R.; Li, W. X.; Nowotny, J. Concentration of Electrons at Grain Boundaries in TiO_2 (Rutile): Impact on Charge Transport and Reactivity. *Catalysis Today* **2014,** *224*, 200-208.
(138) Bak, T.; Nowotny, J.; Nowotny, M. K. Defect Disorder of Titanium Dioxide. *Journal of Physical Chemistry B* **2006,** *110*, (43), 21560-21567.
(139) U.S. Environmental Protection Agency. Technical Fact Sheet--1,4-Dioxane. EPA -505-F-14-011; Office of Solid Waste and Emergency Response, 2014.
(140) Chiang, S. Y. D.; Mora, R.; Diguiseppi, W. H.; Davis, G.; Sublette, K.; Gedalanga, P.; Mahendra, S. Characterizing the Intrinsic Bioremediation Potential of 1,4-Dioxane and Trichloroethene Using Innovative Environmental Diagnostic Tools. *Journal of Environmental Monitoring* **2012,** *14*, (9), 2317-2326.
(141) Anderson, R. H.; Anderson, J. K.; Bower, P. A. Co-Occurrence of 1,4-Dioxane with Trichloroethylene in Chlorinated Solvent Groundwater Plumes at Us Air Force Installations: Fact or Fiction. *Integrated Environmental Assessment and Management* **2012,** *8*, (4), 731-737.
(142) U.S. Environmental Protection Agency. Technical Fact Sheet--1,4-Dioxane. Office of Solid Waste and Emergency Response. EPA -505-F-14-011, 2014.
(143) Klecka, G. M.; Gonsior, S. J. Removal of 1,4-Dioxane from Waste-Water. *Journal of Hazardous Materials* **1986,** *13*, (2), 161-168.
(144) Vainberg, S.; McClay, K.; Masuda, H.; Root, D.; Condee, C.; Zylstra, G. J.; Steffan, R. J. Biodegradation of Ether Pollutants by Pseudonocardia Sp Strain Env478. *Applied and Environmental Microbiology* **2006,** *72*, (8), 5218-5224.

(145) Lan, R. S.; Smith, C. A.; Hyman, M. R. Oxidation of Cyclic Ethers by Alkane-Grown Mycobacterium Vaccae Job5. *Remediation Journal* **2013,** *23*, (4), 23-42.
(146) Nakamiya, K.; Hashimoto, S.; Ito, H.; Edmonds, J. S.; Morita, M. Degradation of 1, 4-Dioxane and Cyclic Ethers by an Isolated Fungus. *Applied and environmental microbiology* **2005,** *71*, (3), 1254-1258.
(147) Sekar, R.; DiChristina, T. J. Microbially Driven Fenton Reaction for Degradation of the Widespread Environmental Contaminant 1,4-Dioxane. *Environmental Science & Technology* **2014,** *48*, (21), 12858-12867.
(148) Hand, S.; Wang, B. X.; Chu, K. H. Biodegradation of 1,4-Dioxane: Effects of Enzyme Inducers and Trichloroethylene. *Science of the Total Environment* **2015,** *520*, 154-159.
(149) Zhang, S.; Gedalanga, P. B.; Mahendra, S. Biodegradation Kinetics of 1,4-Dioxane in Chlorinated Ethene Mixtures. *Environmental Science & Technology* **2016**, (in review).
(150) Adamson, D. T.; Anderson, R. H.; Mahendra, S.; Newell, C. J. Evidence of 1, 4-Dioxane Attenuation at Groundwater Sites Contaminated with Chlorinated Solvents and 1, 4-Dioxane. *Environmental Science & Technology* **2015,** *49*, (11), 6510-6518.
(151) *Geotracker*. State Water Resources Control Board, State of California. Accessed May 2016. (http://geotracker.waterboards.ca.gov/).
(152) Li, M.; van Orden, E. T.; DeVries, D. J.; Xiong, Z.; Hinchee, R.; Alvarez, P. J. Bench-Scale Biodegradation Tests to Assess Natural Attenuation Potential of 1,4-Dioxane at Three Sites in California. *Biodegradation* **2015,** *26*, (1), 39-50.
(153) Sun, M.; Reible, D. D.; Lowry, G. V.; Gregory, K. B. Effect of Applied Voltage, Initial Concentration, and Natural Organic Matter on Sequential Reduction/Oxidation of Nitrobenzene by Graphite Electrodes. *Environmental Science & Technology* **2012,** *46*, (11), 6174-6181.
(154) Sun, M.; Yan, F.; Zhang, R. L.; Reible, D. D.; Lowry, G. V.; Gregory, K. B. Redox Control and Hydrogen Production in Sediment Caps Using Carbon Cloth Electrodes. *Environmental Science & Technology* **2010,** *44*, (21), 8209-8215.
(155) Jasmann, J. R.; Borch, T.; Sale, T. C.; Blotevogel, J. Advanced Electrochemical Oxidation of 1,4-Dioxane Via Dark Catalysis by Novel Titanium Dioxide (TiO_2) Pellets. *submitted* **2016**.
(156) Chen, G.; Betterton, E. A.; Arnold, R. G. Electrolytic Oxidation of Trichloroethylene Using a Ceramic Anode. *Journal of Applied Electrochemistry* **1999,** *29*, (8), 961-970.
(157) Gedalanga, P. B.; Pornwongthong, P.; Mora, R.; Chiang, S.-Y. D.; Baldwin, B.; Ogles, D.; Mahendra, S. Identification of Biomarker Genes to Predict Biodegradation of 1,4-Dioxane. *Applied and Environmental Microbiology* **2014,** *80*, (10), 3209-3218.
(158) Mahendra, S.; Petzold, C. J.; Baidoo, E. E.; Keasling, J. D.; Alvarez-Cohen, L. Identification of the Intermediates of in Vivo Oxidation of 1,4-Dioxane by Monooxygenase-Containing Bacteria. *Environmental Science & Technology* **2007,** *41*, (21), 7330-7336.
(159) Cabiscol, E.; Tamarit, J.; Ros, J. Oxidative Stress in Bacteria and Protein Damage by Reactive Oxygen Species. *International Microbiology* **2000,** *3*, (1), 3-8.
(160) Schaefer, C. E.; Andaya, C.; Urtiaga, A. Assessment of Disinfection and by-Product Formation During Electrochemical Treatment of Surface Water Using a Ti/Iro2 Anode. *Chemical Engineering Journal* **2015,** *264*, 411-416.

(161) Gibbs, P. A.; Seviour, R. J. Does the Agitation Rate and/or Oxygen Saturation Influence Exopolysaccharide Production by Aureobasidium Pullulans in Batch Culture? *Applied Microbiology and Biotechnology* **1996,** *46*, (5-6), 503-510.
(162) Hrapovic, L.; Sleep, B. E.; Major, D. J.; Hood, E. D. Laboratory Study of Treatment of Trichloroethene by Chemical Oxidation Followed by Bioremediation. *Environmental Science & Technology* **2005,** *39*, (8), 2888-2897.
(163) Jefferson, K. K. What Drives Bacteria to Produce a Biofilm? *Fems Microbiology Letters* **2004,** *236*, (2), 163-173.
(164) Arp, D. J.; Yeager, C. M.; Hyman, M. R. Molecular and Cellular Fundamentals of Aerobic Cometabolism of Trichloroethylene. *Biodegradation* **2001,** *12*, (2), 81-103.
(165) Tseng, N.; Wang, N.; Szostek, B.; Mahendra, S. Biotransformation of 6:2 Fluorotelomer Alcohol (6:2 Ftoh) by a Wood-Rotting Fungus. *Environmental Science & Technology* **2014,** *48*, (7), 4012-4020.
(166) Grostern, A.; Sales, C. M.; Zhuang, W. Q.; Erbilgin, O.; Alvarez-Cohen, L. Glyoxylate Metabolism Is a Key Feature of the Metabolic Degradation of 1,4-Dioxane by Pseudonocardia Dioxanivorans Strain Cb1190. *Applied and Environmental Microbiology* **2012,** *78*, (9), 3298-3308.
(167) Liao, C.-H.; Kang, S.-F.; Wu, F.-A. Hydroxyl Radical Scavenging Role of Chloride and Bicarbonate Ions in the H 2 O 2/Uv Process. *Chemosphere* **2001,** *44*, (5), 1193-1200.
(168) Brophy, P.; Farmer, D. A Switchable Reagent Ion High Resolution Time-of-Flight Chemical Ionization Mass Spectrometer for Real-Time Measurement of Gas Phase Oxidized Species: Characterization from the 2013 Southern Oxidant and Aerosol Study. *Atmospheric Measurement Techniques* **2015,** *8*, (7), 2945-2959.
(169) Sakurai, K.; Mizusawa, M. X-Ray Diffraction Imaging of Anatase and Rutile. *Analytical Chemistry* **2010,** *82*, (9), 3519-3522.

APPENDIX A

SUPPORTING INFORMATION FOR CHAPTER 2

Fabrication of titanium dioxide pellets. Figure S2.1(a) includes photos of key steps in the process of making stable TiO_2 pellets starting from > 99.6% anatase TiO_2 powder (≤ 325 mesh or 40 µm). The sintering process was performed in a muffle furnace for 4 hours at 700°C, 800°C, 880°C, and 1,000°C attempting to cement loosely aggregated pellets into a stable form.

Flow-through electrochemical reactor (FTER) design. Figure S2.1(b-d) shows photos of the larger 10 cm I.D. FTERs used to investigate electro(cata)lytic degradation of 1,4-dioxane. The photos show a catalyzed reactor packed with TiO_2 pellets as inter-electrode material in (b), a control reactor with glass beads as inter-electrode material in (c), and a photo in (d) of a mesh Ti/IrO_2-Ta_2O_5 electrode before installation into an FTER. Figure S2.2 has a schematic of the smaller 5 cm I.D. FTERs used to perform flow-through electrolytic experiments on the persistent organic pollutants lamotrigine and chlorobenzene in direct comparison to 1,4-dioxane.

Screening for mechanically stable titanium dioxide pellets. Figure S2.1(e-f) shows photos of the equipment used for the mechanical stability tests. To start the mechanical stability tests, six randomly chosen TiO_2 pellets of each type were massed and placed into separate 40-mL glass vials and capped. Vigorous shaking of each glass vial was performed by hand for 35 reps/10 sec (i.e., 210 reps/min). The intact pellets were then separated from the pulverized or powdered TiO_2 remnants with a 0.077 mm sieve (Tyler Standard 200 mesh). The intact pellets (those pellets > 0.077 mm mesh sieve opening) were then massed again. These intact pellets were again placed into the glass vial, capped, and shaken at 210 reps/min for 15 more seconds

(25 seconds total), pulverized TiO_2 was separated, and intact pellets were weighed again. The percentage mass of intact TiO_2 pellets remaining after each shaking interval was calculated and used to determine mechanical stability based upon criteria as defined in Table S2.1 below. The TiO_2 pellets heated at 880°C and 1,000°C were the only to receive an "excellent pellet stability" ranking, indicating these would be suitable for flow-through systems without easily losing any catalytic material (Table S2.1).

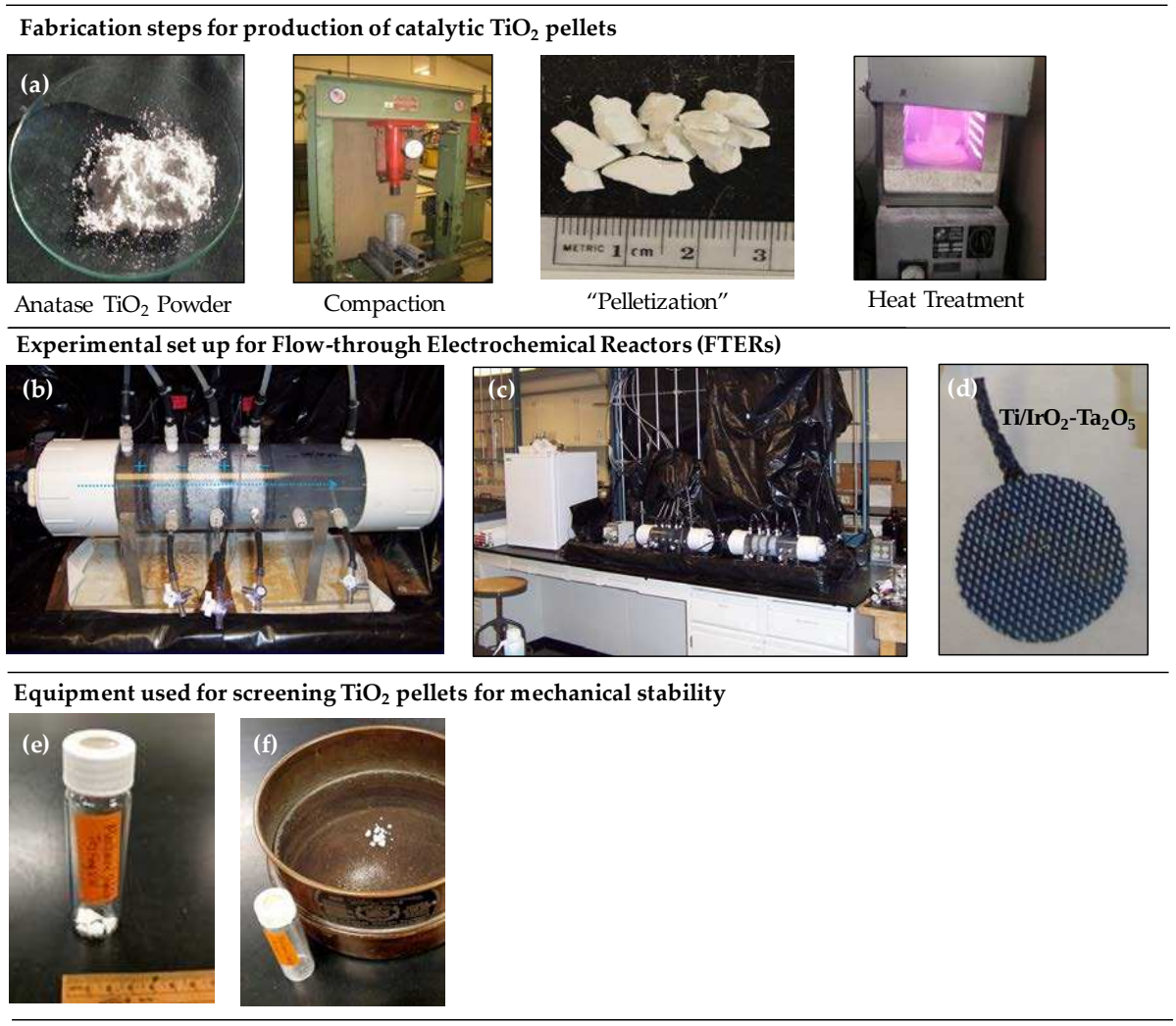

Figure S2.1 (a) Key steps in the process of making catalytic TiO_2 pellets to be used as inter-electrode catalysts including pressure compaction of the fine TiO_2 powder into cylindrical discs, manual chiseling into appropriately sized, loosely adhered pellets with sizes between 3.33 mm and 9.42 mm mesh size, and a heat treatment process. (b) Photo of a flow-through electrochemical reactor (FTER) with inter-electrode TiO_2 pellets between four working

electrodes. (c) Experimental set up showing the non-catalyzed control FTER with inter-electrode glass beads on left and the TiO_2-catalyzed FTER on the right, and (d) circular Ti/IrO_2-Ta_2O_5 mesh electrode before installing into column reactors. (e) Photos showing the 40-mL glass vial used for mechanical stability tests and (f) a top-view of the pulverized TiO_2 after shaking pellets in the glass vial.

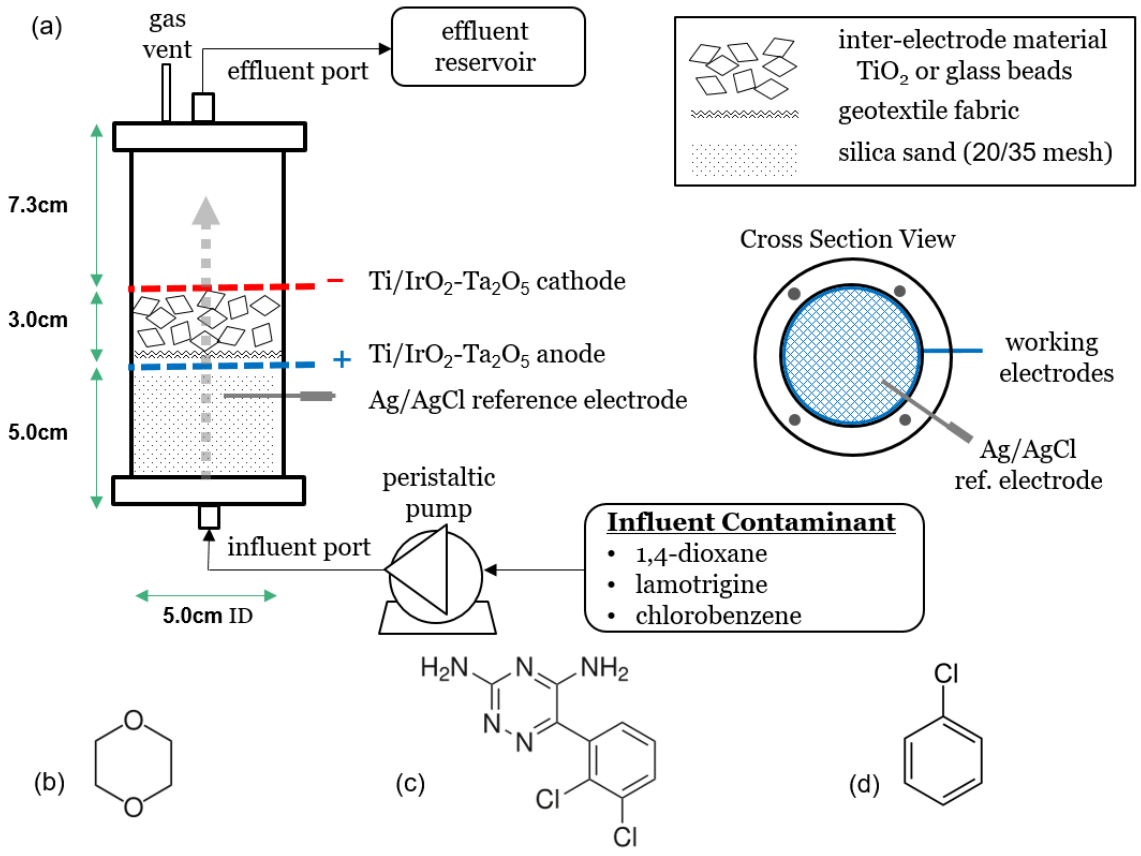

Figure S2.2 (a) Schematic of 5.0 cm internal diameter (I.D.) flow-through electrochemical reactor and list of influent feed pollutants investigated in this study. Small FTER is made from acrylic cylindrical pipe 15.24 cm long, and installed with a single pair of circular electrodes (d = 4.82 cm, A = 18.25 cm^2) spaced with an inter-electrode gap of 2.5cm. Chemical structures of persistent organic pollutants tested are shown for (b) 1,4-dioxane, (c) lamotrigine and (d) chlorobenzene.

Analytical methods used to monitor pollutant concentrations. For identification and quantification of dioxane, liquid-liquid extractions (LLE) into dichloromethane were performed followed by GC/MS full scan and selective ion mode (SIM) analysis (Agilent 6890N GC,

Agilent 5973N MSD). 2 µL injections were made at an inlet temperature of 250°C using a 5:1 split flow ratio. Helium carrier gas was used with initial flow rate of 1.0 mL/min. The initial oven temperature was 40°C for 1 minute, then ramped up at 10°C/min to 90°C, with an additional ramp of 20°C/min to 120°C. The mass spectrometer scanned from 40 to 250 Daltons when operating in full scan, and selected for *m/z* 58 and 88 when quantifying 1,4-dioxane in SIM. For quantification of chlorobenzene and benzene (a reduction transformation product of chlorobenzene), LLE of aqueous samples into methyl-*tert*-butyl ether was performed followed by GC/MS full scan and GC/ECD analyses (Agilent 6890N GC, Agilent ECD). GCs were equipped with a Restek Rxi-624Sil MS capillary column (30m x 0.25mm ID x 1.4 µm). Limits of quantification for 1,4-dioxane and chlorobenzene were 3.2 µg/L and 1.4 µg/L respectively.

Lamotrigine was quantified using an Agilent 1200 series HPLC system equipped with a UV-diode array detector. A Phenomenex Kinetex reversed-phase pentafluorophenyl column (100 mm x 3.1 mm I.D., 2.6 µm particle size) was used as stationary phase and two mobile phase solvents were used: (A) 0.1% v/v formic acid solution with 5 mM ammonium acetate, and (B) acetonitrile. Separation was carried out using a gradient elution program with 0-4 min, 10% B; 4-9.5 min, 10-65% B; 9.5-13.5 min, 100% B; 13.5-18 min 10% B. For all lamotrigine samples, the injection volume was 10 µL, the flow rate was 300 µL/min, and the column temperature was controlled at 30 °C. The samples were quantified at 270 nm using a seven-point external calibration curve (method detection limit < 0.1 mg/L).

Influent and effluent samples from the FTER experiment performed with 207 µM 1,4-dioxane feed solution (10 mM Na_2SO_4, 8.0 V, 0.65 mL/min flow) were analyzed for transformation products using LC/ESI-TOF-MS (Agilent 1100 Series LC connected to an Agilent G3250AA MSD TOF). Electrospray ionization was operated in both positive and

negative mode. However, the transformation products observed in this study were all detected in negative mode. Injection volumes of 50 µL and a flow of 0.5 mL/min were used. The isocratic mobile phase consisted of 0.1% formic acid and 2% acetonitrile. The reversed-phase column was a 150 mm Waters Xterra Phenyl, an organic-inorganic hybrid with 2-phenylpropyl ligands bonded to tetraethylsiloxane & methyltriethylsiloxane. The capillary, fragmentation, and skimmer voltages of the MSD were 800 V, 130 V, and 60 V, respectively. The temperature of drying gas (N_2) was 350°C with a flow rate of 10 mL/min, and the pressure of the nebulizer gas (N_2) was 50 psi. The mass analyzer was calibrated from *m/z* 30 to 600 in negative ionization mode using three reference ions and the elemental composition was determined for each *m/z* peak detected using the high mass accuracy results.

A Shimadzu TOC-L Analyzer was used to perform total organic carbon analysis using 40 mL glass VOC vials with triplicates of aqueous influent and effluent samples from a special TiO_2 catalyzed FTER (large 10 cm I.D.) experiment at 8.0 V and 30.6 cm/d with 10 mM Na_2SO_4 electrolyte and 470 µM 1,4-dioxane. The higher 1,4-dioxane concentration was used to assure TOC levels would remain within the quantification range of the analyzer even if 90% TOC was removed.

Experimental data were plotted using Microsoft Office 2010 (for TOC art, Fig. 1-5, Fig. S1-S4, and all tables) and Igor™ Pro 6 (for Fig. S3c XRD data). The 1,4-dioxane degradation pathway in Fig. 3 was created using ChemBioDraw Ultra version 14.0. Statistical computing was performed using R version 3.2.5 (released April 14, 2016) and RStudio Desktop version 0.99.896 (released April 18, 2016). Statistical computing included (i) Student's t-tests (two-tailed, unpaired) and (ii) a linear model for analysis-of-covariance using "ls means package" (least-squares means).

Methods used to monitor operational parameters of FTERs. Flow rates were measured by volumetric analysis of reactor influent tubing and reactor effluent reservoir measured each day. On a daily basis, measurements were made of pH, voltage and current between working electrodes using a Fluke Multimeter, and aqueous redox potential between the electrodes using Ag/AgCl reference electrodes (World Precision Instruments). These measurement values are all recorded in Table S2.2. In electrolytic degradation experiments of 1,4-dioxane performed with starting pH values of 1.7, 7.0 and 12.4, Choi, et al. demonstrated that initial pH did not have a significant effect on anodic oxidation rates of 1,4-dioxane. Therefore, pH was not varied in our experiments and instead a circumneutral pH of 7.2 ± 1.0 was used in all experiments.

Characterization of titanium dioxide (TiO_2) pellets. Scanning electron microscopy (SEM) was performed to observe surface morphology using a JEOL JSM-6500F Model FE-SEM at 5 kV accelerating voltage. TiO_2 pellet samples were sputter-coated with Au prior to analysis. Figures S2.3a and S2.3b show the uniform porosity seen at the surface of a TiO_2 pellet (after heat treated at 880 °C for 4 hours).

Crystallinity and phase composition of TiO_2 pellets were determined by comparison to anatase and rutile standards using powder X-ray diffraction (XRD) with a synchrotron X-ray light source, beamline 11-3 (λ= 0.972413 Å) at Stanford Synchrotron Radiation Lightsource. Percentage of anatase composition was calculated using the Spurr & Meyer equation and the crystalline shape constant K = 0.7905 specific to TiO_2 crystals. Diffraction intensity data were collected using step size of 0.002° and varying 2θ between 20° and 50°. Figure S2.3(c) shows that the diffraction patterns seen for TiO_2 heat treated at 700°C and 880°C closely match the peaks observed for the anatase standard that did not undergo heat treatment, thus indicating no

major phase transformation to rutile phase. The fraction of anatase and rutile was estimated using the TiO_2-specific crystalline shape constant K = 0.7905 and the Spurr-Meyer equation as shown:[73, 169]

$$f_A = \frac{w_A}{w_A + w_R} = \frac{1}{1 + \frac{1}{K}(\frac{I_R}{I_A})} = \frac{1}{1 + 1.265(\frac{I_R}{I_A})}$$

The fraction of anatase (f_A) by weight (w) is calculated from the intensities of the anatase (101) and rutile (110) lattice peaks, I_A and I_R, located at 15.8° 2θ and 17.2° 2θ, respectively with the synchrotron light source XRD.

Spurr-Meyer calculations confirm that the fraction of anatase remaining in these two TiO_2 specimens to be 97.7 % anatase (Figure S2.3(d)). However, TiO_2 pellets heat treated at 1,000°C clearly show a shift in the diffraction peak pattern that is consistent with the rutile phase, and Spurr-Meyer calculations confirm only 14.1% remains in the anatase phase. The TiO_2 pellets heat treated at 800°C were not analyzed by XRD. These results indicate the compacted TiO_2 pellets are resistant to the typical phase transformation from anatase to rutile, the more thermodynamically stable form, often reported to occur at temperatures above 600°C. Our compacted pellets did not show any significant phase transformation until the 1,000°C heat treatment scheme. We believe that the compression process may have created lattice compaction and distortion in the crystal geometry which inhibits atomic diffusion processes need for lattice rearrangement to occur.

BET specific surface area and porosimetry was performed on TiO_2 pellets using nitrogen physisorption at 77 K with a Micromeretics ASAP 2020 system. The specific surface areas were calculated according to the Brunauer-Emmett-Teller (BET) method (P/P_0 = 0.1-0.3). Total pore volume of the TiO_2 pellets was determined by nitrogen desorption at P/P_0 = 0.99. Barrett-

Joyner-Halenda (BJH) analysis was employed to characterize pore size distribution and using average values from both adsorption and desorption techniques. Prior to adsorption/desorption measurements, samples were outgassed at 573 K for 24 h and duplicate samples were analyzed and reported values to within ± 0.05 relative standard deviation of original samples. Figure S2.3(d) summarizes these results including the BET surface areas determined to be 8.44, 7.48, and 8.15 m^2/g for TiO_2 pellets heat treated at 700°C, 800°C, and 880°C, respectively. The average pore widths for these same pellets were 117, 167, and 147 Å, respectively. In all three of these pellet types, 80 – 82% of their total surface area was due to surface are from pores between the sizes of 17 and 3000 Å.

Table S2.1 Results and test criteria used to evaluate mechanical stability of finished TiO_2 pellets

TiO_2 Pellets Annealing Treatment	mass (g) of intact TiO_2 pellets			% by mass remaining as intact TiO_2 pellet		
	initially	at 10 sec	at 25 sec	at 10 sec	at 25 sec	Pellet Stability
500°C for 4 hours (AA)	0.972	0.631	0.272	65%	28%	Poor
700°C for 4 hours (AA)	1.266	0.874	0.342	69%	27%	Poor
800°C for 4 hours (AA)	1.141	0.965	0.81	85%	71%	Good
880°C for 4 hours (AA)	1.857	1.783	1.693	96%	91%	Excellent
1000°C for 4 hours (AA)	0.996	0.986	0.958	99%	96%	Excellent

Criteria used to categorize TiO_2 pellet mechanical stability after shaking at 210 rpm

Final Pellet Integrity	**% by mass remaining as intact pellets**
Excellent Stability (can be used in FTERs)	> 90% after 10 seconds shaking AND > 80% after 25 seconds shaking
Good Stability	> 70% after 10 seconds shaking AND > 50% after 25 seconds shaking
Poor Pellet Stability	≤ 50% after 10 or 25 seconds shaking

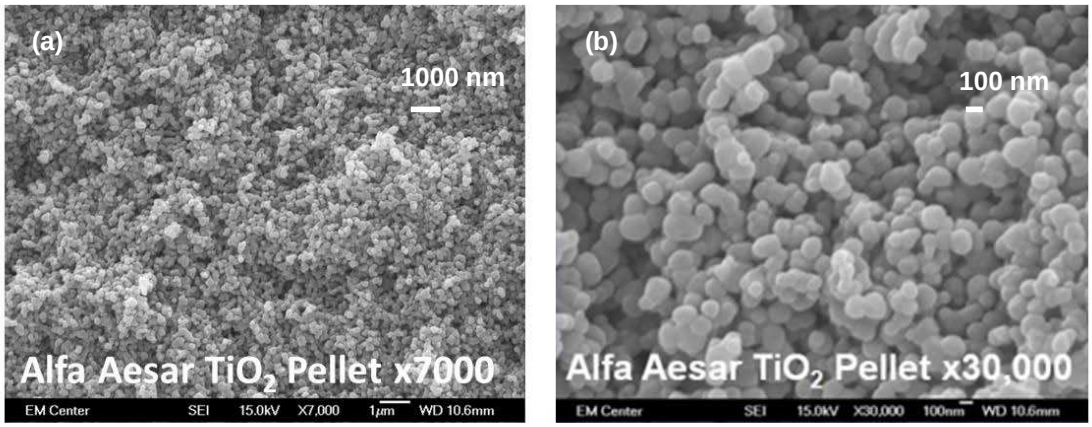

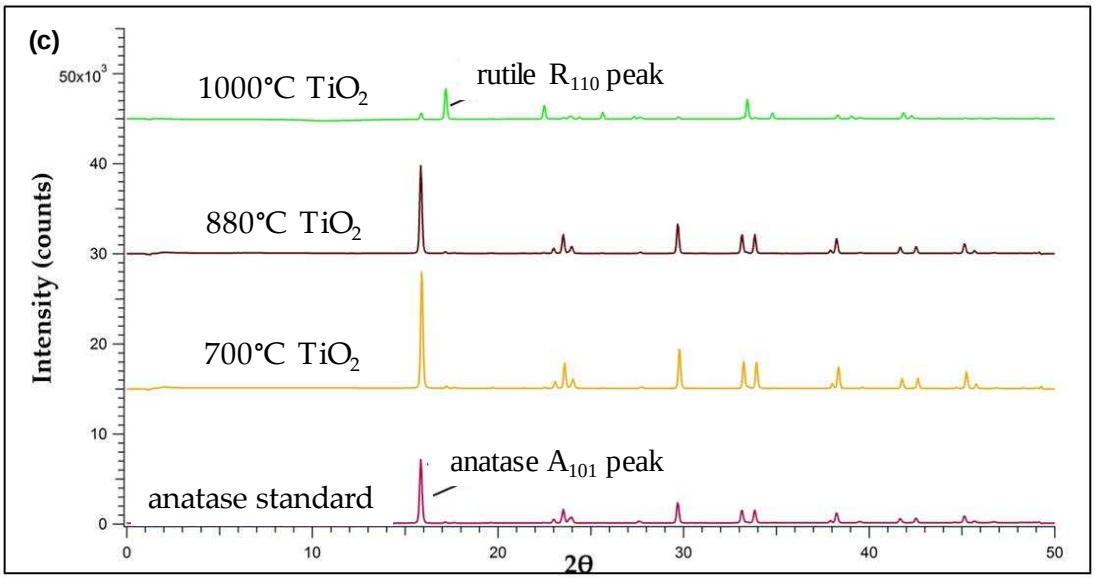

(d) **Characterization of Inter-electrode TiO_2 Pellet using XRD and Porosimetry Data**

TiO_2 sintering temp. (°C)	Fraction anatase (by wt)	Fraction rutile (by wt)	BET SA (±0.03 m^2/g)	% SA due to pores	Avg. pore width (Å)
700	0.977	0.023	8.44	82%	117
800	*NM*	NM	7.48	82%	167
880	0.977	0.023	8.15	80%	147
1000	0.141	0.859	*NM*	*NM*	*NM*

NM: not measured *BET SA: Brunauer, Emmett & Teller surface area*

Figure S2.3 SEM images of TiO_2 pellet surface after 4 hour heat treatment at 880°C using (a) 7,000x magnification and (b) 30,000x magnification. (c) Synchrotron XRD data for TiO_2 pellets heat-treated for 4 hours at 700 °C, 880 °C and 1,000 °C compared to anatase powder standard (purity >99.6%) not treated by heat. (d) Data characterizing TiO_2 pellets sintered for 4 hours at 700°C, 800°C, 880°C and 1000°C using XRD, BET surface area and porosimetry. Percentage of anatase and rutile composition were calculated using the Spurr & Meyer equation and the crystalline shape constant K = 0.7905 specific to TiO_2 crystals.

Electrochemical degradation of 1,4-dioxane in FTERs. In Figure 2.2, electrochemical degradation efficiencies are expressed as percentage of dioxane degraded according to equation S1, where C_{eff} is effluent and C_{inf} is influent dioxane concentration.

$$\text{Degradation (\%)} = [1 - (^{C_{eff}}/_{C_{inf}})] \cdot 100 \qquad \text{(Eq. S1)}$$

Table S2.2 summarizes the 10 different experimental regimes performed in TiO_2-catalyzed FTERs and non-catalyzed FTERs. This table records the pH of the effluent, current density, the pseudo-first order rate constant k_{obs}, and the percentage of dioxane degraded under different operational parameters. The overall degradation efficiency of TiO_2 pellets vs. the control experiments is compared from all treatment regimes as a performance enhancement ratio. Table S2.3 displays how the pore volume and flow rates of the FTERs were used to calculate Darcy velocity, seepage velocity and hydraulic residence time (e.g., HRT is 17.9 hours at a seepage velocity of 30.6 cm/d), which was then used to calculate the k_{obs} values. The pseudo-first order observed rate constants, k_{obs}, were determined according to equation S2 used by Carbonaro, et al. for continuous-flow experiments.

$$k_{obs} = \frac{-\ln(^{C_{eff}}/_{C_{inf}})}{HRT} \qquad \text{(Eq. S2)}$$

Table S2.2 Summary of results from FTER experiments

#	Applied voltage (V)	[Dioxane]$_0$ (μM)	Electrolyte [Na_2SO_4] (mM)	Flux V_s ($cm^3 \cdot cm^{-2} \cdot d^{-1}$)	Inter-electrode material	pH (± SD) of effluent*	Redox potential (V vs SHE)	Current density ($mA \cdot cm^{-2} \pm 0.2$)	k_{obs} (hr^{-1})	Dioxane degraded (%)	PE ratio
1	**8.0**^{BM}	**3.4**^{BM}	**10.0**^{BM}	**30.6**^{BM}	TiO_2 pellets	9.5 ± 2.6	4.1	3.5	0.065	69.0 ± 1.3	1.4
2	**0.0**	-	-	-	TiO_2 pellets	3.8 ± 0.1	0.6	0.0	0.001	2.3 ± 1.0	0.6
3	**11.0**	-	-	-	TiO_2 pellets	5.1 ± 2.1	5.7	5.3	0.074	73.3 ± 7.5	1.6
4	**14.0**	-	-	-	TiO_2 pellets	2.6 ± 0.1	6.9	8.3	0.094	81.4 ± 1.1	1.8
5	-	-	**3.0**	-	TiO_2 pellets	6.1 ± 1.1	4.4	2.5	0.066	69.6 ± 3.5	∞
6	-	-	**30.0**	-	TiO_2 pellets	4.8 ± 1.2	4.3	7.0	0.107	85.2 ± 1.6	1.4
7	-	-	-	**61.1**	TiO_2 pellets	6.3 ± 3.8	4.5	3.2	0.088	53.7 ± 3.1	2.1
8	-	-	-	**15.3**	TiO_2 pellets	11.1 ± 0.2	3.9	3.4	0.045	79.8 ± 1.8	3.9
9	-	**40.0**	-	-	TiO_2 pellets	10.4 ± 0.1	4.2	3.8	0.053	61.2 ± 1.2	2.1
11	-	**207**	-	-	TiO_2 pellets	5.3 ± 2.5	4.2	3.0	0.026	37.6 ± 3.1	2.8
12	-	**470**	-	-	TiO_2 pellets	5.1 ± 0.9	4.1	3.1	0.032	43.8 ± 3.7	4.6
13	**5.0**	**98**	**30.0**	**61.1**	TiO_2 pellets	10.5 ± 0.6	2.9	2.7	0.058	40.4 ± 2.6	2.5
1	**8.0**^{BM}	**3.4**^{BM}	**10.0**^{BM}	**30.6**^{BM}	glass beads	9.8 ± 0.4	4.1	1.5	0.038	49.4 ± 4.4	NA
2	**0.0**	-	-	-	glass beads	3.9 ± 0.04	0.6	0.0	0.002	3.8 ± 1.8	NA
3	**11.0**	-	-	-	glass beads	9.0 ± 0.9	5.7	2.2	0.033	45.0 ± 1.8	NA
4	**14.0**	-	-	-	glass beads	4.2 ± 0.5	6.9	3.3	0.034	45.8 ± 3.6	NA
5	-	-	**3.0**	-	glass beads	5.1 ± 1.1	4.1	1.1	0.000	0 ± 7.6	NA
6	-	-	**30.0**	-	glass beads	3.9 ± 0.6	4.4	3.4	0.052	60.7 ± 6.8	NA
7	-	-	-	**61.1**	glass beads	7.1 ± 1.5	4.4	1.4	0.034	26.5 ± 1.5	NA
8	-	-	-	**15.3**	glass beads	9.6 ± 0.7	4.3	1.5	0.006	20.6 ± 11.2	NA
9	-	**40.0**	-	-	glass beads	8.5 ± 1.0	4.2	1.6	0.019	28.8 ± 1.8	NA
11	-	**207**	-	-	glass beads	6.7 ± 2.0	4.3	1.4	0.008	13.4 ± 4.6	NA
12	-	**470**	-	-	TiO_2 pellets	9.4 ± 1.1	4.3	1.4	0.006	9.46 ± 2.9	NA
13	**5.0**	**98**	**30.0**	**61.1**	TiO_2 pellets	9.9 ± 1.7	3.0	1.4	0.020	16.3 ± 1.2	NA

^{BM} represents the "benchmark level or quantity" from which one or more operational parameters are varied for each flow-through electrochemical

\- signifies that this operational parameter is equal to the "benchmark level"

* pH of unbuffered feedstock influent for all cycles was 7.2 ± 1.0 and SD signifies standard deviation

SHE signifies standard hydrogen electrode and $k_{obs} = [-\ln(C_{eff}/C_{inf})] / HRT$

PE ratio (Performance Enhancement Ratio) is a ratio of % 1,4-dioxane degraded by the TiO_2-catalyzed FTER vs. non-catalyzed FTER under same co

Table S2.3 Flow parameter calculations using hydraulic mass continuity and Darcy equations

measured	The "reactive region" of large 10cm ID FTER is the 22.9 cm from first to last electrode including small buffer
measured	to either side with a measured void volume or "reactive pore volume"(RPV) of 700 cm^3
$v_d = Q / A$	Darcy discharge velocity (v_d) is a flux, thus flow rate (Q) through a cross-section area (A), disregarding porosity
$v_s = v_d / \eta$	Seepage velocity (v_s), also a flux, is dependent on flow rate Q through the void spaces of the cross-sectional area
$\eta = V_v/V_T$	The void volume (V_v) of reactive region and total volume (V_T) are used to determine porosity (η)
$HRT = V_v / Q$	Hydraulic residence time (HRT) is average time a compound (eg.dioxane, water) remains in reactive region

Darcy Discharge Velocity ($L^3/L^2/T$) Calculation: $v_d = Q/A_{total}$ --> flux disregarding porosity of cross-sectional area

	Cross-Section Calculation	Cross-Section Calculation	Cross-Section Calculation
Electrode Area	78.50 cm^2	78.50 cm^2	78.50 cm^2
Column radius	5 cm	5 cm	5 cm
	At Benchmark (BM) Flow	At flow rate < BM	At flow rate > BM
flow rate Q	0.65 mL/min	0.325 mL/min	1.3 mL/min
flow rate Q	39 mL/hr	19.5 mL/hr	78 mL/hr
flux $v_d = Q / A$	11.9 cm/d darcy flux	6.0 cm/d darcy flux	23.8 cm/d darcy flux
column length	0.75 ft	0.75 ft	0.75 ft
column length	22.9 cm	22.9 cm	22.9 cm
V_{void} (cm^3)	700 cm^3 RPV or V_{void}	700 cm^3 RPV or V_{void}	700 cm^3 RPV or V_{void}
$V_{total} = \pi r^2 h$ (cm^3)	1797 cm^3 Max V_{total}	1797 cm^3 Max V_{total}	1797 cm^3 Max V_{total}
porosity $\eta = V_v/V_T$	0.3895 $\eta = V_v/V_T$	0.3895 $\eta = V_v/V_T$	0.3895 $\eta = V_v/V_T$

Seepage Velocity ($L^3/L^2/T$) Calculation: $v_s = v_d/\eta$ --> a flux expressed as an average velocity in porous media in consideration of flow only happening within void space; thus $v_s > v_d$ always and HRT uses v_s

Seepage velocity	1.0 ft/d	0.5 ft/d	2.0 ft/d
Seepage velocity	30.6 cm/d	15.3 cm/d	61.2 cm/d

Hydraulic Residence Time (HRT): represents average time a compound (e.g. dioxane) remains in region of reactivity

$HRT = V_v / Q$	17.9 hr	35.9 hr	9.0 hr

Electrochemical degradation products of 1,4-Dioxane. The total organic carbon measurements of influent and effluent were used to calculate the amount of 1,4-dioxane fully mineralized to CO_2 after treatment of 470 µM 1,4-dioxane with 8.0 V (10 mM Na_2SO_4 electrolyte and 30.6 cm/d seepage velocity). Based upon the mass transfer limitation experienced in our laboratory-scale FTERs, this relatively high concentration of 470 µM 1,4-dioxane is not expected to be at optimal conditions for full mineralization of 1,4-dioxane. However, this higher concentration was necessary to obtain TOC levels above detection limits on our Shimadzu TOC analyzer. Figure S2.4 summarizes the TOC results for this experiment. Effluent samples were analyzed by LC-ESI-TOF-MS to look for possible transformation products from electrochemical

oxidation of 1,4-dioxane. Four organic acid transformation products were detected. The chromatographic retention times and other mass spectra data of these four chemical species are summarized in Table S2.4. A possible degradation pathway was proposed in Figure 2.3 that includes these four intermediates, along with other intermediates known to possible based upon other advanced oxidation treatment of 1,4-dioxane in the literature.

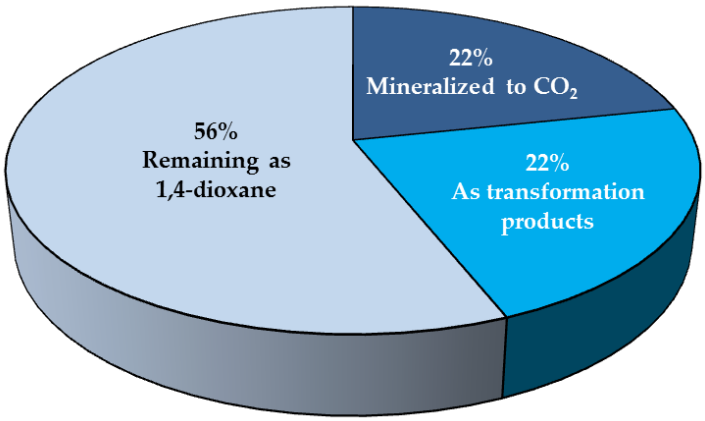

	Total organic carbon (mg/L)		
	Influent	Effluent	% Mineralized to CO_2
Replicate 1	23.08	17.63	23.61
Replicate 2	22.90	18.08	21.05
Replicate 2	22.74	18.11	20.36
Average	22.91	17.94	21.67
SD	0.17	0.27	0.36
RSD	0.007	0.015	0.017

SD, standard devation; RSD, relative standard deviation

Figure S2.4 a) Pie chart showing relative distribution of initial TOC, all from 1,4-dioxane as the sole organic carbon parent compound in the system. A treatment (i.e., single pass) through a TiO_2-catalyzed FTER at 30.6 cm/d, with 8.0 V applied to a 10 mM Na_2SO_4 feed solution spiked with 470 µM 1,4-dioxane. b) Table of triplicate TOC data for the same FTER experiment, with means, standard deviation and relative standard deviation for influent and effluent.

Table S2.4 Chromatographic retention times and ESI-TOF-MS data for intermediates

Species (intermediates)	Retention time (min)	Molecular formula [M]	Base peak ion	Observed *m/z*	Theoretical *m/z*	Error (ppm)	Base peak ion formula
succinic acid	16.1	$C_4H_6O_4$	$[M-H]^-$	117.0188	117.0193	4.52	$C_4H_5O_4^-$
malic acid	18.0	$C_4H_6O_5$	$[M-H]^-$	133.0126	133.0142	11.98	$C_4H_5O_5^-$
mesoxalic acid	19.7	$C_3H_2O_5$	$[M-H]^-$	116.9829	116.9821	-8.05	$C_3HO_5^-$
glycolic acid	13.6	$C_2H_4O_3$	$[M-H]^-$	75.0127	75.0088	-51.2	$C_2H_3O_3^-$

Dark activation of TiO_2 without direct electrode contact. Non-insulated pellets were in direct contact with both anode and cathode, while insulated pellets had a geotextile barrier (polypropylene felt layer) separating the TiO_2 from any contact with either electrode. All experiments, including the non-catalytic control column, were conducted in 5.0 cm I.D. column reactors operated under the following conditions: 91 µM 1,4-dioxane, 20 mM Na_2SO_4 electrolyte, 27.3 cm/day and 8.0 V applied. Figure S7 shows that the catalyzed reactors with (36%) and without (44%) the insulating geotextile layer both were able to provide increases in 1,4-dioxane degradation efficiency compared to the non-catalytic column (15% degradation).

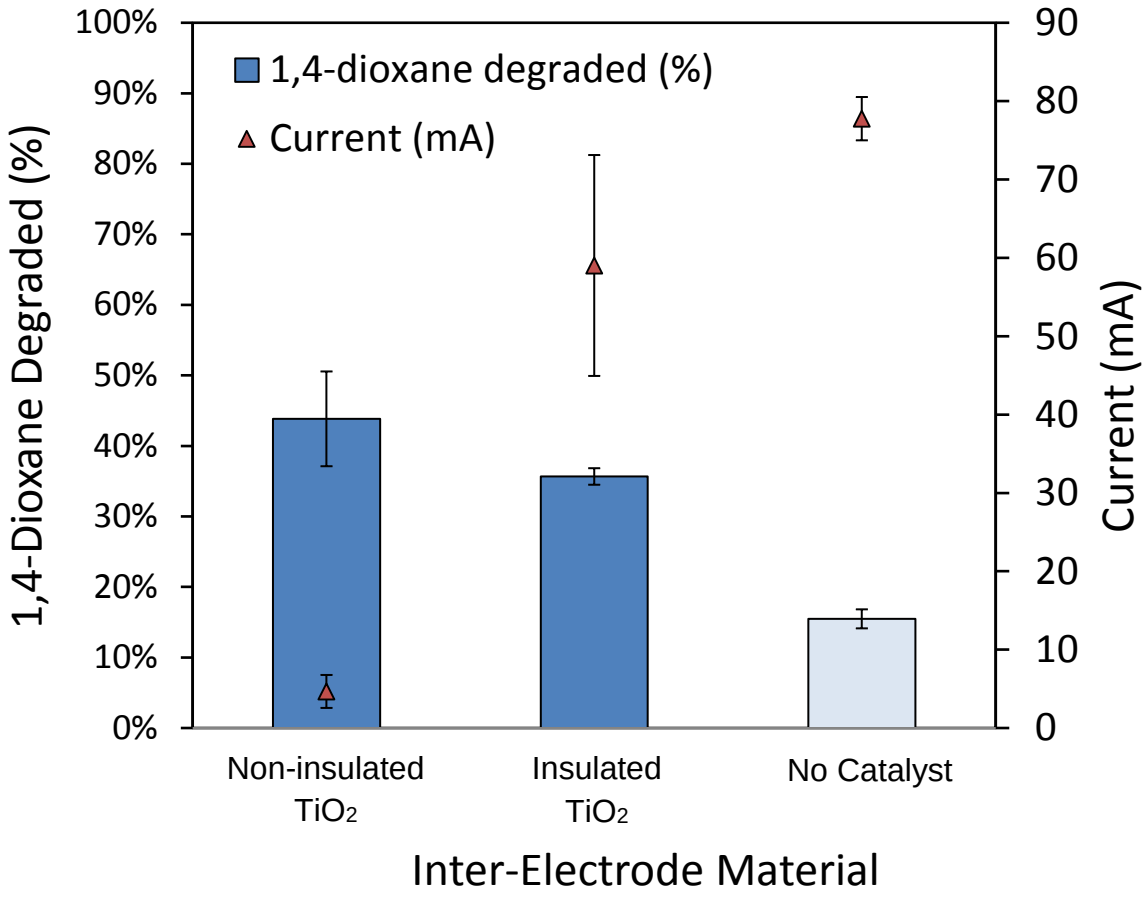

Figure S2.5 Degradation efficiencies of 1,4-dioxane in 5.0 cm I.D. flow-through electrochemical reactors operated under the following conditions: 91 µM 1,4-dioxane, 20 mM Na_2SO_4 electrolyte, 27.3 cm/day and 8.0 V applied. The "No Catalyst" control had inert glass beads in between electrodes. The secondary y-axis plots the average steady state current for each column experiment. Error bars indicate standard deviation ($n \geq 3$) for samples taken during steady-state.

APPENDIX B

SUPPORTING INFORMATION FOR CHAPTER 3

Mechanistic investigations. Many experiments were designed to investigate possible mechanisms for the dark activation of the TiO_2 pellets. Studies were performed in flow-through electrochemical reactors (Figure S3.1) with different types of inter-electrode TiO_2 pellets. Other studies were performed in electrochemical batch reactors, sometimes using a Nafion NRE-212 membrane to operate in conditions where anode and cathode chamber were chemically isolated (Figure S3.2). The Nafion only allows proton exchange to maintain electrical current, while blocking the transport of organic molecules like 1,4-dioxane, carbon tetrachloride, 1,4-benzoquinone (BQ), and *tert*-butylalcohol (TBA).

Catalyst characterization. Multiple analyses were used to characterize the finished TiO_2 pellets fabricated from different starting materials and sintered at different temperatures. Powder X-ray diffraction (P-XRD) plots were overlaid in Figure 3.3 to show how the kinetics of transformation from anatase to rutile is inhibited by the compaction step in fabrication. The AP-C880 and AP-F880 TiO_2 pellets made from the coarse anatase (Huntsman) and fine anatase (Alfa Aesar) powders are resistant to the calcination/transformation process even after 19 hours of heat treatment at 880 °C. Lattice distortion from the compaction step may make inhibit atomic diffusion needed for rearrangement of Ti and O atoms. In contrast, the RP-F880 TiO_2 pellets made from Evonik P25 powder, composed of 20% rutile and 80% anatase, did exhibit rapid transformation to 100% rutile with just 4 hours at 880 °C, possibly due to having rutile nucleation sites able to stimulate phase transformation. P-XRD analysis of the raw Huntsman

and Alfa Aesar anatase powders after heating at 880 C, but without compaction, showed that gradual transformation from anatase to rutile does occur as seen at the 4 hr, 9 hr, and 19 hr diffractograms shown in Figure S3.3(b,c).

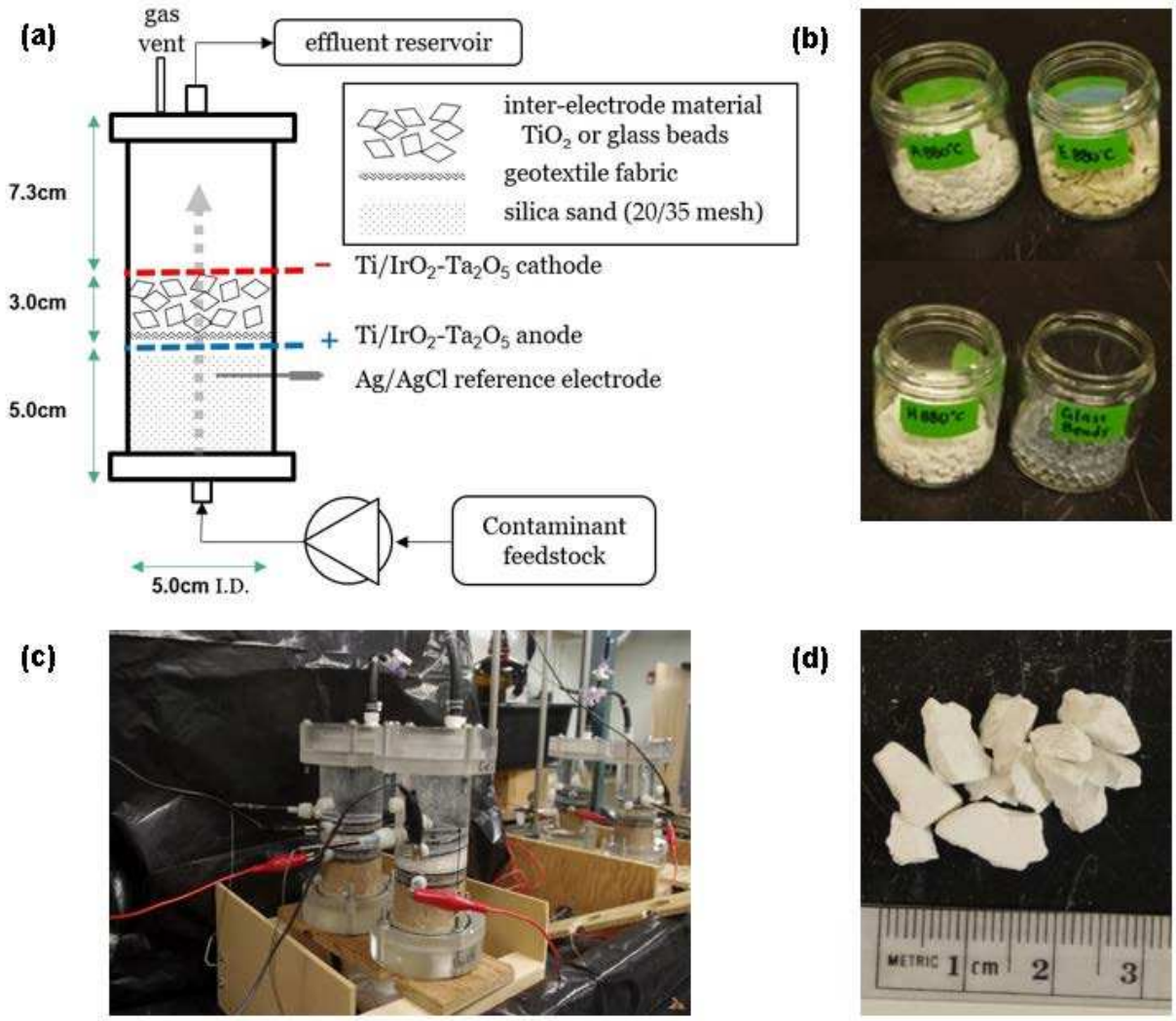

Figure S3.1. (a) Schematic of 5.0-cm internal diameter (I.D.) flow-through electrochemical reactor (FTER) with flow directed upward. Photos of (b) inter-electrode material in clockwise direction are AP-F880, RP-F880, Glass beads, and AP-C880. (c) Four FTERs running simultaneous experiments and (d) a zoomed-in view of AP-F880 TiO_2 pellets. The inter-electrode TiO2 pellets were separated from the electrodes with an insulating geotextile (polyprolylene felt) layer adhered to a HDPE geonet grid.

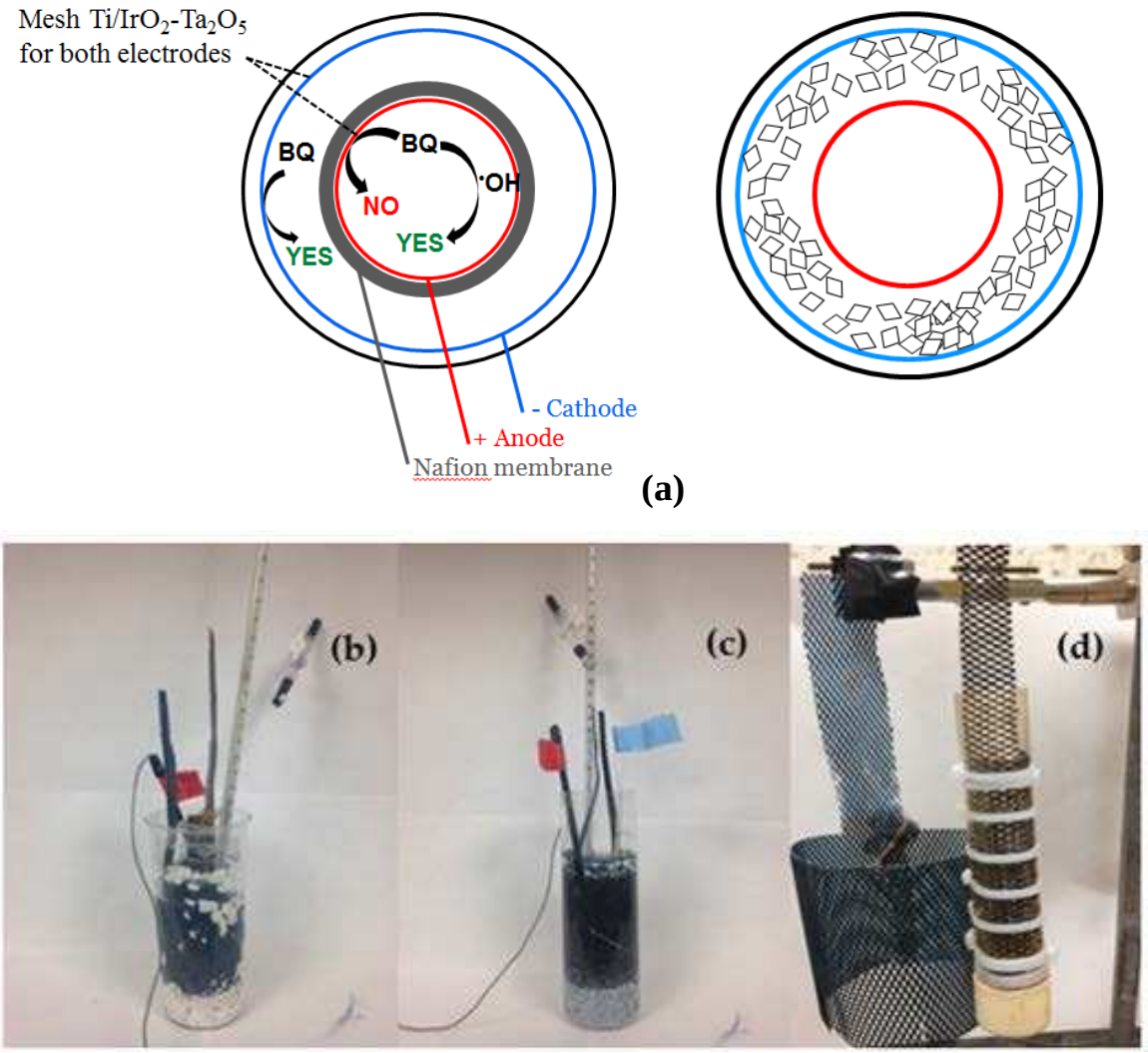

Figure S3.2. (a) Schematic showing the top view of a concentric cylindrical electrode batch reactor with Nafion NRE-212 membrane and without Nafion separation, but with TiO_2 pellets. Nafion is used to separate inner anodic chamber from the outer cathodic chamber. Nafion NRE-212 membrane has technical properties of 0.05 mm thickness and 0.92 meq/g exchange capacity and is composed of $Rf[OCF_2CF(CF_3)_2]_nOCF_2CF_2SO_3H$ (Alfa Aesar PN 45036). Photos of these batch reactors with (b) TiO_2 pellets as packing material, (c) glass beads as packing materials for the control experiments, and (d) showing the outer cylinder electrode and the inner electrode when sealed with a Nafion membrane.

Scanning electron microscopy images shown in Figure S3.3 shows that (d) AP-F880 and (e) AP-C880 TiO_2 pellets exhibit spherical crystalloids with uniform porosity (typical other anatase catalysts), while (f) RP-880 pellets show crystal aggregration effects and shallower, less abundant pore morphology. The (a) Absorbance at different wavelength using UV-Vis diffuse

reflectance analysis, (b) N_2 adsorption/desorption isotherm, and (c) relative pore size distribution.

(a)

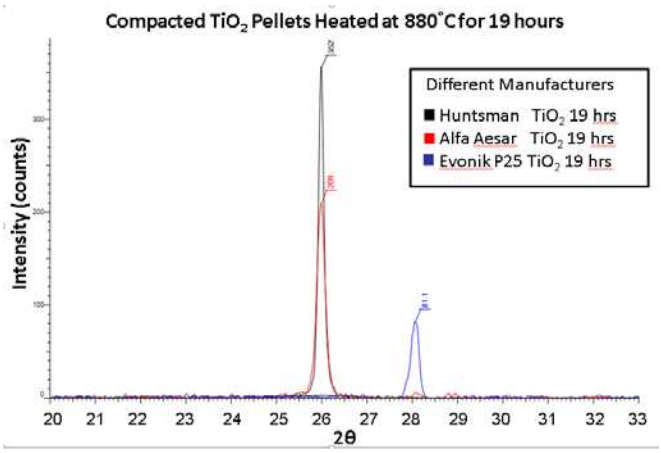

(b)

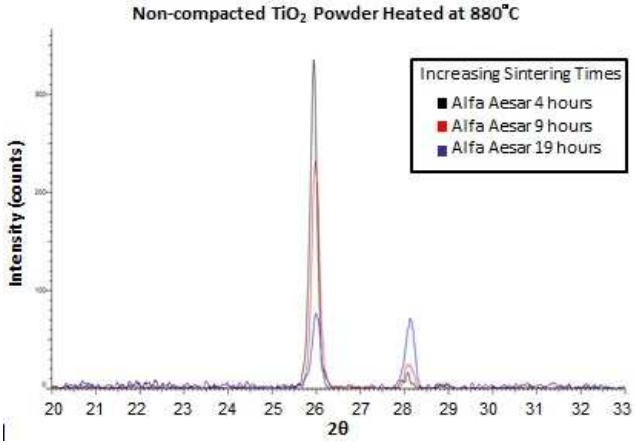

(d)

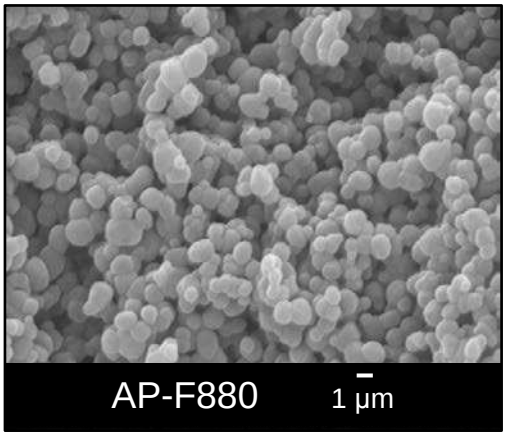

(e)

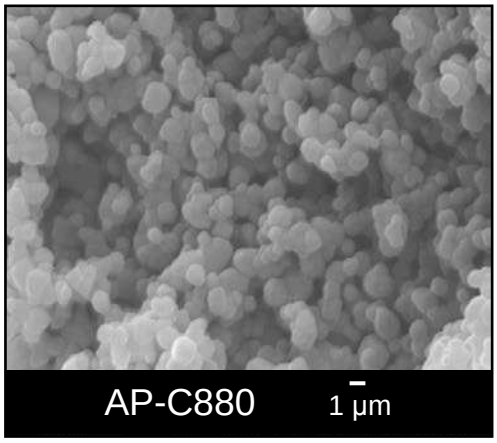

(c) (f)

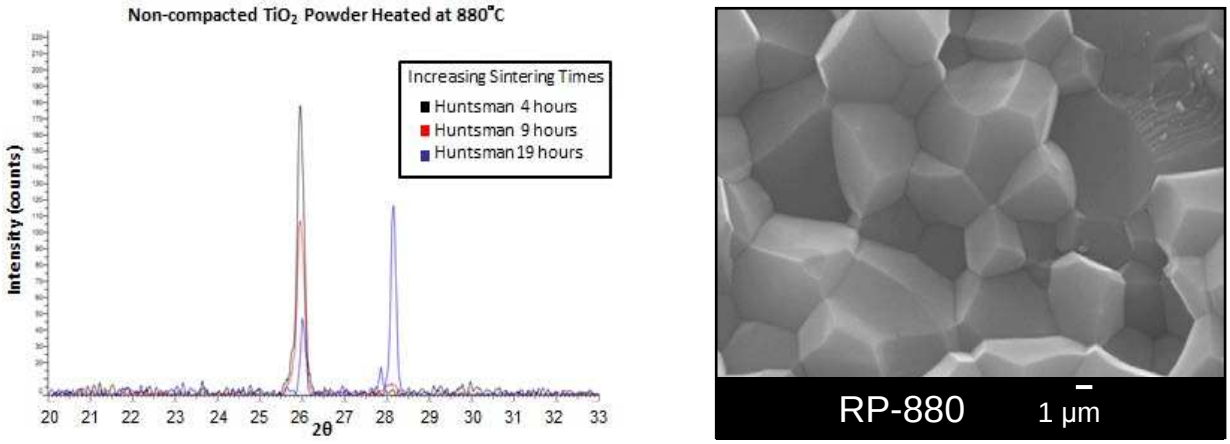

Figure S3.3. Powder XRD Diffractograms after 880°C calcination of a) compacted TiO_2 pellets after for 19 hours, b) AP-F880 for 4, 9 and 19 hours, c) AP-C880 for 4, 9 and 19 hours. SEM images at 30,000x magnification of d) AP-F880, e) AP-C880, and f) RP-880 TiO_2 pellets.

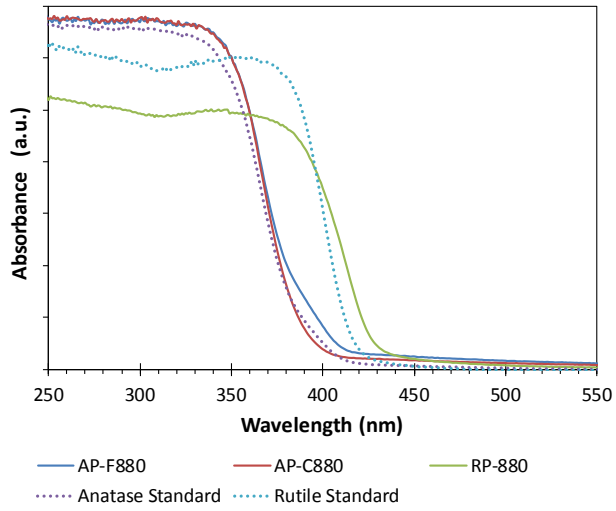

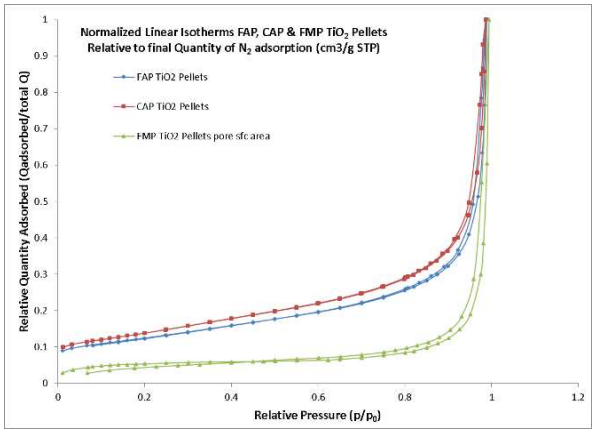

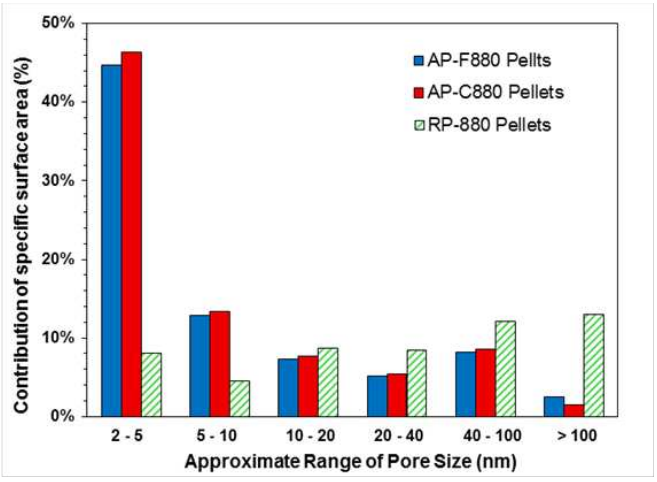

Figure S3.4. Plots comparing electronic and physical properties of three different TiO_2 pellets: AP-F880, AP-C880, and RP-880. (a) Absorbance at different wavelength using UV-Vis diffuse reflectance analysis, (b) N_2 adsorption/desorption isotherm, and (c) relative pore size distribution.

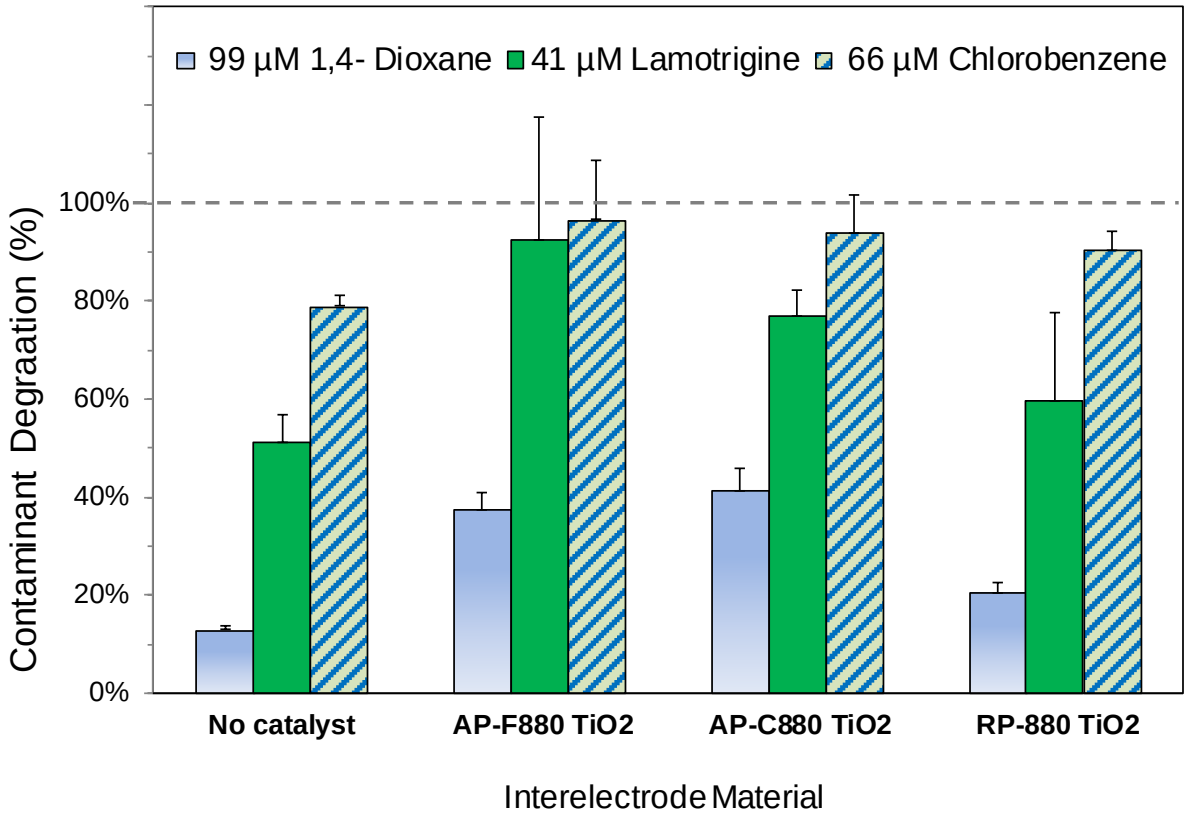

Figure S3.5. Contaminant degradation (%) shown for three persistent pollutants (1,4-dioxane, lamotrigine, and chlorobenzene) using flow-through electrochemical reactors with four different inter-electrode materials with the "no catalyst" reactor using inert glass beads between the electrodes. The experiments were conducted using 8.0 V and seepage velocity of 27.4 cm/d to treat influent spiked with either 99 µM 1,4-dioxane, 41 µM lamotrigine, or 66 µM chlorobenzene into 10 mM Na_2SO_4 electrolyte. Error bars represent standard deviation, n =3.

Table S3.1. Characterization of various compositions of TiO_2 pellets.

TiO_2 pellet type[a]	X_A (by wt)[b]	X_R (by wt)		avg crystallite size[c] (nm)	band gap energy (eV)	BET sfc area (± 0.03 m^2/g)	% SA due to pores	avg. pore width (nm)	Bulk Density ρ (g/cm^3)	mass (g) per inter-electrode space[e]
AP-F880	0.977	0.023	A	45 ± 11	3.20	8.15	80.8%	14.6	0.76	30.3
			R	- -						
AP-C880	0.995	0.005	A	51 ± 7	3.21	8.09	81.3%	13.8	0.73	29.4
			R	- -						
AP-C700	0.995	0.005	A	32 ± 4	NM[d]	8.44	NM	NM	0.73	29.1
			R	- -						
RP-F880	0.000	1.000	A	- -	2.880	0.016	82.4%	51.5	1.56	62.5
			R	35 ± 9						
MP-F800	0.925	0.075	A	47 ± 4	NM	NM	NM	NM	0.84	33.7
			R	55 ± 11						

[a]Sample names represent the phase composition of the final TiO_2 pellets with AP (>97% anatase), RP (100% rutile), MP (mixed phase) before the dash and after the dash, is the size of the precursor powder F (fine < 45 μm) or C (coarse) followed by the temperature used for the 4 hr thermal treatment

[a]Spurr-Meyer calculations were performed on Synchrotron PXRD data for AP-F880, AP-C880, and RP-880, while Scintag X2 data was used for others

[b]Estimated average of Scherer's equation applied to Scintag X2 lattice peaks for anatase @ 2θ = 25.5°, 38.0°, 55.2°; rutile @ 2θ = 28.1° & 36.3°

[d]NM indicates not measured for that specific sample

[e]the 2.54 cm space between electrodes had a measured of $40cm^3$ which was filled to capacity with each pellet type

Flow-through treatment: electrocatalytic behavior at steady state. Table S3.2 includes quantitative data to support Figure 3.3 of the main manuscript.

Table S3.2. Measurements of FTER experiments using different inter-electrode fill material.

Inter-electrode material	[a]AP-F880*	AP-F880	AP-C880	AP-C700	RP-880	MP-800	No Catalyst
Fraction of 1,4-dioxane removed	0.438	0.357	0.397	0.615	0.187	0.177	0.155
Standard deviation	0.067	0.012	0.017	0.121	0.006	0.006	0.013
Current (mA)	4.67	59.025	149.883	167.128	79.913	96.463	77.760
Standard deviation	2.10	14.096	4.315	13.254	4.947	14.048	2.764
Redox potential (V) vs SHE	7.29	1.485	1.730	1.585	1.558	1.290	1.274
Standard deviation	0.28	0.086	0.153	0.243	0.065	0.009	0.031
pH	4.67	6.000	10.333	11.333	6.000	5.833	7.167
Standard deviation	0.76	0.866	1.528	1.155	0.500	0.577	2.466
Conductivity (mS/cm)	4.10	4.608	4.976	5.605	4.599	4.699	4.687
Standard deviation	0.38	0.111	0.068	0.033	0.213	0.030	0.131

[a]AP-F880* is the only reactor purposely lacking a geotextile insulating barrier between the catalytic pellets and electrodes

Electrical current experiments. Experiments were performed electrochemical batch reactors to determine if higher current could be shown to occur when greater pore space (void space between TiO_2 pellets or glass beads) was available. Experimental set up included using a plastic 9"L x 2.5'W x 2"H bin as an "open tray reactor" filled with 500 mL of 10 mM sodium sulfate electrolyte and having a pair of mesh Ti/IrO_2-Ta_2O_5 electrodes spaced 2.5" (6.35 cm) apart. The inter-electrode space was filled to the top of the water line with 150 cm^3 of either AP-F880 TiO_2 pellets (~ diameter range 3.3 – 9 mm), large glass beads (d ~ 6 mm), or small beads (d ~ 2 cm) and the electric current between the electrode pair was measured after an electrical bias applied of 5 V, 8 V, 11 V, and 14. Similarly, current measurements were made with the open tray reactor only half-full of each inter-electrode material to monitor current changes with this

increase in pore volume. Detailed information regarding porosity, pore volume and electrical current measurements are provided in Table S3.3. Results did show that there was increasing current values measured when the pore volumes increased while having the same material reduced from filling inter-electrode space to only half filling the space. For example, the current increased from 18.8 to 29.4 mA at 14.0 V when large glass bead filling material was reduced by half. However, with TiO2 as the filling material, the current appears to plateau. The results also indicate that at 8.0V, higher currents are observed with TiO_2 as the fill material (33.3 mA) compared to large glass beads (9.3 mA) and small glass beads (17.5 mA). However there was not a direct correlation of decreasing current with decreasing pore volumes (filled with conductive electrolyte solution) since the large glass beads with porosity of 0.42 had a much lower current at 8.0 V when compared to the small bead experiment with a porosity of 0.34. Thus, the variance in current between TiO_2 pellet columns and glass bead columns can not be explained well by the differences in porosity between them, since pore volumes in the columns differed by less than 3%. In addition, the pore volume difference are even less when comparing between different TiO_2 pellets used as inter-electrode material and thus this effect is not sufficient to explain the significant current difference observed in FTER experiments between AP-F880*, AP-F880, AP-C880, and AP-C700.

Table S3.3. Porosity characteristics and current measurements of inter-electrode fill material.

Inter-electrode Material	**Filling inter-electrode space**		**Pore volume properties**	
	mass per 150mL (g)	bulk density (g/cm^3)	V_p per $150cm^3$ (mL)	porosity (mL/mL)
Tiny Glass Beads	260 ± 5	1.73 ± 0.03	51.1 ± 0.1	0.34 ± 0.01
Large Glass Beads	220 ± 5	1.47 ± 0.03	63.4 ± 0.1	0.42 ± 0.01
A880 TiO_2 Pellets	140 ± 5	0.93 ± 0.03	110.2 ± 0.1	0.73 ± 0.03
Electrolyte Sol'n only	NA	NA	*NA*	NA
	V_p (volume of pores) per 150 mL		*Porosity (ϑ) = V_p / V_t in (mL/mL)*	

Inter-electrode material	**Electrical current measurements**					
	Current at 5V (mA)	Current at 8V (mA)	Current at 11V (mA)	Current at 14V (mA)	1/2 full at 14V (mA)	1/4 full at 14V (mA)
Tiny Glass Beads	8.6	17.5	26.6	35.8	57.9	68.9
Large Glass Beads	4.6	9.3	14.0	18.8	29.4	39.2
A880 TiO_2 Pellets	16.0	33.3	51.5	70.6	53.0	53.7
Electrolyte Sol'n only	9.6	20.4	32.6	44.2	NA	NA

APPENDIX C

SUPPORTING INFORMATION FOR CHAPTER 4

Experimental approach. Figure S4.1 displays schematic and photo of flow-through sand columns used for abiotic control, biotic control and combined electro-bioremediation experiments. Each clear PVC column reactor is 10 cm I.D. x 45 cm long with two circular mesh electrodes (cross sectional area = 78.5 cm^2 each) spaced 5.0 cm apart. The expanded mesh Ti/IrO_2-Ta_2O_5 electrodes used in the column reactors were 1.0 mm thick with 1.0 x 2.8 mm diamond shaped openings. RE_1 and RE_2 are Ag/AgCl reference electrodes (World Precision Instruments) to monitor relative redox potential of the aqueous solution. Sampling ports S1, S2 and S3 allow for liquid and solid (sand) sampling events and are located 2.5, 12.5 and 22.5 cm downstream of the anode, respectively. S_{inf} and S_{eff} ports are ports for liquid samples only. A schematic diagram of the experimental approach is shown in Figure S4.2.

Flow-through column reactors. Feedstock solutions of 1,4-dioxane and trichloroethene (TCE) were made in Ammonium Mineral Salts (AMS) medium which had a conductivity of approximately 3.6 mS/cm. Starting feedstock pH was adjusted to 6.8 ± 0.3 using NaOH before adding phosphate buffer. Measurements of pH (± 0.3) at influent, effluent and liquid ports 1, 2, and 3 were made with pH paper strips (Sigma-Aldrich PANPEHA pH 1.0-14.0; Electron Microscopy Sciences PEHANON pH 6.0-8.1; Baxter Scientific Products pH 1.7-3.8). Daily measurements were made of voltage and current between working electrodes (Fluke Multimeter) along with aqueous redox potential between and downstream of electrodes. Flow rates were measured by volumetric analysis each day to confirm a flow rate of 1.07 mL/min, corresponding

to seepage velocity of 46 cm/d (volume per porous cross-sectional area per time, $cm^3/cm^2/d$) based upon column porosity of ~0.43. To minimize sorption impacts, the feedstock was pumped through every sand column before each experiment until influent and effluent contaminant concentrations were equal. Once steady-state conditions were achieved at target voltage, a minimum of each three influent and effluent samples were collected for chemical analysis.

Analysis of chemical contaminants. For experiments only containing dioxane in the feedstock, aqueous samples were filtered with 0.45-μm syringe filters (Pall Scientific Acrodisc nylon membrane, 13 mm diameter) and extracted into dichloromethane (99.96%, OmniSolv, EMD Chemicals, Inc.) before analysis by GC/MS. For experiments containing 1,4-dioxane and TCE, aqueous samples were filtered with 0.20-μm syringe filters (Microliter Analytical Supplies PTFE membrane, 25 mm diameter), then extracted into dichloromethane before GC/MS analysis. Filtering and extraction in methyl *t*-butyl ether (99.5%, OmniSolv) was performed when analysis was done by GC/ECD. All GCs were equipped with a mid-polarity Restek Rxi-624Sil MS column (30 m x 0.25 mm ID x 1.4 μm df). Contaminant degradation rates in $mg \cdot h^{-1} \cdot m^{-2}$ were determined for averaged triplicate (or more) analyses according to the equation:

$$\text{Degradation rate } (mg \cdot h^{-1} \cdot m^{-2}) = [(C_{inf} - C_{eff}) / A] * Q$$

where $(C_{inf} - C_{eff})$ are influent and effluent contaminant concentrations, A is the cross-sectional area of mesh electrode of 0.00785 m^2, and Q is the flow rate of 0.0642 L/h.

Monitoring microbial activity and viability. *Pseudonocardia dioxanivorans* strain CB1190 was grown aerobically in Ammonium Mineral Salts (AMS) medium within 4.0-L polycarbonate Nalgene containers, maintaining 1,4-dioxane concentrations of 50-100 mg/L (Figure S4.3(a-c)). Aqueous cultures were incubated at 30 °C while shaking at 100 rpm for ~ 2

weeks, then 8/12 mesh sand was added once high CB1190 bacteria abundance was present and increasing ATP concentrations were observed (Figure S4.3(b)). The sand and CB1190 culture was monitored in order to transfer inoculated sand to pack the column reactors once high CB1190 abundance and increasing ATP concentrations were observed (~3-5 days). 1,4-Dioxane biodegradation rates were also monitored by GC/MS to confirm that CB1190 cultures were metabolizing 1,4-dioxane at suitable rates before transfer steps were performed.

Bacterial abundance was monitored by counting bacterial colonies on 3M Petrifilm Aerobic Count Plates following manufacture protocol at 1:1000 dilutions of the aqueous culture. (Figure S4.3(c)). To track ATP concentration curves over time, ATP analysis was completed within two hours of sampling using the BacTiter-Glo™ Microbial Cell Viability Assay (Promega Corporation, Madison, WI) following Promega *Technical Bulletin #TB337* and *Protocol for Measuring ATP from Bacteria Bulletin*. Briefly, an opaque-walled 96-well plate was prepared with 100 µL of non-filtered sample and 100 µL reagent in each well. The plate contents were mixed, allowed to equilibrate in the dark for five minutes, and then immediately analyzed on a BioTek Synergy HT plate reader (BioTek Instruments, Winooski, VT). Calibration curves ranged from 0.01 - 100 nM ATP and samples from different reactors were spaced out on the well plate in order to avoid interference of luminescence. Figure S4.3(c) provides an ATP concentration curve showing peak activity 27 hours after the addition of a 100 mg/L dioxane spike.

Sterilization and disinfection protocol. All glassware, micropipette tips, sand for abiotic control experiments, and most equipment was dry heat-sterilized at 232 °C for 12-18 hours or autoclaved at 121 °C and 23 psig for 20 minutes (Tuttnauer 2870 EP Autoclave). Non-

autoclavable materials, i.e. work bench surface and the PVC sand column reactors, were disinfected either with 70% ethanol or 10% bleach.

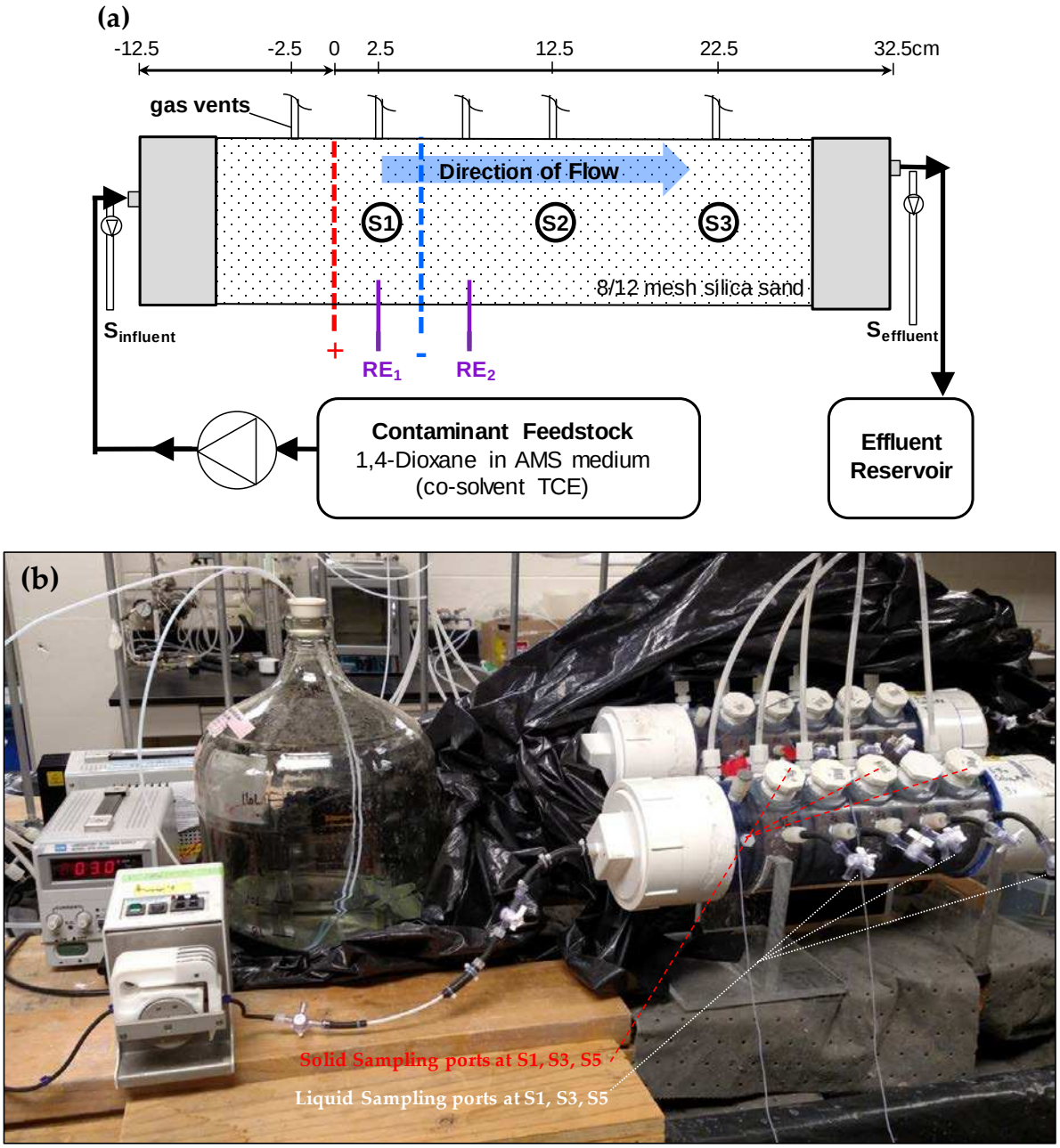

Figure S4.1 (a) Schematic and (b) photo of flow-through sand columns used for abiotic, biotic and combined electro-bioremediation experiments, all conducted in the dark by covering with black plastic.

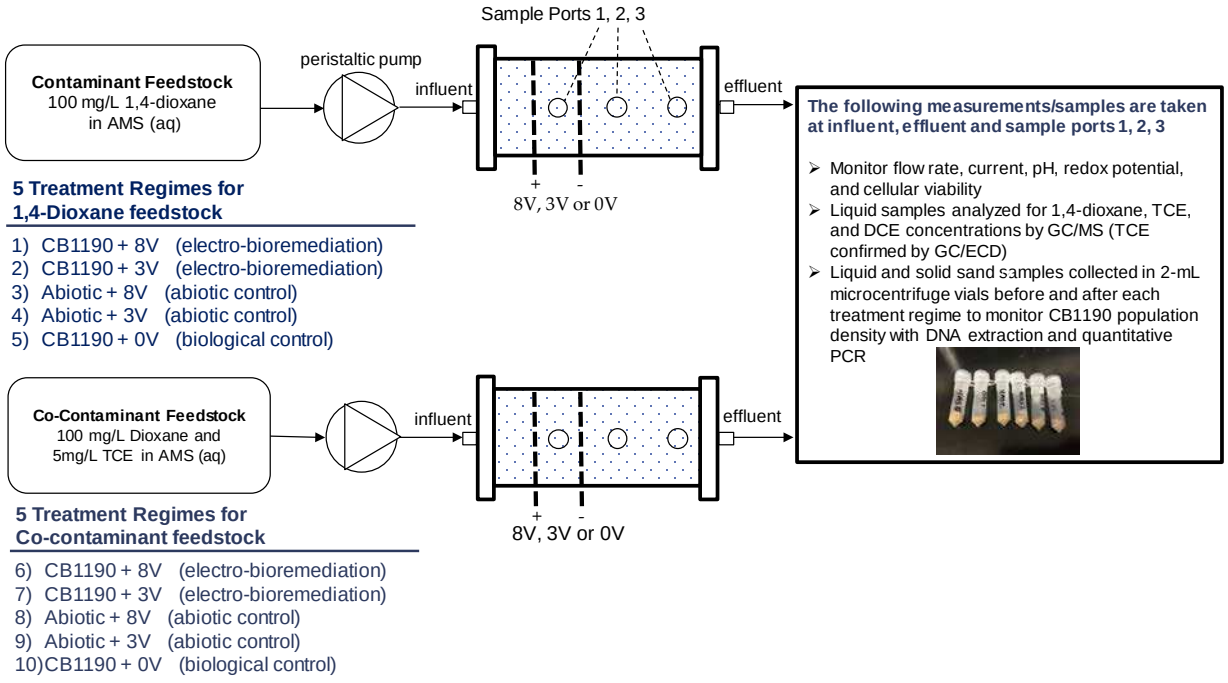

Figure S4.2 Schematic of experimental approach outlining the ten different experimental regimes tested in sand column reactors and measurements taken.

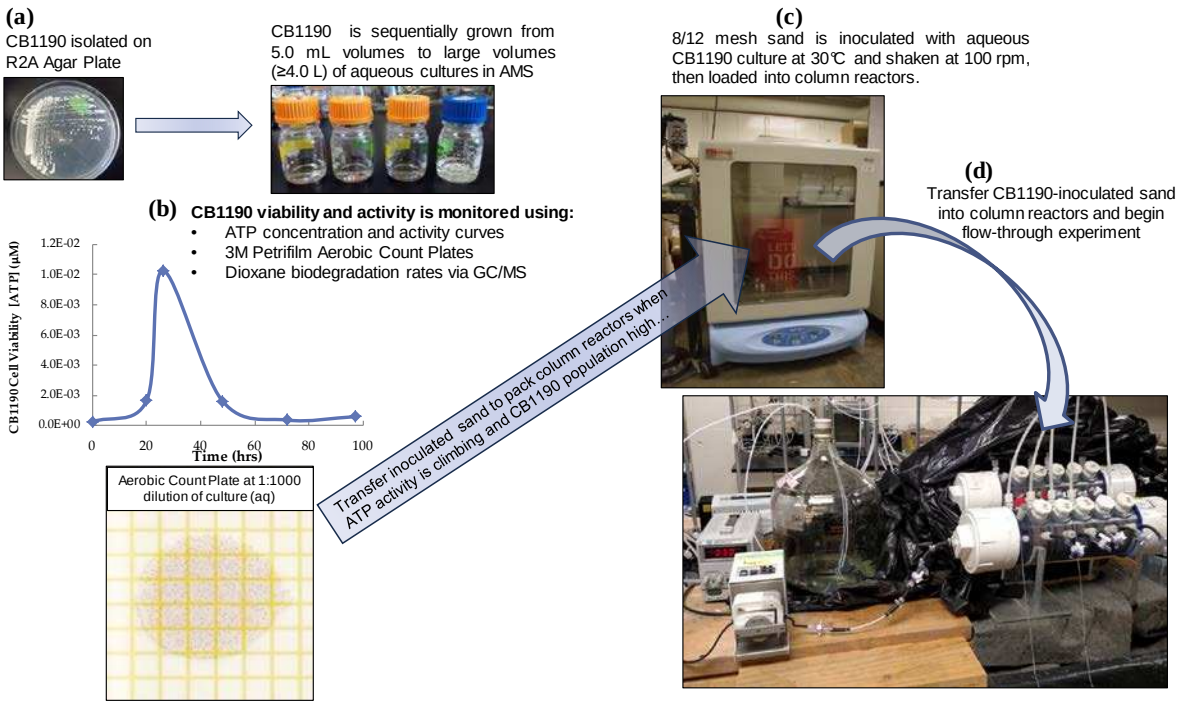

Figure S4.3 Workflow of sand inoculation process: (a) isolated *Pseudonocardia dioxanivorans* CB1190 strain is grown into large volumes of aqueous culture, (b) aqueous culture is added with sand for inoculation once high bacteria abundance is present on petrifilm aerobic count plates and increases in ATP concentrations are observed, (c) inoculation on sand occurs for 3-5 days, continually monitoring ATP and bacteria abundance, (d) the inoculated sand is packed into column reactors and flow-through experiment is started.

Measurements of pH and CB1190 counts. Electrolysis can produce dissolved molecular oxygen at voltages above the oxygen evolution potential, (E_H^0 = 1.23 V vs. SHE), stimulating aerobic biodegradation. However, since electrolytic treatment can also be used for disinfection purposes, we investigated the pH and CB1190 population abundance at different locations along the flow path. Figures S4.4 and S4.5 show measurements taken at the influent and at 4 other sampling ports along the column reactor with locations 1, 2, 3 and effluent positioned at distances of 2.5, 12.5, 22.5, and 32.5 cm downstream of the anode. Figure S4.4 shows the planktonic and biofilm cell counts for CB1190 bacteria in the abiotic sand column experiments. The unexpected detection of CB1190 in several abiotic control samples is likely due to the fact that abiotic experiments were conducted after biotic experiments. Although all column reactors

had been submerged in 70% ethanol for 30 minutes and air dried after biotic experiments, and heat-sterilized sand was used in the columns, it is possible that remnants of DNA could have remained in the column reactor fittings or sand even after cellular death had occurred during the disinfection process since qPCR detects the (dxmB) genes coding for dioxane monooxygenase.

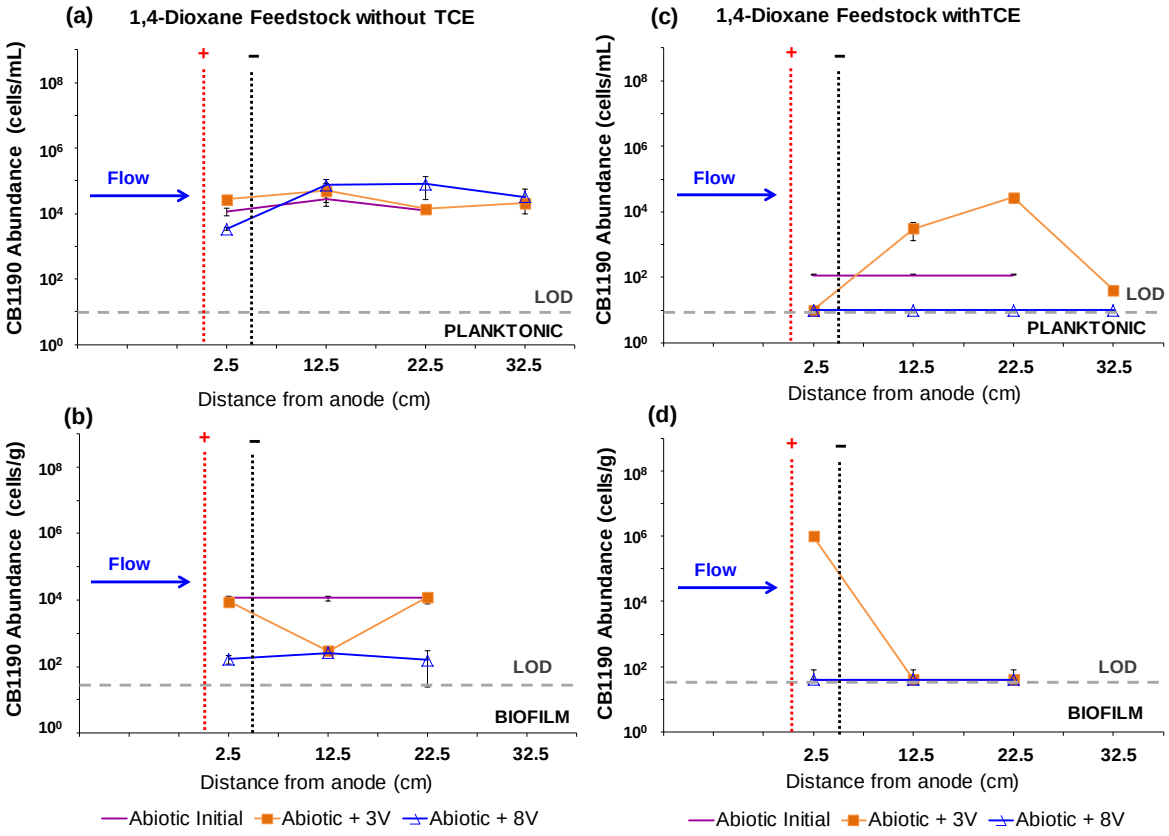

Figure S4.4. Plots of (a) planktonic abundance and (b) biofilm abundance of CB1190 in the abiotic flow-through sand columns with 100 mg/L 1,4-Dioxane in AMS liquid media as feedstock. Plots of (c) planktonic abundance and (d) biofilm abundance of CB1190 in the abiotic flow-through sand columns when 5 mg/L TCE was also present. Any samples that were below the detection limit of the qPCR analysis were plotted at the respective method detection limit (1×10^1 cells/mL for planktonic abundance and 4×10^1 cells/g for biofilm abundance).

Figure S4.5 plots pH measurements along each column reactor for the CB1190 experiments and the abiotic controls, in conditions with TCE absent and TCE present. Figure S4.5 shows the greatest extremes in pH conditions occur between the electrodes, ranging from

highly alkaline at pH of 12.0 to extremely acidic at pH of 2.3. However, after passing the second electrode, pH levels return to near neutral levels, except for the CB1190 + 8V experiment.

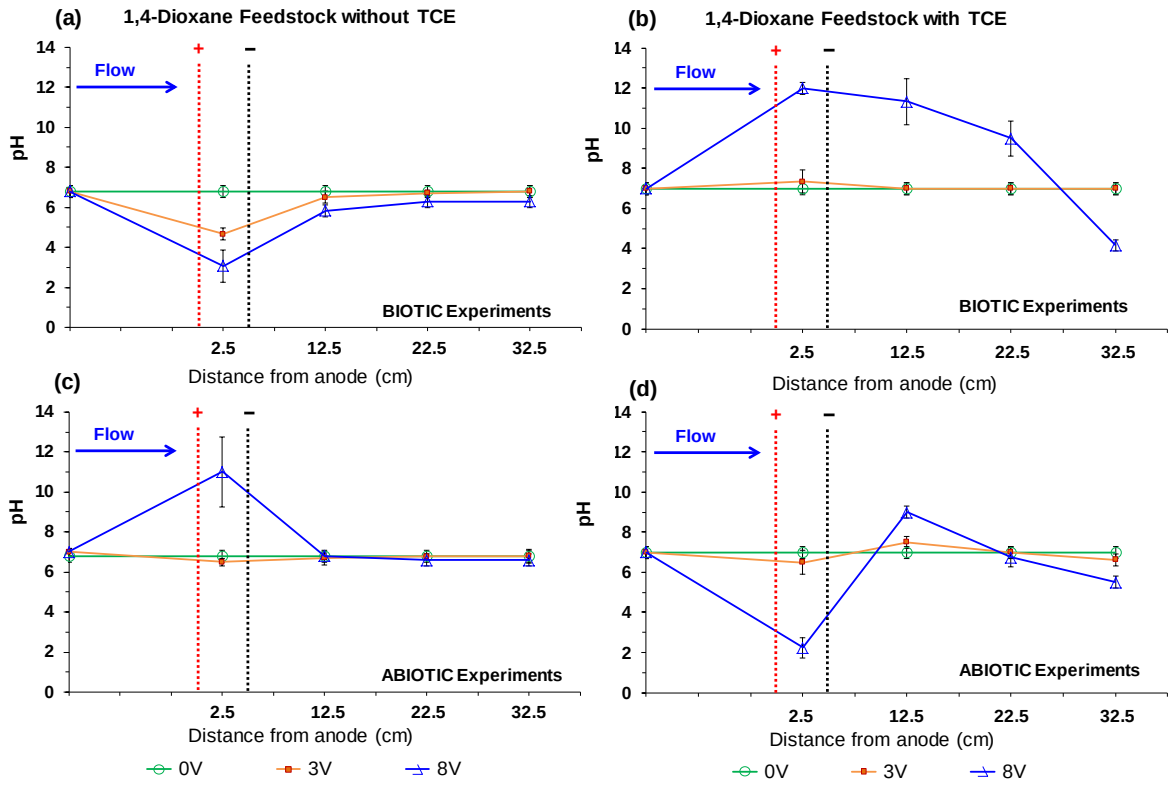

Figure S4.5. Plots of pH along the *P. dioxanivorans*-inoculated sand column reactors with feedstock of (a) 100 mg/L 1,4-dioxane in AMS liquid media and (b) 100 mg/L 1,4-dioxane with 5 mg/L TCE also present. Plots of pH along abiotic control columns with (c) 100 mg/L 1,4-dioxane in AMS liquid media and (d) 100 mg/L 1,4-dioxane with 5 mg/L TCE also present. All column experiments were operated at room temperature with a seepage velocity of 46 cm/d.

Measurements of dissolved oxygen and conductivity. Dissolved O_2 (DO) and conductivity values were measured using a Hach HQ40d Meter with rugged LDO101 probe in conjuntion with CDC401 conductivity cell. Specific conductivity consistently measured around 3,400 µS/cm with all experiments. Dissolved O_2 values were measured in the influent and 3 ports along the column flow path for the co-contaminant experiments having AMS media spiked with 100 mg/L 1,4-dioxane and 5 mg/L TCE. Replicate measurements and averaged DO values (mg/L) are included in Table S4.1 below. At 2.5 cm downstream of the anode, higher dissolved

O_2 concentrations were measured in the electrochemically stimulated FTERs, 10.98 mg/L (at 3.0 V) and 15.3 mg/L (at 8.0 V) compared to 5.51 mg/L in the biological control column (CB1190 + 0V). This data supports the claim that more favorable aerobic conditions were being produced downstream (downgradient) from the electrodes when the electrodes were charged.

Table S4.1 Dissolved O_2 (DO) measurements in co-contaminant experiments

Replicate DO (mg/L) measurements (n = 3)	Influent	Distance from anode (cm) 2.5 cm	12.5 cm	22.5 cm
CB1190+ 0V	2.77	5.59	4.87	4.60
CB1190+ 0V	2.63	5.30	4.97	4.62
CB1190+ 0V	3.10	5.64	4.76	4.55
DO average (mg/L)	**2.83**	**5.51**	**4.87**	**4.59**
Standard deviation	0.24	0.18	0.11	0.04
CB1190 + 3V	2.81	9.04	6.58	6.28
CB1190 + 3V	2.69	12.32	4.74	6.01
CB1190 + 3V	2.68	11.58	4.00	6.04
DO average (mg/L)	**2.73**	**10.98**	**4.83**	**6.11**
Standard deviation	0.07	1.72	1.33	0.15
CB1190+ 8V	2.81	9.81	7.29	7.65
CB1190+ 8V	2.69	20.86	7.57	6.17
CB1190+ 8V	2.68	15.31	7.54	6.23
DO average (mg/L)	**2.73**	**15.33**	**7.47**	**6.68**
Standard deviation	0.07	5.53	0.15	0.84

APPENDIX D

SUPPORTING INFORMATION FOR CHAPTER 5

The salt concentrations necessary for treatment of 1,4-dioxane in electrochemical batch reactors made the analysis for organic acid transformation products difficult. The 10 mM Na_2SO_4 electrolyte used caused swamping of the detector when using LC-HR-TOF(MS) due to swamping the mass detector signal with easily ionizable sulfate ions. Thus, in collaboration with Patrick Brophy of the Delphine Farmer laboratory group at Colorado State University, a novel experimental set up was constructed to allow for real-time analysis of volatile organic acid transformation products in the headspace during electrochemical degradation of 1,4-dioxane (Figure S5.1). The analysis was performed using high resolution time-of-flight chemical ionization mass spectrometry with a head space apparatus (HS-HR-CIMS(TOF)). The interference effect of sulfate was removed by collecting volatiles from the headspace rather than using liquid samples. Moreover, this technique can rapidly provide vast amounts of mass spectra data for non-targeted analytes from complex aqueous samples without any pre-separation chromatography, pre-concentration or sample preparation. Due to the sensitivity of the instrument and abundance of mass spectra being continuously collected, it is very important to measure a representative background spectrum for both normalization and data quality control and assurance.[168] We obtained background spectra for the blank, unfilled electrochemical reactor and time zero analysis for the liquid sample from the headspace of the reactor (for real-time analysis) or from headspace of a sample vial (for aliquots from timed reactions). The details of

this analysis technique are described in Brophy and Farmer 2015[168] and in Chapter 4 of Patrick Brophy's Ph.D. dissertation 2016.

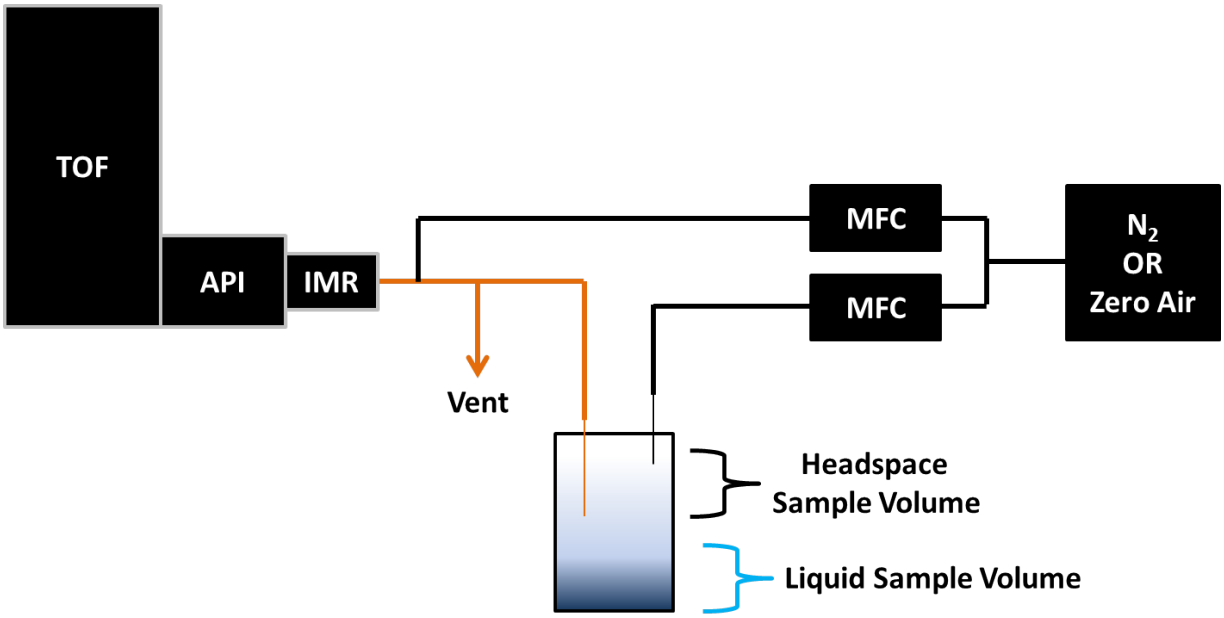

Figure S5.1 Experimental set up of HS-CIMS(TOF) experiments for real-time transformation product analysis from electrochemical batch reactor degradation of aqueous 1,4-dioxane.

Electrochemical batch reactor conditions used for this preliminary study were 1.0 Amp constant current applied to 10 μM 1,4-dioxane in 10 mM Na_2SO_4 electrolyte filled with inert glass beads for sample Glass_120min and filled with AP-F880 TiO_2 pellets for TiO_2_00min and TiO_2_120min. The Fenton _120min sample is the result of 120 minutes of Fenton's reagent oxidation using 0.1 mM $FeSO_4$ and 0.20 mM H_2O_2, with no voltage applied. HS-HR-TOF-CIMS was used to analyze the headspace and the background-subtracted mass defect plots are displayed in Figure S5.2 and S5.3. Figure S5.2 demonstrates the powerful filtering of mass spectra that can be done to determine the peaks with the highest confidence of being different than background. Starting with the full amount of peaks plotted in (a), and the peaks remaining after filtering (b) by calculating the percent change for every detected species and rejecting those that change by < 5% from background. The top plot (c) shows the result of applying both the 5%

cutoff and applying a S/N >3 cutoff and still many new organic acid homolog peaks persist, some showing higher O:C ratio from the 2:1 to 4:1 range. The relevance and likelihood of these long carbon chain carboxylic acids products was not deeply investigated at this time.

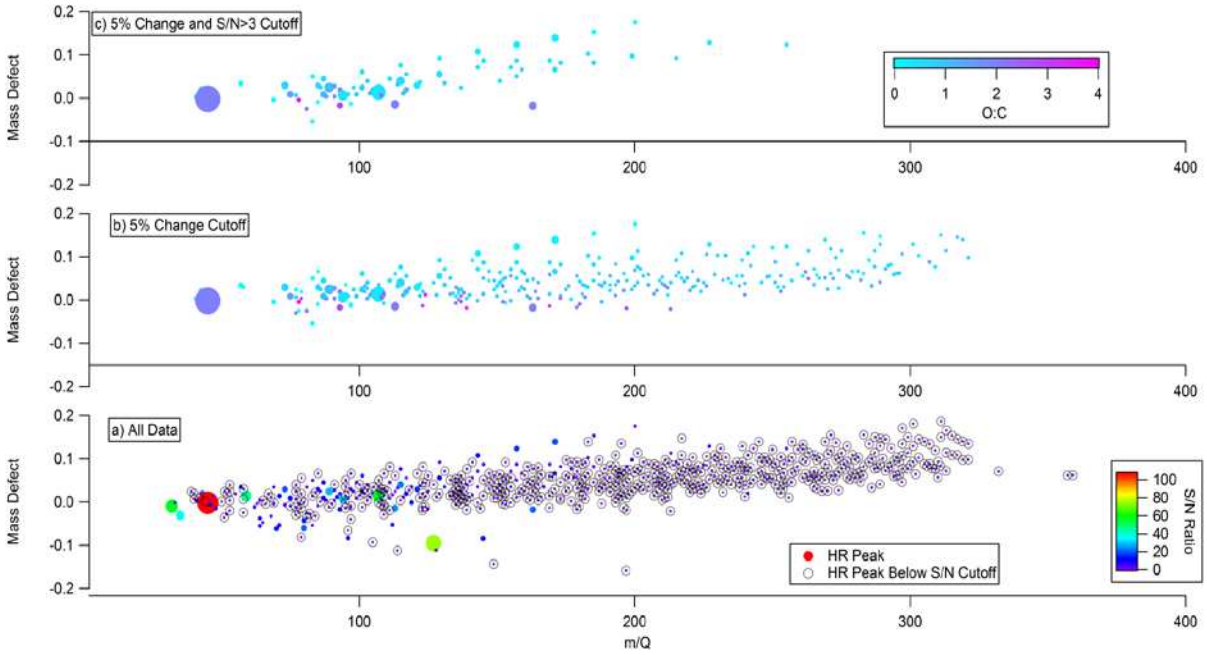

Figure S5.2 Mass defect plots of a sample after 120 minutes of electrochemical degradation in an electrochemical batch reactor held at 1.0 Amp constant current (TiO_2_120 min). Electrochemical batch reactor conditions included 10 µM 1,4-dioxane in 10 mM Na_2SO_4 electrolyte filled with AP-F880 TiO_2 pellets between electrodes. Plots (a) and (b) show all peaks in the mass spectrum colored by O:C ratio. Plot (c) shows all peaks in the mass spectrum colored by S/N ratio. The full amount of mass spectra peaks obtained are plotted in (a), and the peaks remaining after filtering by calculating the percent change for every detected species and rejecting those that change by < 5% from background are shown in (b). The top plot (c) shows the result of applying both the 5% cutoff and applying a S/N >3 cutoff.

Figure S5.3 shows the difference between four aqueous samples with all peaks in the mass spectra colored by O:C ratio with red having the highest oxygen to carbon ratio, indicating a more oxidized species. The appearance of numerous lower mass defects appear when comparing initial time 0 solution (c) to the reactor solution after 120 minutes (d) of electrochemical degradation by 1.0 Amp constant current. This typically corresponds to an increase in oxidation state which is consistent with the electrochemical oxidation process

occurring. Additionally, the peaks enclosed by the red circle indicate that these peaks were detected above the established threshold limits: signals that differ from background spectrum by >5% and have S/N >3. Thus these are data points with a high degree of confidence that they are the result of detected compounds, and not interferences happening in the ion source due to large volumes of sample continually flooding into the MS. The reactant solution after 120 minutes of electrochemical degradation with TIO_2 catalytic pellets present shows a higher amount of lower mass defect peaks (more oxidized products) than the one degraded in the presence of glass beads. From this data comparison alone, it cannot be concluded that more oxidized transformation products were formed in the TiO_2 reactor. An alternative explanation could be that the same oxidized products were present in the glass beads reactor at some other time point and have subsequently been fully oxidized to CO_2. The mass defect plot of Fenton's reagent solution after 120 minutes does not show any new mass peaks that overcome the threshold requirements. In the Fenton's reagent reaction, 100% of the 1,4-dioxane was removed and so it is possible that ongoing reactions fully mineralized any of the organic acid intermediates. Figure S5.4 shows another version of a mass defect plot showing chemical formulas of detected ions collected in real-time in headspace above batch reactor at 1.0 Amp with TiO_2, 10 µM 1,4-dioxane, 10 mM Na_2SO_4. This could be a very powerful tool for detecting transformation products in real-time as treatment is taking place.

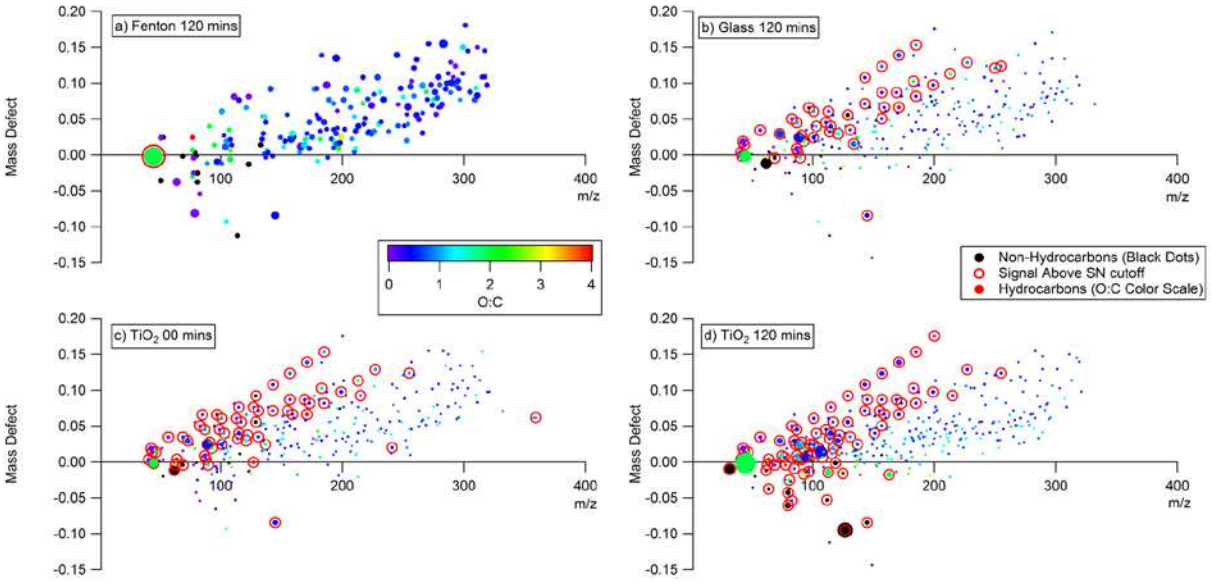

Figure S5.3 Mass defect plots of four samples. The (a) Fenton _120min sample is the result of 120 minutes of Fenton's reagent oxidation using 0.1 mM $FeSO_4$ and 0.20 mM H_2O_2 on a 10 µM 1,4-dioxane solution, with no voltage applied. The other samples were from electrochemical batch reactors at 1.0 Amp constant current with 10 µM 1,4-dioxane in 10 mM Na_2SO_4 electrolyte filled with inert glass beads for sample (b) Glass_120min and filled with AP-F880 TiO_2 pellets for (c) TiO_2_00min and (d) TiO_2_120min.

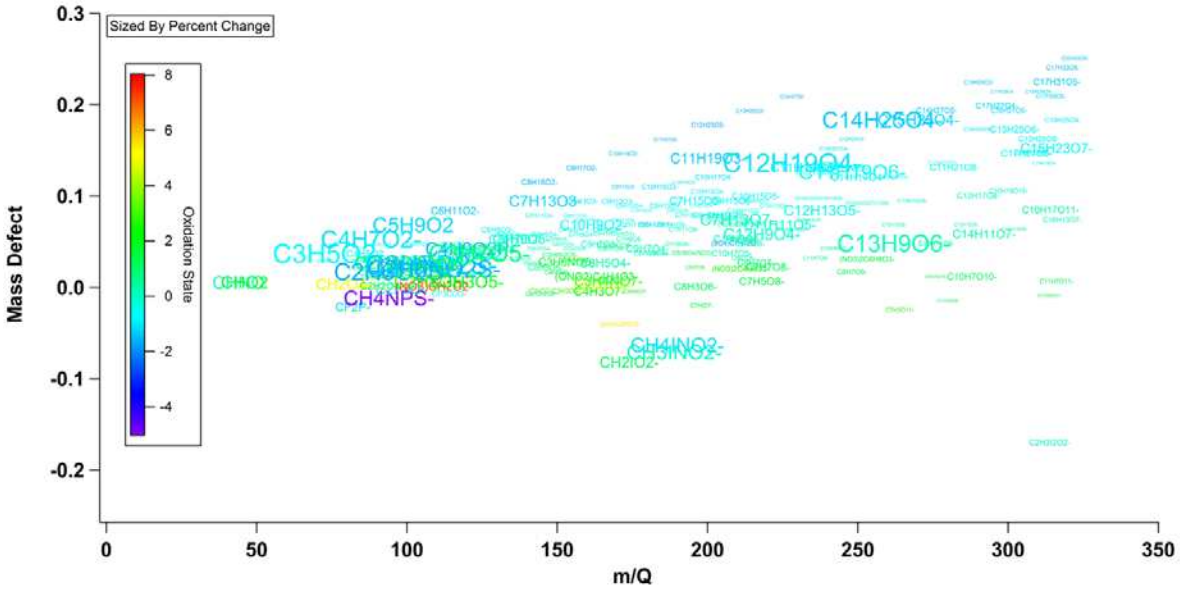

Figure S5.4 Mass defect plot showing chemical formulas of detected ions collected in real-time in headspace above batch reactor at 1.0 Amp with TiO_2, 10 µM 1,4-dioxane, 10 mM Na_2SO_4.